THE EXPLORATION FOR, AND POSSIBLE GENESIS OF, SOME ARCHAEAN GRANITE/GNEISS-HOSTED GOLD DEPOSITS IN THE PIETERSBURG GRANITE-GREENSTONE TERRANE.

THESIS

Submitted in partial fulfilment of the

requirements for the Degree of

MASTER OF SCIENCE (ECONOMIC GEOLOGY)

of Rhodes University

by

MICHAEL ANTHONY LEONARD FLANDERS LINKLATER

January, 1992.

ABSTRACT

The gold mineralization event within Archaean granite-greenstone terranes occurred during the late Archaean, and followed the intrusion of syn- to late-tectonic granitic plutons into previously deformed greenstone belts.

An Archaean granite/gneiss-hosted gold deposit, in terms of this project, is classified as having a gold-assay cutoff of 1g/metric ton over widths of at least several metres, or higher grades over narrower widths and/or verbal descriptions that indicate such values.

Fluid inclusion studies and isotopic data identify two possible origins for the auriferous fluids; namely magmatic and metamorphic. The exploration target according to the magmatic model, is a late-Archaean, hydrothermally altered, mineralized and fractured granitic intrusion preferably with a granodioritic or quartz-dioritic composition. The exploration target according to the metamorphic replacement model is a granitic stock that has intruded a zone of crustal weakness such as a shear zone, active during the late Archaean. Alternatively, the granitic intrusion should be affected by regionally extensive late-Archaean shearing. It should be hydrothermally altered, deformed and mineralized.

Five areas within the Pietersburg granite-greenstone terrane were selected for the 'Regional Area Selection' phase of exploration for Archaean granite/gneiss-hosted gold deposits; namely Roodepoort, Waterval, Ramagoep, Moletsie and Matlala. Roodepoort contains a known granodiorite-hosted gold deposit; the Knight's Pluton, and served as an orientation survey for this project. The use and interpretation of LANDSAT images formed an integral part of exploration techniques; to assess their usefulness in the exploration of Archaean granite/gneiss-hosted gold deposits.

Area selection criteria for granite/gneiss-hosted gold mineralization at Roodepoort are the major ENE-trending shear zone, the NNW-trending lineament and hydrothermal alteration, shearing, quartz-stockworks and sulphide mineralization within the Knight's Pluton. The origin of the gold within the Knight's Pluton is uncertain; both magmatic and metamorphic models are possibilities. Ongoing exploration is in progress at Roodepoort.

The only area selection criterion for granite/gneiss-hosted gold mineralization at Waterval is the sericitized, subcropping granites located within trenches. Gold mineralization is insignificant. No area selection criteria for Archaean granite/gneiss-hosted gold mineralization were located at Ramagoep, Matlala and Moletsie. No further exploration is recommended for all these areas.

The MES image interpretations were successful in identifying lineaments, granitic outcrops, greenstones, vegetation and soil cover. The Clay-iron images adequately differentiated betweeen iron-rich and clay-bearing areas. However, not all clay-bearing areas were associated with hydrothermal alteration; field checks were necessary to discriminate between weathered granites and hydrothermally altered granites. The Wallis images served to locally enhance the contrasts of the MES and Clay-iron images.

List of Contents

List of Figures

List of Tables

1. Introduction

The Pietersburg granite-greenstone terrane is one of the major granite-greenstone terranes preserved within the Kaapvaal Craton of South Africa. It is located within the Highveld of the Northern Transvaal, about 300 km northeast of Johannesburg (Fig. 1).

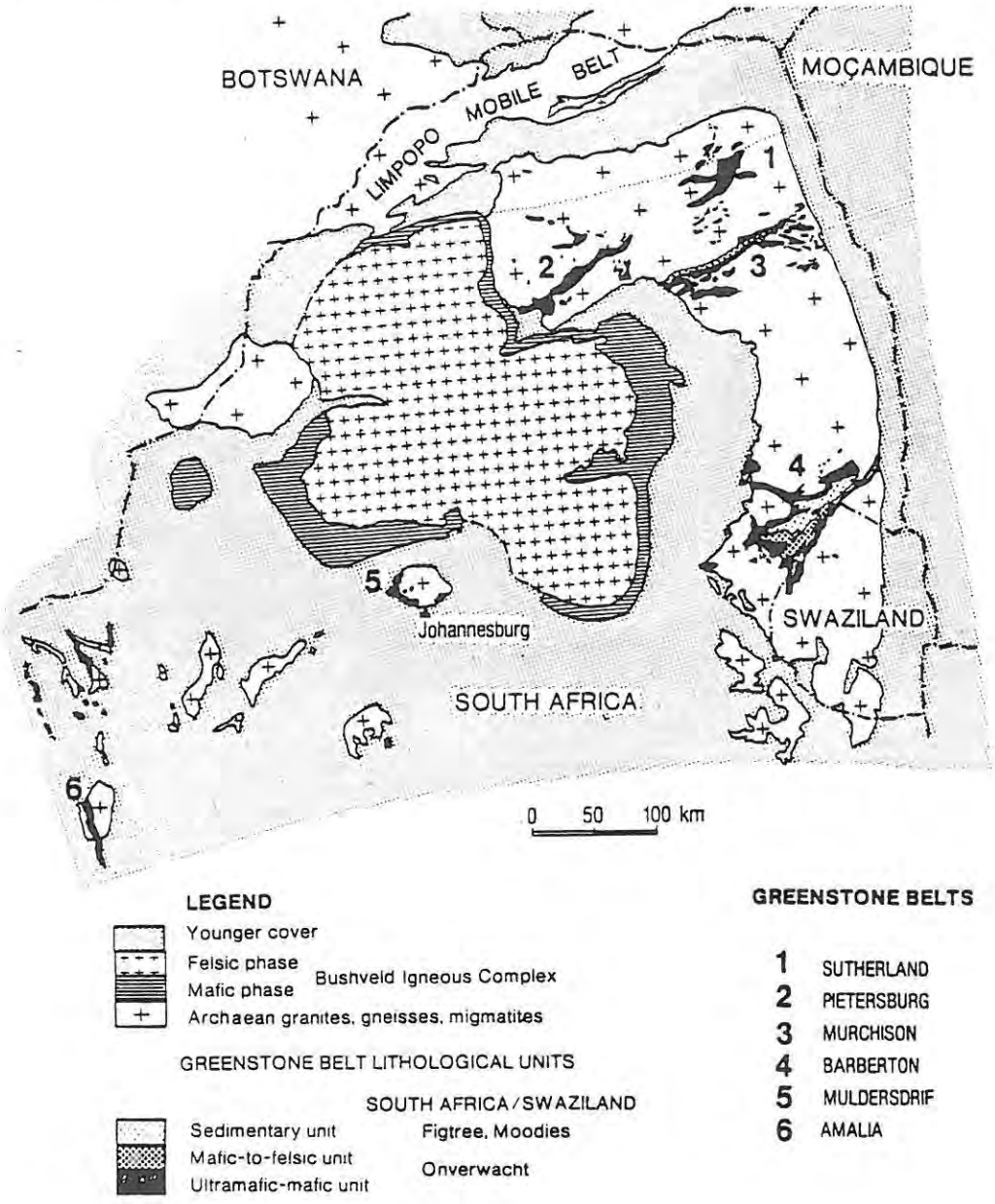

Figure 1. Map illustrating the exposed Archaean granite-greenstone terrane of the Kaapvaal Craton, Southern Africa (after Anhaeusser, 1973, 1976).

The area has an average altitude of more than 1300m above sea level, a mild and healthy climate, and summer rainfall of about 400mm per year (Willemse, 1938). Towards the south of Pietersburg, the area is quite hilly, and dissected by numerous streams. Extensive low-lying planes between the ridges are generally soil covered. In the north of Pietersburg, the areas underlain by ancient gneisses are flat and soil-covered. This topography is broken by younger, rounded granitic intrusions in places. Occasional streams drain the areas surrounding these granitic intrusions.

To date, Archaean gold exploration is concentrated in the greenstone belts rather than the granitic rocks. However, a number of old granite-hosted gold workings exist within the Pietersburg granite-greenstone terrane and therefore, exploration for Archaean granite/gneiss-hosted gold deposits is warranted. The term 'granite' is used very loosely, and covers alkali granites, granites, granodiorites and quartz diorites. Individual rock compositions are named, where necessary.

Five granitic areas near Pietersburg, within the Pietersburg granite-greenstone terrane, were selected for gold exploration. One area (Roodepoort) contains a known gold deposit (Knight's Pluton), hosted by an altered Archaean granodiorite, and served as an orientation survey.

Apart from Roodepoort, this project is restricted to the 'Regional Area Selection' phase of exploration (Appendix 1). The procedure followed is illustrated in figure 2.

At Roodepoort, in addition to completing the 'Regional Area Selection' phase of exploration, logging and petrographic examination of an old vertical drill core through the Knight's Pluton (RDP2) was done. Furthermore, a series of unaltered and altered granitic samples were collected and geochemically analysed to determine possible pathfinder -elements applicable to the exploration of Archaean granite/gneiss-hosted gold deposits, using the analytical techniques available to exploration geologists (Appendix 3).

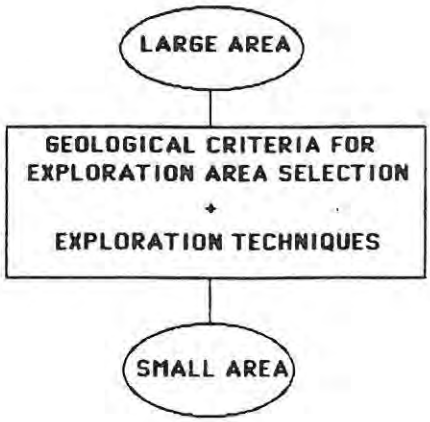

Figure 2. Schematic representation of the exploration process (after Hodgson and Troop, 1988).

The initial part of this project involved a literature survey covering:

1). the evolution of Archaean granite-greenstone terranes.

2). Archaean gold mineralization within Archaean granite-greenstone terranes.

3). the magmatic- and metamorphic-replacement models for Archaean granite/gneiss-hosted gold mineralization.

Area selection criteria (Fig. 2), incorporating favourable geological features spatially and genetically associated with Archaean granite/gneiss-hosted gold deposits, were acquired from (3).

The use and interpretation of LANDSAT images formed an integral part of the exploration techniques (Fig. 2); to assess their usefulness in the exploration for Archaean granite-gneiss-hosted gold deposits (Fig. 2). They also represent a potentially cost-effective exploration tool; an important component of a good exploration strategy (Hodgson, 1990). The LANDSAT images used in this project were processed and made available by the **Remote Sensing Department, Anglo American Corporation of South Africa Limited.** The images were interpreted with emphasis on identifying the 'area selection criteria' mentioned above.

The fieldwork was completed during December, 1989 to March, 1990; part of June, 1990 and part of June, 1991. It consisted of locating the LANDSAT features on the ground, geological mapping and trenching where necessary, and confirming the presence or absence of 'area selection criteria' for granite/gneiss-hosted gold mineralization in the areas chosen for exploration. Lithogeochemical samples were collected and analyzed using the techniques described in Appendix 3. A substantial part of this thesis, in addition to the fieldwork, involved petrographic examinations of selected granitic samples from each of the five areas chosen for exploration. Finally, recommendations for the future of each area, in terms of gold exploration, were offered.

An overview of the 'exploration strategy' used in this project and the various phases of exploration applicable to Archaean granite/gneiss-hosted gold deposits is given in Appendix 1. A brief description on the processing techniques of LANDSAT images is given in Appendix 2. Appendix 3 describes the geochemical analytical techniques used in this project and Appendix 4 lists the analytical data.

2. Archaean granite-greenstone terranes.

Archaean granite-greenstone terranes broadly comprise discontinuous greenstone belts engulfed in a sea of intruded granitic plutons (Condie, 1989; Anhaeusser and Robb, 1980; Watkins et al., 1991), and are surrounded by extensive high-grade gneissic terranes (Hunter, 1991). A diagram of a typical Archaean granite-greenstone terrane is given in figure 3, and an idealized Archaean greenstone belt stratigraphic column is illustrated in figure 4.

The Superior and Slave Provinces of North America, the Zimbabwe and Kaapvaal Provinces of Southern Africa, and the Yilgarn and Pilbara Provinces of Western Australia are amongst the economically important granite-greenstone terranes.

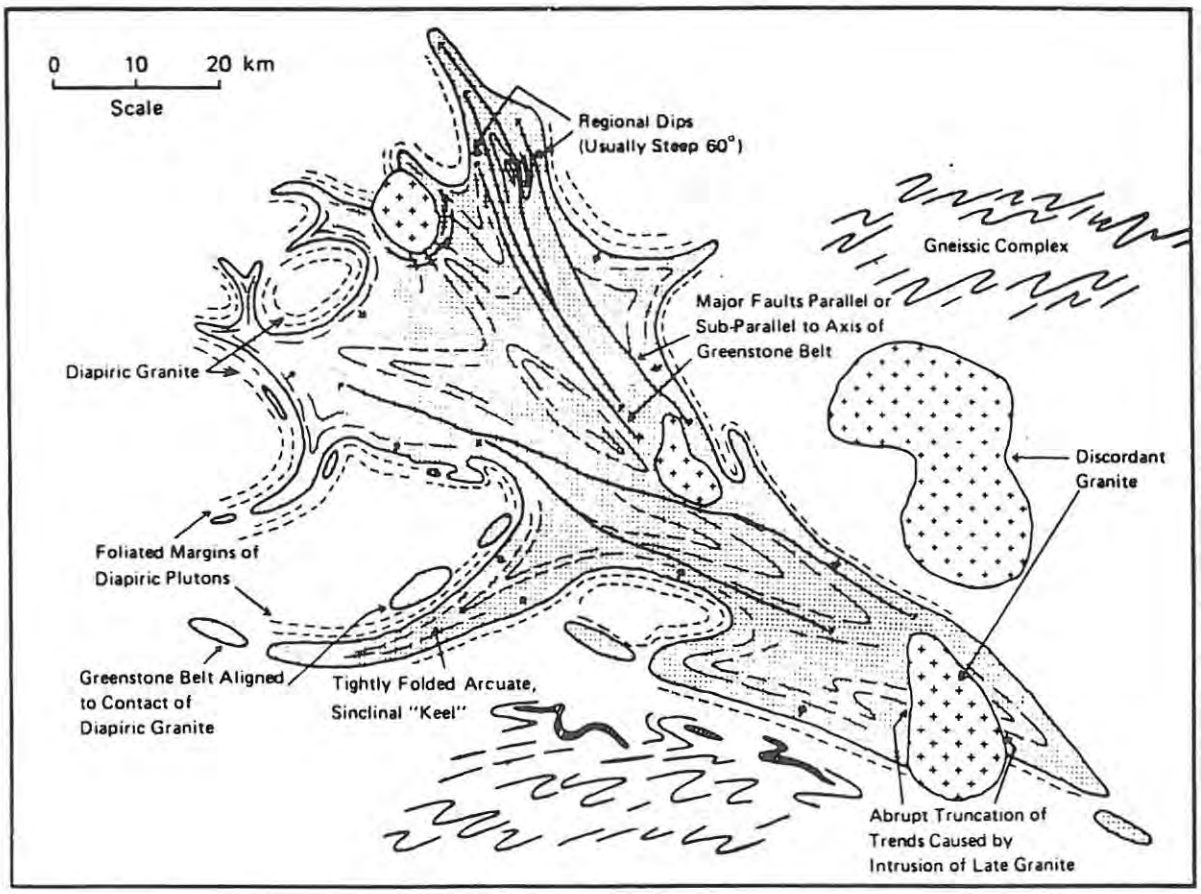

Figure 3. Map of an idealized Archaean granite-greenstone terrane (after Anhaeusser et al., 1969).

FIGURE 4

HYPOTHETICAL ARCHAEAN STRATIGRAPHIC COLUMN

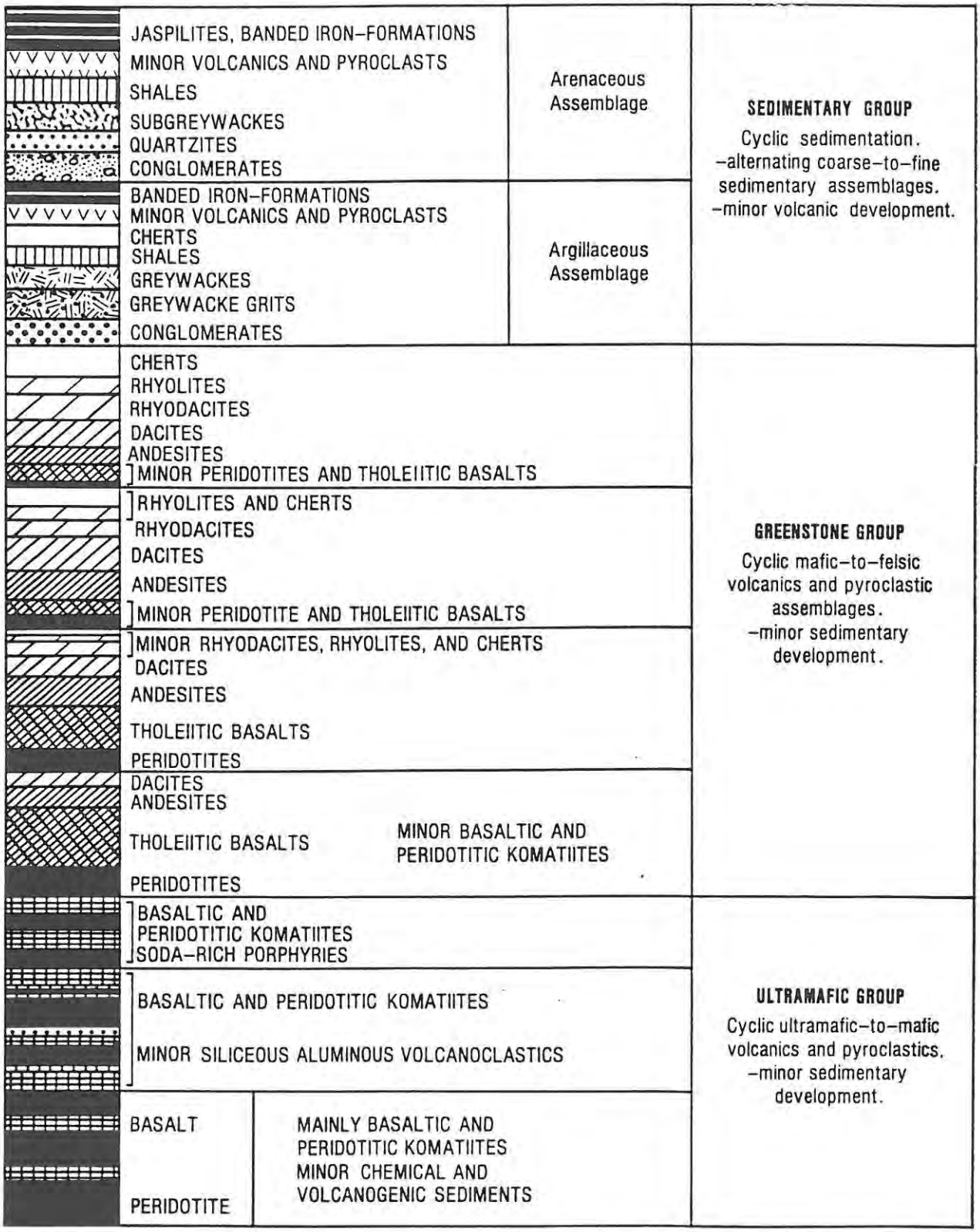

(after Anhaeusser and Viljoen, 1986).

2.1. The greenstone belts

Archaean greenstone sequences are composed of areally restricted remnants of volcanic rocks, commonly metamorphosed at greenschist facies, with or without sequences of clastic and chemical sedimentary rocks that structurally and/or stratigraphically overlie the volcanic piles (Hunter, op. cit.).

The volcanic rocks (Fig. 4) are subdivided into a lower, primarily ultramafic group and an upper volcanic group in which calc-alkaline, mafic-to-felsic rocks predominate. Cyclicity is common, with individual belts containing between 5 and 10 major volcanic cycles (Windley, 1984).

The predominantly clastic sedimentary succession (Fig. 4) consists ideally of a lower argillaceous deep-water assemblage comprising shales, pelitic sandstones and greywackes, and an upper arenaceous, shallow-water assemblage with conglomerates, quartzites and chemically precipitated limestones and banded iron formations that tend to occupy the tops of cyclic units (Windley, op. cit.).

2.2. The granitic rocks.

Anhaeusser et al., (1969) and Anhaeusser and Robb (1980) have subdivided the Archaean granites within the Barberton Mountainland and parts of Swaziland into three magmatic cycles. Watkins et. al., (1991) proposed a similar classification of granites within the Murchison Province of the Yilgarn Craton in Western Australia. These cycles reflect possible stages in the formation and genetic evolution of the early sialic crust in these regions, and are possibly applicable to other Archaean granite-greenstone terranes.

The earliest magmatic cycle involved the formation of Na-rich tonalites and trondhjemites, and a complex series of bimodal gneisses and migmatites. The tonalite/trondhjemite material was derived from about 30-50 per cent melting of a mafic source similar to the basal stratigraphic units of the greenstone belts into which the above-mentioned tonalites/trondhjemites intruded (Anhaeusser and Robb, 1980). This cycle commenced approximately

3550 Ma ago within the Barberton Mountainland and parts of Swaziland (Anhaeusser and Robb, 1980) and approximately 2900 Ma ago within the Murchison Province (Watkins et. al., 1991).

The second magmatic cycle involved the emplacement of enormous volumes of K-rich magma into the crust, such that by the end of the Archaean era, the thickness of the continental crust had probably reached 30-35 km. Watkins et. al., (op. cit.) state that these rocks were probably derived by partial melting of mafic source rocks similar in composition to those of the first magmatic cycle. These granites were emplaced at relatively high crustal levels in the form of batholiths and sheet-like masses over earlier-formed sialic crust, belonging to the preceding magmatic cycle. The batholiths are multi-component bodies comprising homogenous, often medium-to-coarse-grained, occasionally porphyritic, granites, granodiorites or adamellites (Anhaeusser and Robb, 1980). Pegmatitic and aplitic phases are associated with these granites, and areas marginal to the batholiths are characterized by K-rich migmatites and gneisses that represent zones of interaction between the intrusive granitic massifs and the surrounding host rocks. The batholith margins seldom display sharp contacts (Anhaeusser and Robb, op. cit.). This cycle began approximately 3200-2900 Ma ago within the Barberton Mountainland and parts of Swaziland (Anhaeusser and Robb, op. cit.), and approximately 2700 Ma ago within the Murchison Province (Watkins et. al., 1991).

The third magmatic cycle commenced about 2900 Ma ago within the Barberton Mountainland and parts of Swaziland , and was associated with the intrusion of late to post-tectonic, granitic-, adamellitic-, granodioritic- and syenitic-plutons into an already consolidated and tectonically stable crustal regime (Anhaeusser and Robb, 1980). This same cycle commenced about 2600 Ma ago within the Murchison Province (Watkins et al., 1991). Essentially, these granitic bodies caused a minimum amount of structural disturbance and metamorphic alteration (Anhaeusser and Robb, 1980; Watkins et al., 1991).

Anhaeusser and Robb (1980) have identified two groups of plutons within the Barberton Mountainland and parts of Swaziland that are associated with the third magmatic cycle; namely an older group and a younger group. The older

group comprises granodiorites that range in age from 2927 ± 59 Ma to 2784 ± 53 Ma. The younger group consists of granites and adamellites that are 2608 ± 123 Ma to 2496 ± 176 Ma in age (Anhaeusser and Robb, op. cit.).

Similarly, Watkins et al., (1991) have identified two distinct suites of post-tectonic granites within the Murchison Province. One suite (Suite I) comprises tonalite, trondhjemite, granodiorite and monzogranite plutons that are approximately 2663 ± 74 Ma old. The other suite (Suite II) consists of quartz-rich monzogranite and syenogranite plutons that are approximately 2365 ± 161 Ma old. The different compositions of Suites I and II are thought to reflect the differing compositions of the deep crust at the level of partial melting. Suite I granites were probably derived from mafic rocks which underplated or intruded the base of the crust, whilst Suite II granites originated from dominantly silicic parental rocks (Watkins, et al., op. cit.).

2.3. Metamorphism

Low pressure greenschist facies metamorphism is most common in the granite-greenstone terranes, however the grade of metamorphism can increase to amphibolite facies from the centre to the margins of the greenstone belt, and also towards intrusive granitic plutons (Windley, 1984). Condie (1989) suggested that the numerous granitic intrusions surrounding and possibly underlying greenstone belts, provided a major source of heat for later periods of low-grade regional metamorphism.

2.4. Structure

Archaean granite-greenstone terranes are structurally very complex with most of these areas having undergone two or three periods of major deformation and metamorphism. Deformation of the greenstone sequences apparently involved thin-skinned tectonism, as geophysical data (e.g. Burley et al., 1970; Darracott, 1975 and de Beer et al., 1984) indicate that greenstone belts do not persist to depths greater than about 5 km below surface (Hunter, 1991).

2.5. Tectonic Setting

The reader is referred to Windley (1984) for a general model of Archaean crustal evolution. It combines the idea of an original back-arc marginal setting for the formation of Archaean greenstone belts with a main-arc setting for high-grade gneissic complexes.

Greenstone belts generally contain mixtures of components from different tectonic environments (e.g., the Pietersburg and Barberton greenstone belts). Both greenstone belts contain a record of early sedimentation on oceanic crust which may have been created at similar times (i.e. circa 3.5 G.a.). Subsequent clastic sedimentation within the Pietersburg greenstone belt (500 Ma later) is recorded in a subaerial sequence of rocks that formed in tectonically active compressional basins during the imbrication of the old oceanic crust. At present, it is not known whether the simatic basement of the Pietersburg greenstone belt was already allochtonous before its imbrication (De Wit, 1991).

The late clastic sedimentation within the Barberton greenstone belt, on the other hand, occurred in a submarine environment in tectonically active, compressional regimes restricted to within a period of 250 million years during, and following, the obduction of the oceanic crust and its associated sediments (De Wit, op. cit.). Both the Barberton and Pietersburg greenstone belts were subjected to transpressional and transtensional processes at a late stage in their history (De Wit, op. cit.).

Watkins et al., (1991) stated that the modes and sites of intrusion of all Archaean granites were controlled either by active tectonic processes or by structural features of the crust.

3. Archaean Gold Mineralization.

Most significant Archaean gold deposits occur within or immediatly adjacent to Archaean granite-greenstone terranes. This chapter is restricted to the latter. An overview of gold mineralization within Archaean granite-greenstone terranes is discussed in terms of lithology, structural setting, alteration, metamorphism, fluids and timing. Chapter 4 describes the major models of Archaean granite/gneiss-hosted gold mineralization.

3.1. Lithology

Gold mineralization within Archaean granite-greenstone terranes occurs within a variety of lithologies, such as ultramafic- and mafic-lavas and sills, felsic to intermediate lavas and volcaniclastic rocks, chemical- and clastic-metasedimentary rocks, granites and schists (Perring et al., 1991).

The spatial association between small granitic intrusions and epigenetic gold mineralization in Archaean terranes is well known. In Canada, this association is particularly striking and there is much literature on the subject (see Colvine et al., 1988, and references therein). There, intrusions range in composition from granodiorites and quartz monzonites to syenite and monzonite (Perring et al., 1991). Generally, the granodiorites and quartz monzonites are preferentially associated with the richer deposits. All types of intrusions mentioned above occur more commonly in the environs of gold mines than they do in the Abitibi Belt as a whole (Hodgson and Troop, 1988).

To date, no such correlation between late Archaean felsic intrusions and gold deposits is known to exist within the Norseman-Wiluna Belt of Western Australia (Perring et al., 1991). However, paucity of outcrop within the deeply weathered Norseman-Wiluna Belt and scale of regional mapping by the Geological Survey of Western Australia (1:250000 and 1:100000 in more highly mineralized areas) may hamper this assessment. Perring et al., (op. cit.) proposed that the spatial association of granitic intrusions with gold mineralization could often be genetically attributed to the presence of granitic batholiths, and that the parental magmas probably exploited the same zones of crustal weakness as the mineralizing fluids.

The above-mentioned controversy remains the source of heated debate. The Canadians support a magmatic origin for the gold-bearing fluids, whilst the Australians tend to support a 'metamorphic replacement' origin. These models are discussed in Chapter 4.

3.2. Metamorphism and Alteration

The majority of Archaean epigenetic lode gold deposits within Archaean granite-greenstone terranes, formed at sub-greenschist to lower-amphibolite facies metamorphic conditions, commonly at pressures and temperatures estimated to range from 1-3 kb and 250°-400°C respectively (Groves et al., 1991).

Alteration is a common characteristic of many Archaean lode gold deposits. It is generally represented by retrograde mineral assemblages consistent with greenschist facies pressure-temperature conditions, and most likely resulted from overprinting due to hydrothermal alteration (Colvine et al., 1988). In most cases, the intensity of the alteration increases with proximity to mineralized structures. Gold deposition is caused predominantly by fluid-wallrock interactions, and is more fully discussed in Chapter 4. The associated sulphide mineralization varies according to prevailing metamorphic conditions; ranging from pyrite at low metamorphic grades to pyrite-pyrrhotite-dominated assemblages at medium metamorphic grades (Groves et al., 1991).

The timing of the alteration probably post-dates peak metamorphism, which possibly occurred during the granulitization of the lower crust and coeval generation of the late Archaean plutons (Colvine et al., 1988).

3.3. Structural Setting

Eisenlohr et al., (1989) stated that many large Archaean epigenetic gold deposits show a broad spatial relationship to regional lineaments, and have subdivided these lineaments into first- and second-order structures. This is illustrated in figure 5.

The first-order structures are generally greater than 100km in strike length, and appear to be transcurrent structures that extend into the lower crust and mantle. They appear to control the distribution of deep crustal, or upper mantle felsic melts (porphyries) and mantle derived lamprophyres, as well as regional carbonation zones. Some appear to be reactivated syn-volcanic faults (Groves and Batt, 1984). The second-order fault structures are commonly up to 10km in length, and have widths varying from centimetres to hundreds of metres. They represent regional stress orientations and are subsidiary to the larger first-order structures (Eisenlohr et al., 1989).

Gold mineralization is more commonly associated with the second-order structures rather than first-order structures. A possible reason for this is the physiochemical gradients between first- and second-order structures which cause migration (infiltration) of fluids and/or selective transport (diffusion) of gold within fluids into second-order structures (Eisenlohr et al., op. cit.).

The occurrence of gold mineralization within these structures implies that gold concentration was related to the major, latest tectonic event that formed this faulting. Strain analyses of gold deposits within the Superior Province of Canada, show that the present sites of gold mineralization represent zones of dilation produced by shear deformation and that these fabrics post-date previous fabrics produced by folding or tilting (Colvine et al., 1988).

Deformation zones can also form in response to the ascent and emplacement of major granitic batholiths that are external to greenstone belts, and smaller plutons that occur within greenstone belts (Colvine et al., op. cit.). Examples of gold occurrences within this environment are the Red Lake deposits within the Superior Province of Canada. Although these deposits occur within regional deformation zones, the ore zones are controlled by structures caused by the ascent and emplacement of adjacent batholiths, rather than by structures resulting from transcurrent displacement (Colvine et al., op. cit.).

In summary, two types of deformation zones are associated with gold deposits. One results from large scale crustal movement or shortening; the other results from emplacement of plutons and batholiths. The most significant gold deposits are generally associated with the first process. Both types of deformation are late-Archaean tectonic events.

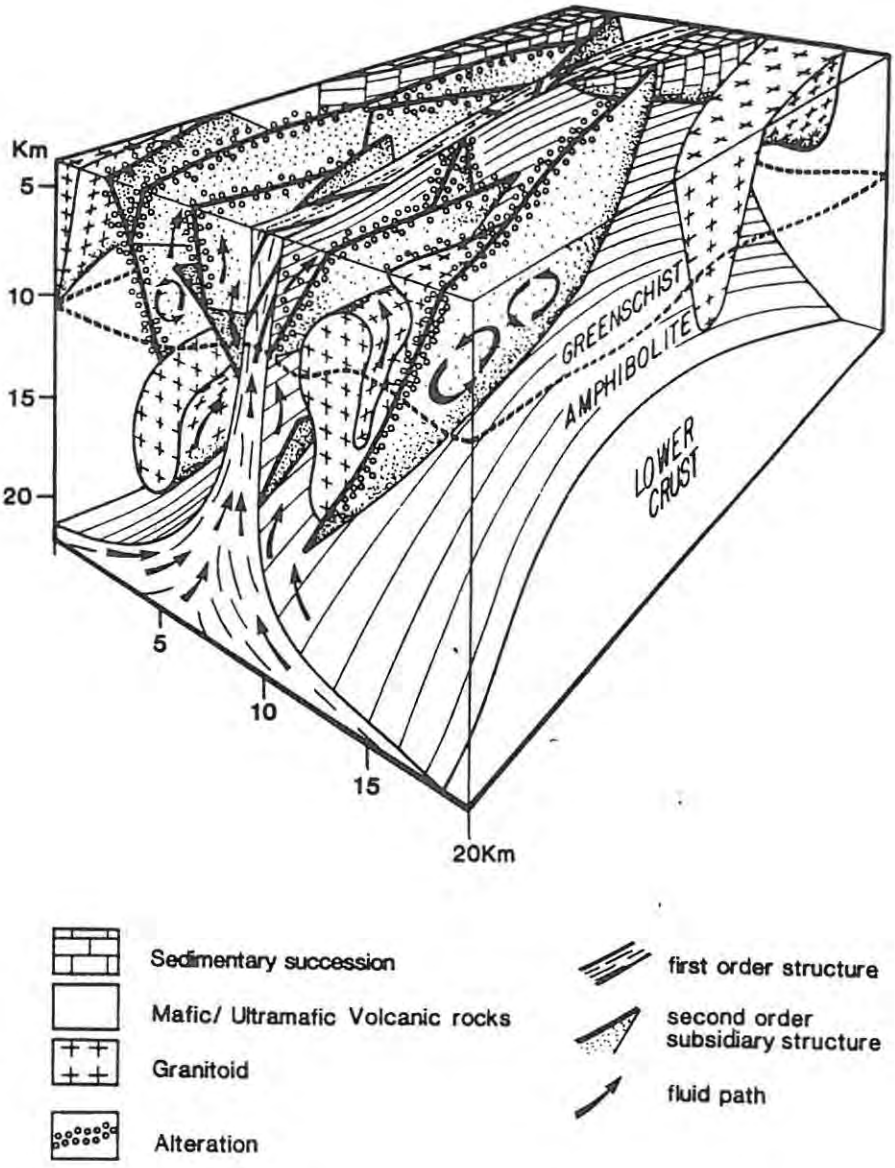

Figure 5. Schematic block diagram illustrating fluid path through the crust via first-order fault zones into second-order subsidiary structures (after Eisenlohr et al., 1989).

3.4. Fluids

Fluid-inclusion and stable-isotope data provide some insight into the origin of the fluids, and are described below.

3.4.1. Fluid inclusion characteristics

Fluid inclusion studies of quartz veins interpreted to be syn-mineralization, indicate that the majority of Archaean gold deposits were formed from similar ore fluids. The fluid was a relatively reduced H_2O-CO_2 fluid (≈75 mole % H_2O-CO_2 fluid (≈75 mole % H_2O, 25 mole % CO_2), $\delta^{18}O$ = 8 - 10 per mil, of low salinity (< 2 wt.% equiv. NaCl) and low density, interpreted to be near neutral to slightly alkaline with depositional temperature and pressure ranges of 250°C - 400°C at 1 - 3 kb. These fluids introduced CO_2, K (and associated minor elements; e.g., Rb and Ba), Au (± Ag, As, Sb, W, B) and S into depositional sites (Groves and Phillips, 1987; Groves et al., 1991). Base metals are generally minor, as these deposits are thought to originate from fluids at 250°C - 300°C, at hydrostatic pressure, $\delta^{18}O$ = 0 to 5 per mil, salinities of 3 - 5 wt. %, H_2O>>CO_2 and Na>>K (Fyfe and Kerrich, 1984). Gold-bearing fluids having the above-mentioned characteristics can originate from low to medium grade metamorphic terranes (Groves and Phillips, 1987). Alternatively, these fluids can also originate from low salinity, CO_2-bearing magmatic fluids, if CO_2 becomes saturated within an H_2O-CO_2 bearing silicate magma (Colvine et al., 1988). Thus fluid inclusion studies indicate that both magmatic and metamorphic processes can produce fluids that are similar to those implicated in the Archaean gold event.

3.4.2. Sulphur Isotope Constraints

$\delta^{34}S$ isotopic data of Archaean gold deposits in Canada and Western Australia tend to cluster near 0 per mil, although two broad groupings are apparent: $\delta^{34}S$ = 0 to +10 per mil (Yellowknife, Red Lake, Belmoral, Owl Creek, Coniarum, McIntyre-Hollinger, Dome and Hard Rock) and $\delta^{34}S$ < 0 per mil (Lakeshore, Macassa, Canadian Arrow, Kelore, Ross, Young Davidson, Consolidated Matachewan and Hemlo; Colvine et al., 1988). The above-mentioned isotopic variation is possibly due to mixing of more than one sulphur source or major isotopic fractionation (Colvine et al., op. cit.).

The latter option is considered to be the dominant factor contributing to the isotopic variation as small changes in temperature, pH and fO_2 can induce large changes in the sulphur isotopic values of sulphur-bearing minerals (Ohmoto and Rye, 1979).

The $\delta^{34}S$ value of 0 per mil suggests two possible sources for the sulphur, namely: direct contribution from magmatic sources, and dissolution of juvenile sulphide minerals by metamorphic fluids. The sulphur isotopic data do not adequately discriminate between the two (Colvine et al., 1988).

3.4.3. Carbon Isotope Constraints

Carbon isotope data from both the Abitibi Subprovince and the Yilgarn Block are similar, and imply a similar auriferous fluid source (Colvine et al., 1988). $\delta^{13}C$ values for total dissolved carbon in the auriferous hydrothermal fluid (based on the $\delta^{13}C$ values of carbonate minerals) range from -8 to -3 per mil, and have a median value of -3,5 per mil (Colvine et al., op. cit.). This is consistent with a magmatic source (Burrows et al., 1986), although a metamorphic origin cannot be ruled out. Possibilities include the dissolution of carbonate related to regional zones of carbonatization and regional faults (Perring et al., 1987).

3.4.4. Oxygen and Hydrogen Isotope Constraints

$\delta^{18}O$ and δD values for the water component of ore fluids within the Yilgarn Block of Western Australia, and the Superior- and Slave-Provinces of Canada, lie in the range +2,5 to +10,0 per mil and 0 to -70 per mil, respectively (Colvine et al., 1988). As illustrated in figure 6, the data lie in the overlapping fields of magmatic and metamorphic fluids, and therefore do not adequately discriminate between them.

3.4.5. Summary of Constraints

Fluid inclusion and isotopic data identify two possible origins for auriferous fluids with similar compositional and isotopic characteristics to those observed within Archaean lode gold deposits, namely metamorphic and magmatic. To date, fluid inclusion studies and stable isotopic data cannot satisfactorily discriminate between the two processes.

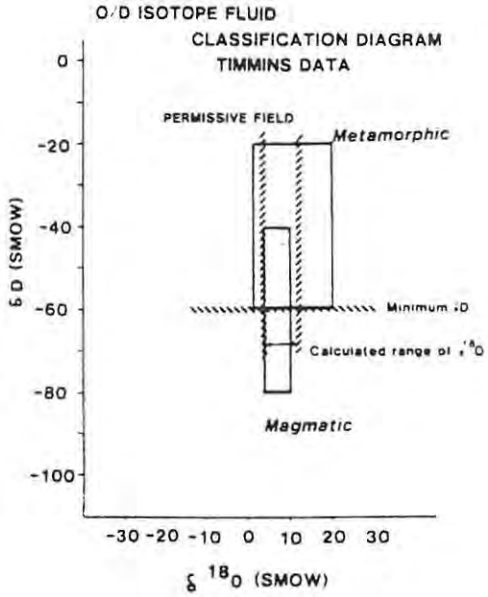

Figure 6. $\delta^{18}O$ vs. δD isotopic fluid classification diagram, showing the empirical fields for magmatic and metamorphic fluids, and the meteoric water line. The fields for data from Archaean gold deposits are indicated (after Colvine et al., 1988).

3.5. Timing

Gold was introduced in a single event that followed the intrusion of syn- to late-tectonic felsic plutons into previously deformed volcano-sedimentary sequences in the greenstone belts (Colvine et al., op. cit.). Barley and Groves (1990) state that this event is closely associated with the final stabilization of Archaean cratons. The approximate age of the gold mineralization event within the Superior Province of Canada ranges from 2718 to 2660 Ma (Colvine et al., 1988). Similar ages for gold mineralization occur within other Archaean granite-greenstone terranes.

4. Models of Archaean Granite/gneiss-hosted Gold Mineralization.

The origin of the Archaean gold-bearing fluids has been a major controversy of the past decade. Two major theories exist. The first, termed the magmatic model, holds that the hydrothermal fluids responsible for gold mineralization are magmatic in origin and are derived from granitic /porphyritic intrusions. The second proposal is that the hydrothermal fluids were derived by metamorphic dewatering during prograde metamorphism, and is known as the metamorphic replacement model. These models are now reviewed.

4.1. Magmatic Model.

The major factor influencing the impetus for this model is the close spatial association between gold deposits and certain granites, particularly in Canada and Zimbabwe. It must be emphasized however, that gold deposits are by no means confined to the vicinity of granitic intrusions, and in many cases there is no evidence that these intrusions could have given rise to the observed mineralization in gold deposits.

Recent reviews of Archaean lode gold deposits believed to be magmatic in origin are supplied by Mann (1984); Wood et. al. (1986); Burrows et al. (1986); Burrows and Spooner (1987); Cameron and Hattori (1987); Burrows and Spooner (1988), Fyon et al. (1988) and Spooner (1991).

The actual magmatic processes involved in the evolution of magmatic-hydrothermal gold deposits can, for convenience, be subdivided into orthomagmatic-, transitional- and hydrothermal-processes. Most of the following summary is based on Burnham and Ohmoto, (1980). Orthomagmatic processes involve the initial generation of silicate melts by partial melting of older rocks. Transitional processes begin when orthomagmatic processes are sufficiently advanced to form a separate aqueous magmatic phase. The lower limit for transitional processes can be arbitrarily set at the H_2O-saturated solidus of the magma. This stage marks the beginning of the hydrothermal processes and involves aqueous fluids and solid phases (hydrothermal fluids and wallrocks).

4.1.1. Orthomagmatic processes

The orthomagmatic processes that are relevant to ore-formation begin with the generation of magmas by partial melting of older rocks. The partial melting is induced by the presence of H_2O, and the amount of melt produced is directly proportional to the H_2O content of the original rock. For a geologically reasonable H_2O content of 1,0 wt.% within the original rock, the amount of melt produced typically ranges from 10 to 25% (Burnham and Ohmoto, op. cit.).

The influence of the total H_2O content of a given source rock on the amount of melt produced is important as it provides a mechanism for greatly enriching early-formed partial melts with certain elements, compared to the concentration of these elements in the original source rocks. The enrichment factors of elements that are contained in minor mineral phases of the source rocks, and which dissolve completely in early formed melts, are inversely proportional to the H_2O content of the source rock. On the other hand, the enrichment factors of elements contained within major mineral solid solutions which coexist with early-formed melts, are dependent upon the partition coefficients amongst the coexisting phases (Burnham and Ohmoto, op. cit.). For example, copper is highly concentrated in the minor iron-rich sulphides of mafic amphibolites and may undergo a five-fold or greater enrichment in early formed melts. However, an element such as lead can easily substitute for potassium in alkali feldspars, and therefore undergoes little, if any enrichment in melts formed from metasedimentary rocks.

In areas of great crustal pressure (depth), such as deep continental crust - and even greater pressures within subduction zones, the parental rocks have essentially zero porosity, and the water probably occurs as the $(OH)^-$ ion (Burnham and Ohmoto, op. cit.). In mafic rocks, the predominant hydrous mineral is amphibole, whilst in felsic metasedimentary rocks, the hydrous minerals are mostly represented by micas. Mafic source rocks tend to have higher average contents of base- and precious-metals compared to felsic metasedimentary rocks; hence their partial melts (magmas) are enriched in these elements. Felsic source rocks, on the other hand, tend to yield partial melts that are enriched in tin, the alkali metals, beryllium etc.,

(Burnham and Ohmoto op. cit.). Therefore, magmas derived from mafic source rocks are favoured for gold mineralization, and should be preferably meta-aluminous in composition (Whitney, 1988).

At depths shallower than about 70 km, a non-porous mafic amphibolitic rock begins to melt at temperatures between 940°C and 1040°C, and the H_2O content of the melt must exceed 2,7 wt.%. At greater depths (75 - 80 km) as in subduction zones, amphibole is not stable at any temperature, and the amphibolitic rock can begin melting at about 660°C. However, for melting to occur at such low temperatures, the melt must contain approximately 27 wt.% H_2O (Burnham and Ohmoto; 1980). This is illustrated in figure 7.

The minimum of 2,7 wt.% H_2O in the initial melt is important because: (1) it ensures that the magma will evolve a separate magmatic aqueous phase upon cooling and crystallization when emplaced in shallow crustal environments necessary for hydrothermal ore processes to operate; (2) it greatly enhances the solubilities of metal sulphides in initial melts compared to solubilities in anhydrous melts of the same silicate composition through equilibrium reactions such as 2FeS (solid) + $2H_2O$ (melt) + SiO_2 (melt) ---> Fe_2SiO_4 (melt) + $2H_2S$ (melt); thereby providing the hydrous magmas with high sulphur carrying capacity; and (3) hornblende and/ or biotite generally crystallizes from these magmas upon cooling at depths greater than about 2 km; thus providing a possible exploration guide for intrusive igneous bodies that might have been associated with hydrothermal ore forming processes. The dioritic to granodioritic compositions of the hydrous magmas formed is important, because most magmatic-hydrothermal ore deposits are associated with intrusive igneous bodies of these compositions (Burnham and Ohmoto, op. cit.).

The intrusive igneous bodies associated with magmatic-hydrothermal ore mineralization are usually emplaced at depths of less than 10 km. Many of these intrusions reach depths as shallow as 1 or 2 km, and some appear to have vented at the surface (Burnham and Ohmoto, op. cit.). It should be noted that granitic magmas with water contents greatly in excess of 4 wt.% are unsuitable for magmatic-hydrothermal deposits as they would become vapour saturated at high pressures, and would tend to crystallize during ascent to a fine-grained granite before reaching shallow depths (Whitney, 1988).

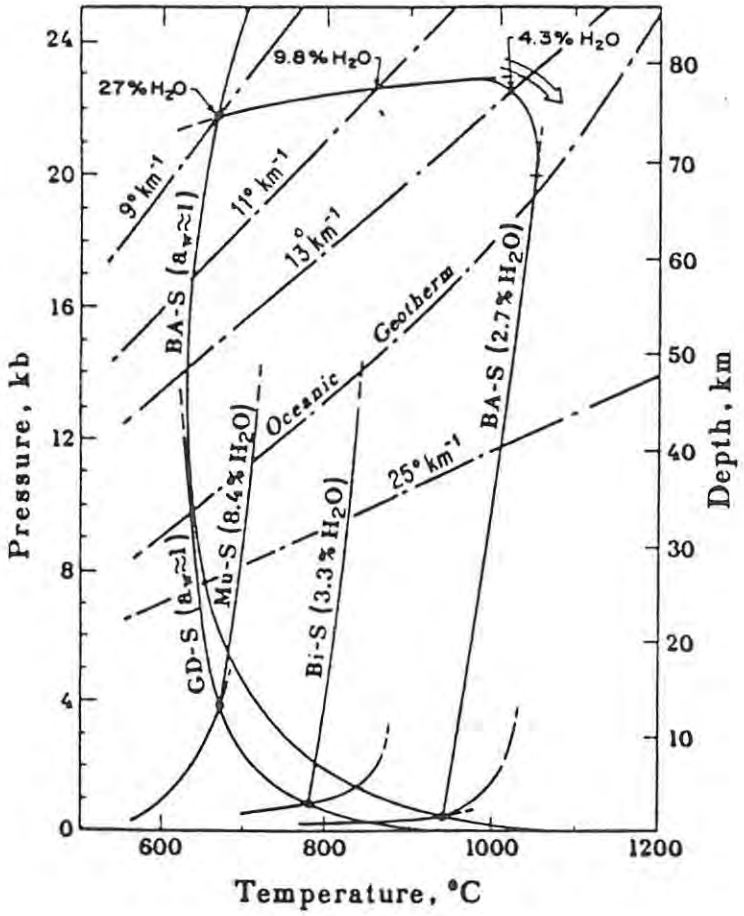

Figure 7. Pressure-temperature projections of melting relations for muscovite- and biotite-bearing schists and gneisses, and hornblende-bearing basaltic amphibolites. The curves labelled GD-S and BA-S($a_w \approx 1$) are the H_2O-saturated solidus for average granodiorites and basaltic amphibolites, respectively; the curves labelled Mu-S (8,4% H_2O), Bi-S (3,3% H_2O), and BA-S (2,7% H_2O) represent the divariant, fluid-absent, beginning of melting of non-porous gneisses and amphibolites. The percentage H_2O figures are the H_2O contents, in weight percent, of the first-formed melts produced by incongruent solutions of muscovite, biotite and hornblende, respectively (after Burnham and Ohmoto, 1980).

During the cooling of granitic melts, fractional crystallization occurs, and results in the concentration of ore metals, sulphur and chlorine in the more hydrous residual melt. Further cooling and resultant fractional crystallization beyond these points of H_2O-saturation (Fig. 7), results in the H_2O separating from the residual melt by retrograde boiling, thus becoming a separate fluid phase. Eventually, all the H_2O content of the

original magma, except the structurally bound fluid within hydrous minerals, evolves as a separate fluid phase (Burnham and Ohmoto, op. cit.).

The evolution of this separate, H_2O-rich (aqueous) volatile phase, is controlled principally by the solubility of H_2O in the melt. This H_2O solubility is strongly pressure dependant, but weakly temperature dependant. For example, at a pressure of 500 bars, which is approximately the lithostatic pressure at a depth of 2 km, the maximum solubility of H_2O in melts of granitic compositions is only 2,7 to 3,0 wt.%, whereas at a pressure of 2000 bars (8 km depth), it is 6,1 to 6,4 wt.%. At 5000 bars (18 km depth), it is 9 to 10%. According to Burnham and Ohmoto (op. cit.), melts initially containing 2,0 wt.% H_2O, would become H_2O-saturated after about 33% crystallization at 2 km, 73% crystallization at 8 km and 83% crystallization at 18 km.

4.1.2. Transitional Processes

In terms of this discussion, transitional processes begin with the formation of a separate magmatic volatile (aqueous) phase by retrograde boiling. Physically, transitional processes are characterized by volume changes that accompany the second boiling reaction: H_2O-saturated melt ---> crystals + volatile phase. Chemically, transition processes are dominated by melt-volatile (aqueous fluid) equilibrium. These processes are now discussed.

Physical Processes

A hydrous magmatic body that is emplaced within colder wallrocks, must lose heat to its surroundings; hence crystallization generally proceeds inwards from the walls of the magma chamber. As there is a very low diffussivity of dissolved H_2O in silicate melts; the magma first becomes H_2O saturated at the margins. The resultant H_2O saturated rind effectively isolates the interior from the transfer of matter (except hydrogen), either in or out (Burnham and Ohmoto, op. cit.).

As second boiling proceeds within the H_2O-saturated carapace, the magma body must either expand or the internal pressure must increase because the

reaction, H_2O-saturated melt ---> crystals + volatile phase, results in an increase in volume at all crustal pressures. This increase in volume is more or less directly proportional to the H_2O content at saturation, and inversely proportional to pressure. An example is a granodioritic melt containing 2,7 wt.% H_2O. As illustrated in figure 8, the rock will expand nearly 50% upon complete crystallization at a depth of 2 km (550 bars). At a depth of 4 km, the same body will expand approximately 15% after complete crystallization. At the shallow depths described above, most wall rocks have high rigidity and cannot accommodate such large increases in volume.

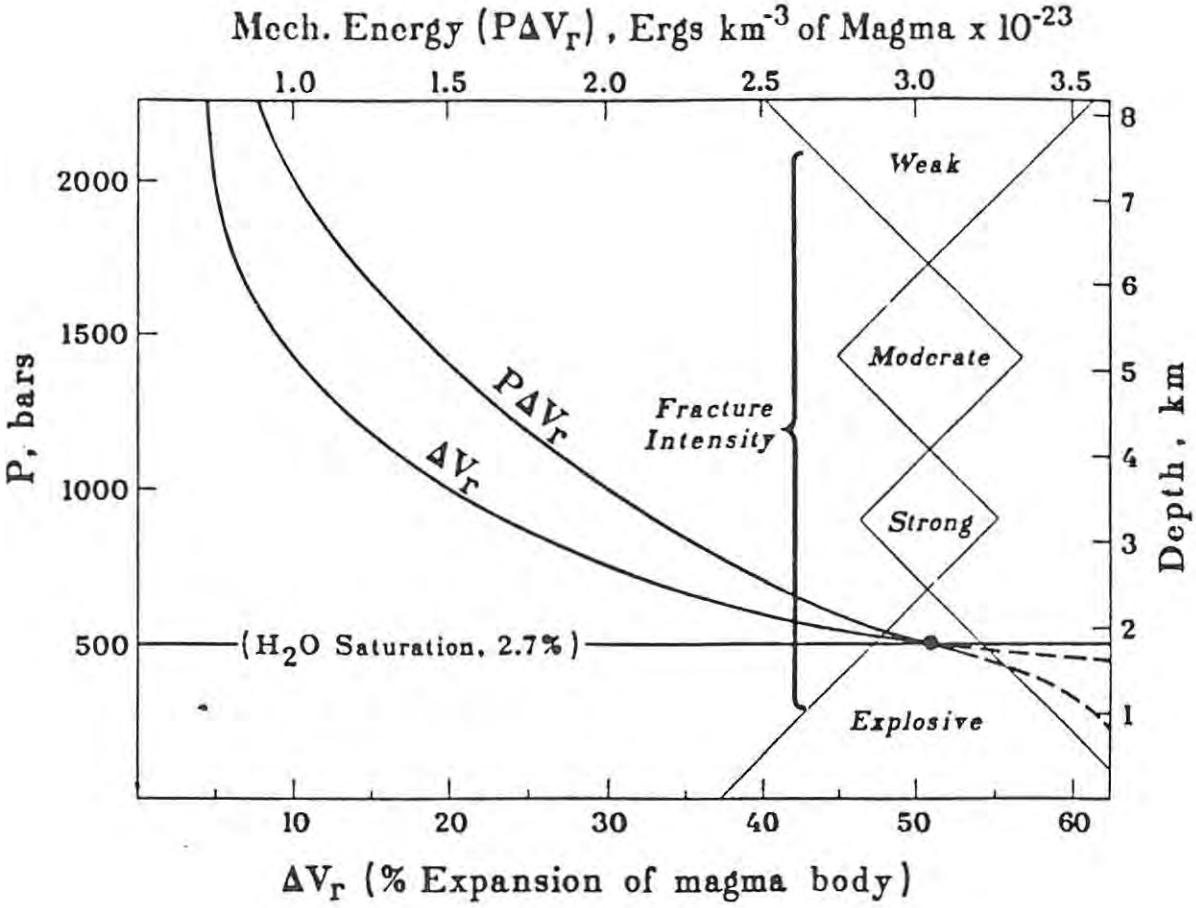

Figure 8. The change in volume (lower abscissa) in the second-boiling reaction: H_2O-saturated melt ---> crystals + vapour. Values of δV_r and $P\delta V_r$ are for complete crystallization of a granodioritic magma with an initial H_2O content of 2,7 wt.%. The depth of transition between 'explosive' (volcanic eruption) and 'strong' fracture regimes is approximate, as it depends upon the size and shape of the magma body (after Burnham and Ohmoto, 1980).

Therefore, as cooling and crystallization proceeds, the internal pressure within the H_2O-saturated carapace must increase and could reach several thousand bars. As the tensile stress of the wall rocks are at most a few hundred bars, brittle failure occurs. Expansion generally occurs within a horizontal plane as this is the plane of least principal stress. The resultant fracturing tends to be subvertical. The expansion of the magma also causes stress within the surrounding host rocks, and results in small, upward propagating fractures. Quartz veins and quartz stockworks are mostly associated with these fractures (Burnham and Ohmoto, op. cit.).

Thus the major cause of fracturing appears to be the mechanical energy released by second boiling during the cooling of a shallow seated hydrous magma. The fracturing is essential in the localizing of the ores in most magmatic-hydrothermal ore deposits, as they represent permeable channelways for the migration of hydrothermal ore forming fluids, irrespective of their origin (Burnham and Ohmoto, op. cit.).

Chemical Processes

The generation of the magmatic aqueous phase by second boiling is accompanied by partitioning of all elements in the system, such that the chemical potential or fugacity of each chemical species is the same in all phases at equilibrium (Burnham and Ohmoto, op. cit.). Chlorine occurs within the silicate melts as the chloride ion (Cl^-) and during second boiling, it is partitioned strongly towards the magmatic aqueous phase as (1); chloride minerals are not stable in magmas of intermediate to felsic compositions and (2); it forms highly stable neutral chloride complexes with hydrogen, alkali metals, alkaline earths, and heavy metals in aqueous solutions at magmatic temperatures and low to moderate pressures. A chemical reaction to account for the transportation of gold as chloride complexes in magmatic fluids is:

$$Au + aHCl + bO_2 \text{ ---> } [Au \text{ complex}] + cH_2O$$

(after Henley, 1973).

Sulphur occurs within hydrous melts principally as thiosulphide complexes, and is also partitioned strongly in favour of the magmatic aqueous phase. Low concentrations of CO_2 occur within felsic melts and also partition into

the volatile phase, but do not greatly affect transitional processes (Burnham and Ohmoto, op. cit.).

Partition coefficients of the above-mentioned volatiles between the aqueous fluid and the melt appear to be relatively insensitive to temperature, and except for sulphur, pressure. The partition coefficient of sulphur is sensitive to both H_2O pressure and to oxygen fugacity (f_{O2}) because sulphur exists within the aqueous phase as H_2S and SO_2, whereas within the hydrous melts, it occurs as thiosulphide complexes (HS^-). At a given phase assemblage and constant fO_2, increasing pressure (fH_2, hence fH_2O) increases the proportion of H_2S to H_2O in the aqueous phase; hence the partition coefficient for sulphur ($\Sigma S^v/\Sigma S^m$) is decreased. If the pressure is kept constant and the fO_2 is increased, the concentration of hydrogen is decreased within the system, and the proportion of SO_2 is increased; hence the partition coefficient for sulphur is increased. The above-mentioned behaviour of S occurs because SO_2 is much less soluble than H_2S in hydrous magmas. Therefore the partition coefficient of sulphur between the aqueous phase and the melt is much higher in magmas with high oxygen fugacity compared to those with low oxygen fugacity. These high fO_2 magmas may therefore contain potentially high concentrations of sulphur and heavy metals (almost entirely as chlorides; Burnham and Ohmoto, op. cit.).

The fO_2 of a magma, prior to the onset of second boiling, is largely controlled by the Fe^{3+}/Fe^{2+} ratio in the magma, and this in turn is controlled by the type of source rock from which the magma is generated. As illustrated in figure 9, the fO_2 in felsic magmas that were generated by partial melting of metamorphic, volcanic and igneous rocks, is generally higher than that of the QFM buffer (Carmichael et al., 1974). The SO_2/H_2S fugacity ratio ranges from 0,1 to 10. The fO_2 of felsic magmas that were generated by partial melting of carbonaceous metasediments, on the other hand, are generally lower than the QFM buffer and the SO_2/H_2S fugacity ratio is generally much smaller than 0,01.

Silica, together with KCl, NaCl, HCl, $CaCl_2$, $FeCl_2$, and $FeCl_3$, form the major portion of the total dissolved solutes in the magmatic aqueous phase of granodioritic magmas. Their relative proportions (e.g. NaCl/KCl ratio) are strongly dependant upon melt composition, pressure and the nature of the coexisting mineral assemblage (Burnham and Ohmoto, op. cit.).

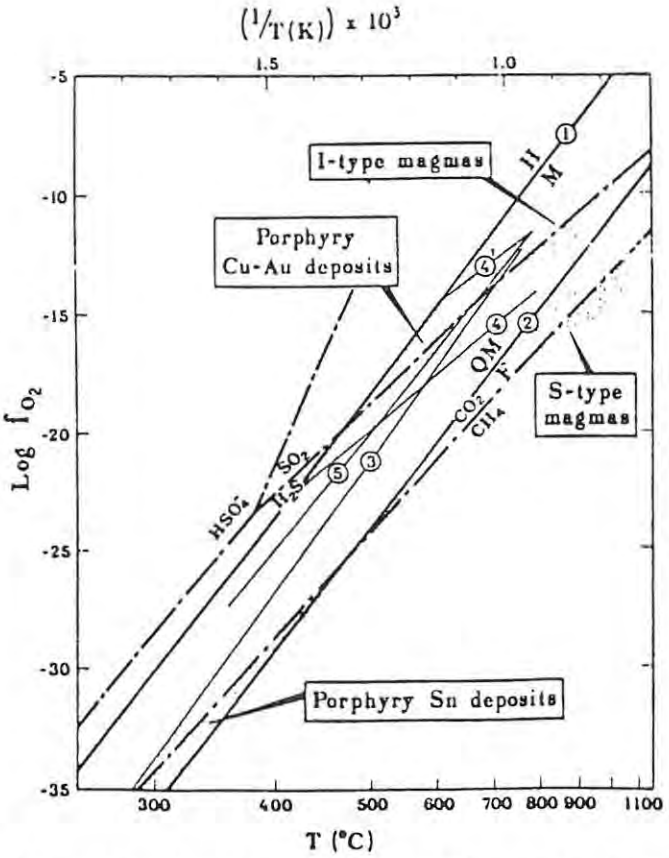

Figure 9. Oxygen fugacity vs. temperature relations for the predominant sulphur species and carbon species (broken lines) in aqueous fluids, and the stability fields of pertinent iron-bearing mineral assemblages (solid lines), all at approximately 1kb. The SO_2/HSO_4^- and HSO_4^-/H_2S boundaries are for unit activity ratios at pH = 4. Mineral equilibria represented are: (1) magnetite + hematite, (2) fayalite + magnetite + quartz, (3) pyrrhotite + pyrite + magnetite, (4) biotite (38% annite) + K-feldspar + magnetite, and (5) anorthite + K-feldspar + pyrite + muscovite + quartz + anhydrite. Also shown (stippled) are approximate fO_2 - T fields for typical magnetite-bearing 'I-type' and 'S-type' felsic magmas, as well as for porphyry copper-gold and porphyry tin types of mineralization (after Burnham and Ohmoto, 1980).

Little is known about the partitioning of most ore metals and aqueous chloride solutions, however as gold is preferentially associated with sulphide metals, it is expected that aqueous chloride solutions in which the fugacity of SO_2 is approximately equal to, or greater than H_2S, should be effective in scavenging a magma and adjacent wallrocks of their metal content. Consequently, aqueous fluids that separate from so-called I-type magmas tend to produce sulphide-rich mineralization, whilst fluids derived

from so-called S-type magmas produce sulphide-poor type mineralization. As gold is prefentially associated with sulphide-related minerals, high fO_2, I-type magmas are preferable for potential gold mineralization.

Finally, it should be noted that fluids originating from chloride-poor magmatic sources are generally poor in HCl, sulphur, iron and other metals; but richer in silica and alumina (Burnham and Ohmoto, op. cit.).

4.1.3. Hydrothermal Processes

The boundary between transitional processes and hydrothermal processes is the temperature, for a given total pressure, below which the hydrous silicate melt is not thermodynamically stable. This boundary may be sharp in some systems and gradational in others. Burnham and Ohmoto (op. cit.) places the boundary at the H_2O-saturated solidus of the magma (Fig. 7). The transition occurs with falling temperature or a marked decrease in fluid pressures, and results in disequilibrium conditions between wallrocks and fluids. The degree of disequilibrium depends on the initial conditions of equilibrium within the magmatic system, and also the extent to which pressure and temperature decrease. It should be noted that transitional processes and hydrothermal processes may coexist in some instances.

Aqueous chloride solutions from high temperature magmatic sources tend to be HCl-rich. At high temperatures, these hydrothermal fluids will react with the wall rocks to produce aluminium-silicate alteration with or without biotite; and muscovite (sericitic, phyllic) alteration at lower temperatures (Fig. 10). Fluids that equilibrated with hornblende-bearing magmas are enriched in KCl relative to NaCl and HCl; hence potassic alteration occurs. This potassic alteration is indicated by the production of biotite and potassic feldspars, and is caused by the exchange of potassium with sodium and especially calcium. These exchange reactions lower the KCl/HCl ratio in the aqueous phase, which leads to entry into the muscovite stability field (H^+ metasomatism; sericitic or phyllic alteration) near its high temperature limit for the prevailing pressure. Therafter, further cooling of the fluids causes the KCl/HCl ratio to increase as K-rich feldspar is converted to muscovite and quartz.

The decrease in pressure and temperature associated with the escape of the magmatic aqueous phase into fractured wallrocks may result in condensation of a chloride-rich liquid consisting mainly of NaCl, KCl and iron-chlorides. Due to differences in density, the liquid may become separated from the gaseous volatile phase, which is enriched in HCl, CO_2, SO_2 and H_2S. It is this acid-enriched volatile phase that may be responsible for part of the sericitic and argillic alteration in the upper (outer), cooler parts of the fracture systems (Burnham and Ohmoto, op. cit.).

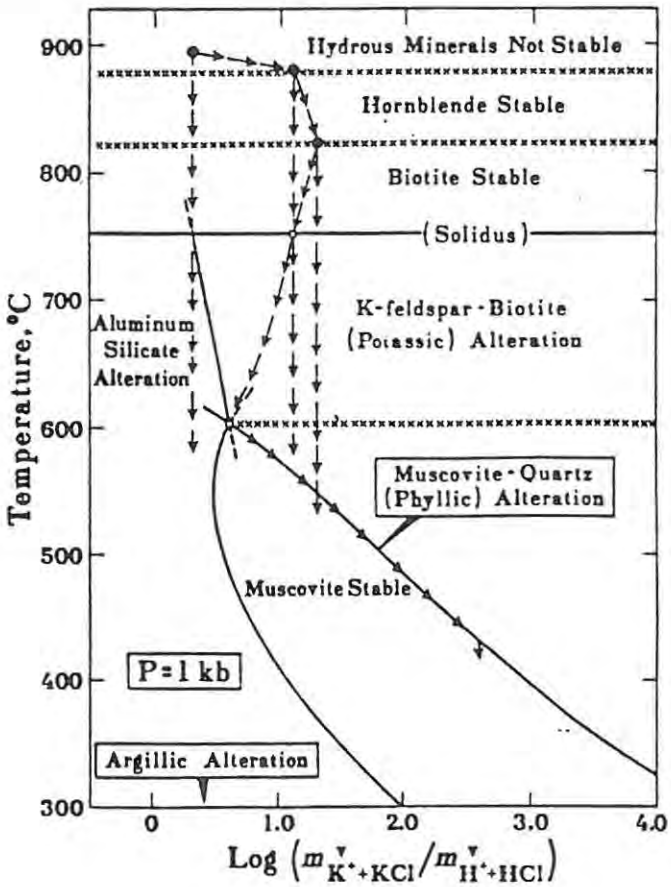

Figure 10. Log $(m^{v}_{K+KCl}/m^{v}_{H+HCl})$ vs. temperature at 1 kb showing variations in m^{v}_{KCl}/m^{v}_{HCl} of magmatic aqueous chloride solutions as a function of phase assemblage, and possible non-equilibrium cooling paths of these fluids in a porphyry fracture system. Solid circles represent compositions of aqueous chloride solutions in equilibrium with granodioritic magmas, and open circles represent fluid compositions at isobaric invariant points (H_2O-saturated solidus and the muscovite + quartz ---> K-feldspar + aluminium silicate + 'vapour' equilibrium), (after Burnham and Ohmoto, op. cit.).

Hydrolysis of SO_2-rich fluids belonging to I-type, high fO_2 magmas ($4SO_2 + 4H_2O$ ---> $H_2S + 3\ H_2SO_4$) results in a continuous increase in the activities and concentration of both H_2S and aqueous sulphates. The temperature at which this hydrolysis occurs depends on several factors, including pH, total fluid pressure, m_{NaCl}, m_{KCl} and m_{CaCl}, but mostly ranges from 500°C to 350°C. The presence of ferrous iron-bearing minerals in wallrocks may cause the activity of H_2S to be increased at the expense of SO_2 ($SO_2 + 6FeO + H_2O$ ---> $H_2S + 3Fe_2O_3$). In either case, the increased activity of H_2S causes precipitation of sulphide ore minerals from the metal chloride complexes (mainly of iron) in aqueous solution which, in turn, produces HCl ($4FeCl_2 + 7H_2S + H_2SO_4$ ---> $FeS_2 + 4H_2O + 8HCl$). Gold is generally associated with these sulphides (e.g., Saager and Meyer, 1984). The production of HCl also results from the precipitation of anhydrite ($CaCl_2 + H_2SO_4$ ---> $CaSO_4 + 2HCl$) from the aqueous $CaCl_2$ produced in K <---> Ca exchange reactions, and by direct reaction of H_2SO_4 with calcium-bearing minerals in the wallrocks.

4.1.4. Styles of gold mineralization

Magmatic-derived, Archaean granitic gold deposits are most likely to consist of quartz veins representative of brittle and brittle-ductile shears, and stockworks associated with small, late-Archaean, hydrothermally altered, preferably meta-aluminous granitic plutons.

Gold deposits in granitic rocks in Zimbabwe most commonly consist of quartz veins confined between well developed shears in the granite (e.g., Golden Oriole Mine in Esigodini; Mann, 1984). The gold occurs in the quartz veins and is generally associated with sulphide mineralization which is concentrated near one or other of the sidewalls. Wallrock alteration is usually confined to greisenization of the granite and the introduction of minor diffuse sulphides into the immediate walls of the vein. Where the veins are associated with megaxenoliths within the granites, sulphide mineralization tends to concentrate on the side closest to the xenolith. Disseminated sulphides; mostly pyrite, occur for distances up to 200cm into the xenoliths (Mann, op. cit.). Stockworks are less common than the vein deposits, and may be subdivided into two types. The one is a network of fine sulphide veinlets, with or without quartz in the granite (e.g.,

Grandeur Mine; Robertson, 1976). The other, typified by the Ayrshire orebody (Stagman, 1961), consists of a series of quartz veinlets in a mafic mega-xenolith in otherwise unmineralized granite (Mann, 1984). Minerals associated with gold deposits in granitic rocks in Zimbabwe are pyrite, arsenopyrite, scheelite, molybdenite, chalcopyrite, galena, sphalerite, stibnite and pyrrhotite (Mann, op. cit.).

4.2. Metamorphic Replacement Model

Groves and Phillips (1987) provide an extensive review of the metamorphic replacement model, which forms the basis of the following discussion. They propose that the hydrothermal ore fluids originated by the dehydration and decarbonation of volcanic rocks deep in the greenstone pile, above 450°C during upper greenschist and amphibolite facies metamorphic conditions, giving rise to low salinity H_2O-CO_2 fluids.

Komatiitic lavas are favoured to be the major source of the gold. According to Keays (1984), the komatiites should be enriched in gold relative to the more widespread tholeiitic basalts as the sulphur solubility is generally low at temperatures required to produce tholeiitic magmas (<0,1 wt.% S), and may be exceeded at or near the source. Therefore, precious metals that partition strongly into immiscible sulphide liquids, are lost from magmas at source, and the resultant basaltic rock has a low gold content. Komatiitic magmas, on the other hand, represent higher degrees of partial melting at higher temperatures where sulphur solubility is enhanced, and the possibility of earlier formation of immiscible sulphides is much lower. Hence, komatiitic magmas may be erupted below sulphur saturation, but exsolve immiscible sulphides, containing gold during crystallization, thereby providing a suitable source of gold and sulphur during later metamorphic leaching (Groves and Phillips, 1987).

4.2.1. The Genetic Model

A diagrammatic representation of the metamorphic replacement model, proposed by Groves and Phillips, (op. cit.) is illustrated in figure 11. The metamorphic fluids originated by devolatilization of volcanic rocks deep in the greenstone pile during prograde metamorphism at amphibolite

facies with high geothermal gradients and in the absence of significant melting. They evolved from grain reactions, and therefore had effective contact with the whole greenstone pile and the ability to extract Au and other ore components efficiently.

The syn-kinematic felsic intrusives and granitoids commonly associated with Archaean gold mineralization may represent emplacement of magmas formed by deep crustal melting during the same thermal event that induced metamorphism in the greenstone belts at higher crustal levels (Groves and Phillips, op. cit.). Both magmas (described above) and hydrothermal fluids used available structural channelways. Possibly, these intrusive rocks helped to redistribute heat and provide some hydrothermal fluids locally. Carbon isotope data suggest that mantle-derived carbonate was the source of CO_2, rather than sea-floor alteration (Groves and Phillips, op. cit.).

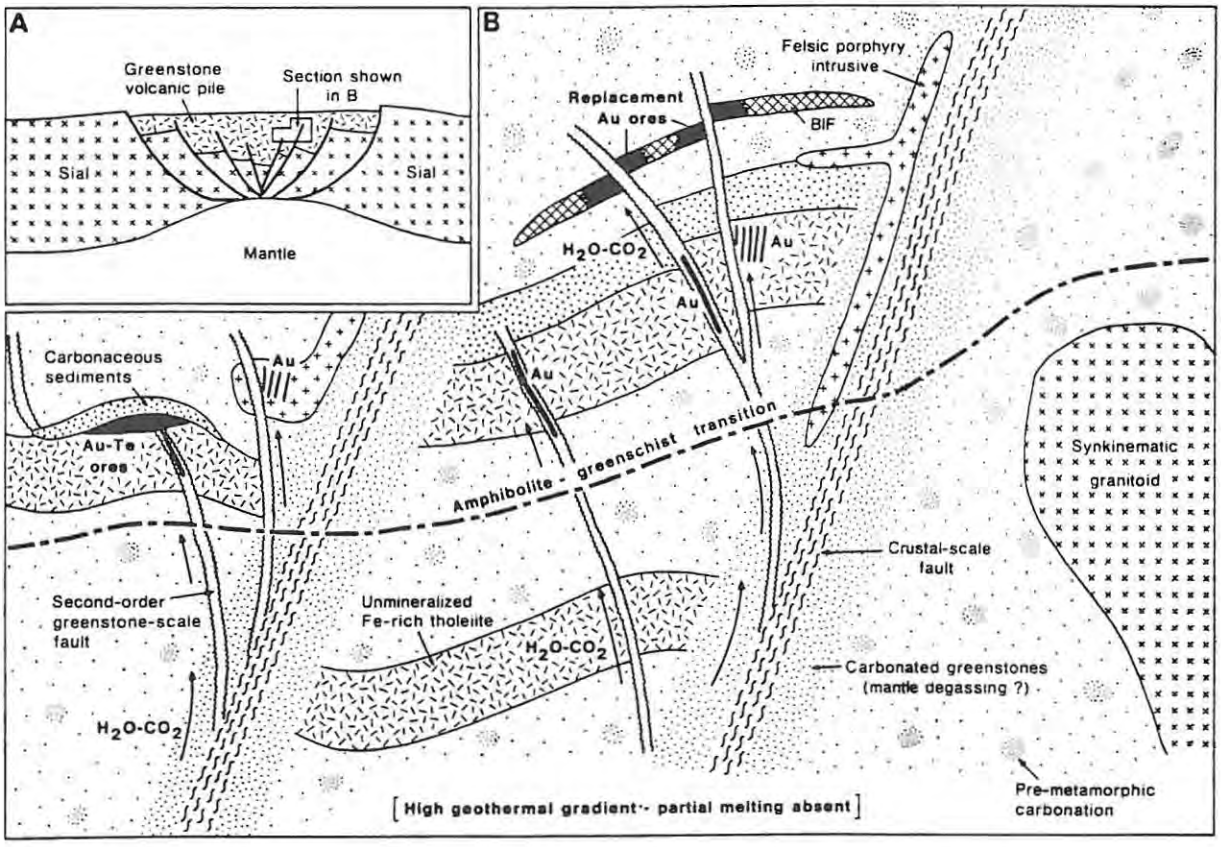

Figure 11. Schematic representation of the metamorphic replacement model for the generation of Archaean gold deposits showing fluid access and siting of gold deposition. Early carbonation is showed schematically (after Groves and Phillips, 1987).

In the source region, conditions of low fluid/rock ratios existed. The hot, CO_2-H_2O-rich, low-salinity and low-density fluids were focussed and channelled upwards by greenstone-scale faults and shear zones. Fluid channelization into fault zones probably took place via mass-transfer processes such as seismic pumping; resulting in high fluid/rock ratios along channelways.

The process of seismic pumping is caused by contrasting fluid-pressure and/or temperature regimes within the first- and second-order fault structures (Chapter 3). Prior to brittle failure, fluid pressures increase, then drop to a minimum after failure. This causes a pressure gradient between the first-order structures with relatively constant fluid pressure, and the second-order structures with periodically varying fluid pressure. The result is a net fluid flow into the latter with a high fluid/rock ratio (Kerrich, 1986; Neall, 1987). Note that this type of environment is more common within sub-amphibolite facies domains.

The derivation and/or interaction of fluids with mafic-ultramafic sequences accounts for their near-neutral to slightly alkaline character, with gold and associated elements being transported as reduced sulphur complexes [e.g., $HAu(HS)_2$; Groves and Phillips, 1987]. The common association of gold with arsenic and antimony suggest that arsenothio- and antimonothio-complexes [e.g., $Au(AsS_2)^0$, Au $(As_3)^{2-}$ and $Au(Sb_2S_4)$-] may also be significant in the transport of gold in hydrothermal solutions (Seward, 1984).

Gold deposition took place mostly within sub-amphibolite facies conditions, in the P-T range 300-450°C at 1-2 Kb, owing to the solubility decrease of reduced sulphur complexes below 500°C (Seward; 1979, 1984). Many large gold deposits formed due to sulphidation of the wallrocks where structural channelways such as faults or shear zones intersected Fe-rich tholeiitic basalts or dolerites within greenschist facies domains. Stratabound, or locally stratiform ores also formed, due to sulphidation of fracture zones within oxide-rich BIF-units (fig 11). Other deposits formed when fluid - wall rock interactions with less Fe-rich rocks caused fluid oxidation or reduction and/or lowering of pH, resulting in significant gold deposition where very large and efficient channelways were present. Felsic intrusions

and granitoids also host gold deposits, but are in the minority, possibly due to their low Fe-content.

The metamorphic replacement model allows some gold deposits that were formed initially at greenschist facies conditions to be overprinted by amphibolite facies metamorphism (e.g. Big Bell in Western Australia). Phillips (1985) states that although the metal associations at Big Bell are similar to greenschist facies Archaean gold deposits, there is a lack of CO_2 and depletion of Na; which may be expected at the prevailing amphibolite facies conditions. He envisages the introduction of gold-rich hydrothermal fluids prior to the peak of metamorphism, probably under greenschist facies conditions as per the metamorphic replacement model. However, the mineralization was overprinted at a later stage due to continuing prograde amphibolite facies metamorphism. Small-scale remobilisation and concentration of gold occurred in response to the introduction of retrogressing fluids after the peak of metamorphism.

4.2.2. Styles of Gold Mineralization

Figure 12 briefly summarises the styles of gold mineralization associated with Archaean epigenetic gold deposits in Western Australia.

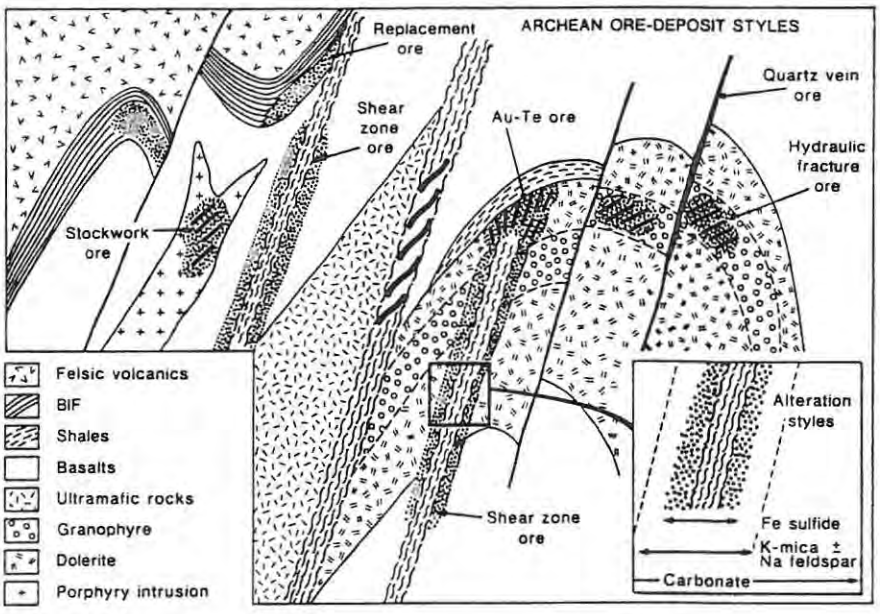

Figure 12. Schematic representation of the nature of Archaean gold mineralization showing various structural styles and host rocks (after Groves and Phillips, 1987).

As illustrated, the gold mineralization appears to be structurally controlled, and varies from alteration haloes (+/- quartz veins) in shear zones, through laminated quartz veins in shear or fault zones, to quartz vein stockwork deposits in volcanic/intrusive hosts, as well as stratabound and locally stratiform deposits in BIF and Fe-rich sediments.

Gold deposits in sub-amphibolite facies domains have distinctive alteration haloes, with zones of intense K-mica (+/- albite), ankerite-dolomite and Fe-sulphide alteration surrounded by broader zones of carbonation. The gold commonly occurs as submicroscopic grains within Fe-sulphides (+/- arsenopyrite) in the alteration assemblage rather than within syn- to post-tectonic quartz veins. This association of gold with sulphides, together with the iron-rich nature of the mafic host-rocks and lack of mobility of Fe, suggests that gold deposition was related to sulphidation of Fe-rich wall rocks (Phillips and Groves, 1983; Neall, 1985) for most large deposits. Ag, As, B, Sb and W are generally associated with the gold mineralization. Base-metals are in the minority (Groves and Phillips, 1987), although exceptions do occur.

4.3. Magmatic or Metamorphic Fluids ?

The close spatial, structural and time relationships between Au-quartz vein mineralization and granite intrusions (Chapter 3) are the major factors supporting a magmatic origin for the gold-bearing fluids. However, Fyfe and Kerrich (1984) maintain that the granite intrusions commonly associated with gold mineralization are volumetrically insignificant and could not have produced the volume of ore fluid necessary to produce a reasonable gold deposit. As previously discussed, granitic melts containing greater than 4 wt.% water are unsuitable for magmatic-hydrothermal deposits as they would become vapour saturated at high pressures, and would tend to crystallize before reaching shallow depths (e.g., Whitney, 1988).

Instead, Groves and Phillips (1987) propose that the magmas and mineralization are a product of the same thermal event, with magmas representing melting at deeper crustal levels. According to the metamorphic replacement model, these magmas may be selectively emplaced along crustal fractures that also localised earlier mantle degassing and controlled the

location of later greenstone scale faults, and hence the siting of gold mineralization.

Metamorphic fluids on the other hand, are an integral part of greenstone belt development and represent a potentially huge reservoir of gold-bearing fluids. Assuming this to be correct, an important question arises - if the fluids are of metamorphic origin, why do all metamorphic terranes not contain gold deposits?

An answer to this question probably lies in the presence of gold in an available form for metamorphic leaching in Archaean mafic-ultramafic sequences, but the P-T conditions of metamorphism are potentially a more critical factor (Groves and Phillips, 1987). An important characteristic of greenstone belt evolution is the typical low pressure metamorphism (e.g. Binns et al., 1976), implying high geothermal gradients. This means that the isotherms may have been closely spaced in the greenstone pile, causing devolatilization to occur over a small interval; thus providing ideal conditions for intense focussing of large volumes of ore fluid (Groves and Phillips, 1987). Furthermore, an important consequence of a high geothermal gradient and low pressures is the increased importance of devolatilization reactions compared to melting reactions. Crustal melting will produce melts with significant amounts of dissolved H_2O, thereby reducing the amount of fluid available for gold transport. Figure 13 illustrates how low pressures and high geothermal gradients are vital for the production of large volumes of metamorphic fluid.

Groves and Phillips, (1987) state that although it is difficult to prove conclusively that the hydrothermal systems responsible for the formation of Archaean epigenetic gold deposits were dominated by metamorphic fluids, such a model is favoured for the following reasons:-

1) It explains the universal occurrence of gold deposits in Archaean greenstone belts.

2) It is consistent with deposit location, primarily in greenschist facies domains in low-pressure metamorphic terranes.

3) It is consistent with broad timing constraints, and with heated wall rocks implied by the lack of vertical zonation.

4) It explains the association of mineralization with faults and shear zones in greenschist terranes.

5) It could potentially explain the limited range of ore fluid compositions if they are buffered by assemblages in largely mafic-ultramafic lithologies during prograde metamorphism.

6) It explains the apparent lack of a consistent association between gold deposits and specific igneous rock types on a world wide scale.

Finally, it is probably correct to say that magmatic and metamorphic-replacement models for Archaean granite/gneiss-hosted gold mineralization form end members of a vast array of types of gold deposits.

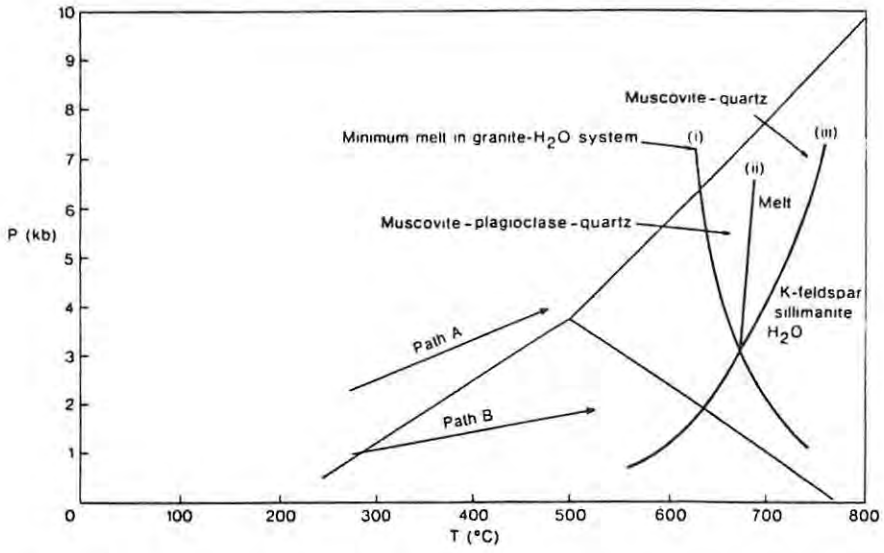

Figure 13. P-T paths illustrating the importance of a high geothermal gradient in the generation of auriferous metamorphic fluids. **Path A** at pressures above the Al_2SiO_5 triple point leads to vapour-absent melting (curve ii), effectively eliminating the potential for substantial fluid generation from dehydration reactions. **Path B**, at lower pressures, leads to dehydration at lower temperatures than melting, with the potential for large volumes of metamorphic fluid with gold leaching and transporting capabilities (after Groves and Phillips, 1987).

4.4. Exploration targets for Archaean granite-/gneiss-hosted gold deposits.

For a gold deposit in the Abitibi greenstone belt, Hodgson and Troop (1988) used a gold-assay cutoff value of 1g/metric ton over widths of at least several metres, or higher grades over narrower widths and/or verbal descriptions that indicate such values (e.g., visible gold, significant values, etc.). It should be emphasized that according to this definition, a deposit is not necessarily an economically exploitable concentration of minerals under present, or any forseeable future economic conditions, although further exploration might lead to the discovery of an economic deposit on the site of a known deposit. These criteria, used by Hodgson and Troop (op. cit.) for a gold deposit within the Abitibi greenstone belt, are also applicable to this project.

The 'magmatic' and 'metamorphic' exploration targets for Archaean granite-/gneiss-hosted gold deposits are similar despite the different processes involved in the formation of the gold deposits.

The exploration target according to the 'magmatic' model is a late Archaean, meta-aluminous, hydrothermally altered granitic intrusion associated with the third magmatic cycle (Chapter 2); preferably (but not necessarily) with a granodioritic/quartz-dioritic composition. The granite should contain extensive shearing in the form of brittle and brittle-ductile quartz veins, and be hydrothermally altered. The hydrothermal alteration should be represented by a potassic alteration zone surrounded by a propylitic alteration zone. These alteration zones may be overprinted by phyllic alteration, consisting of quartz-sericite-pyrite mineralization within stockworks or shears within the intrusion. Carbonate alteration may also be present. Albitization is a common alteration feature of Archaean granite-hosted gold deposits, and is possibly controlled by the hydrolytic breakdown of alkali feldspar to albite plus sericite (Colvine et al., 1988). The gold mineralization should occur within the potassic- and phyllic-alteration zones, quartz veins and quartz stockworks. Gold may be present in its native state, or be associated with sulphide minerals such as pyrite, arsenopyrite, scheelite, molybdenite, chalcopyrite, galena, sphalerite, stibnite and pyrrhotite (Mann, 1984).

Large scale area selection criteria (Fig. 2 and Appendix 1) for magmatic-related gold deposits within granites are: (1) the intrusion should be of late-Archaean age, (2) it should be hydrothermally altered, and (3) possibly be located within a shear zone. Smaller scale area selection criteria are: (1) the intrusion should be extensively sheared with an abundance of quartz veins in brittle and brittle-ductile fractures, and (2) sulphide mineralization should be associated with these quartz veins, and also quartz stockworks. The level of erosion should always be considered as the patterns of hydrothermal alteration and geochemical anomalies can vary. Enrichments of Ba, Sb and As within the primary dispersion environment are considered to be indicators of a supra-ore halo, whilst Mo and W enrichments suggest a sub-ore halo (Levinson, 1980).

The major exploration target for the 'metamorphic replacement model' is a granitic stock that has intruded a zone of crustal weakness such as a shear zone, active during the late Archaean. Alternatively, the granitic intrusion should be affected by late-Archaean shearing. Styles of deformation within the intrusion will change according to P-T variations, and vary from brittle and brittle-ductile structures such as tension- and shear-veins to ductile structures such as replacement-veins. Brittle and brittle-ductile deformation structures predominate in greenschist metamorphic conditions, whilst ductile deformation structures are generally associated with amphibolitic metamorphic conditions (Colvine et al., op. cit.). Hydrothermal- and carbonate-alteration, and possible sulphide mineralization should be present in haloes surrounding the quartz veins within the adjacent wallrocks.

Large scale area selection criteria for metamorphic-related gold deposits in granites are: (1) the granite intrusion should be located within a shear zone, or alternatively the granite intrusion should be affected by regionally extensive, late-Archaean shearing/deformation, and (2) the granite intrusion should display hydrothermal alteration. Smaller scale area selection criteria are: (1) shearing within the granite. The style of shearing could vary from brittle to brittle-ductile to ductile, depending on the grade of local metamorphism, and (2) sulphide mineralization together-with associated hydrothermal and possible carbonate alteration should be present within adjacent wallrocks of the quartz veining, and in

quartz stockworks. Elements commonly associated with the gold mineralization are K, S, As, Sb, W, B and Ag. Base metals such as Cu, Pb and Zn also occur, but are in the minority (Groves and Phillips, 1987). Colvine et al., (1988) add B, Li, Ba, Cr and Rb to the list, but stresses these enrichments are not consistent for all deposits.

Pathfinder elements/ratios applicable to the primary dispersion environment in both the magmatic- and metamorphic-related gold deposits are K/Na, Cu, Ba, Mo, As and Sb. The K/Na ratio should increase as the ore zone is approached (Levinson, 1980). Suitable pathfinder elements for the secondary dispersion environment depend on the sampling medium being used. As and Mo are suggested for stream sediment sampling; as neutral to alkaline conditions generally prevail within the streams (Levinson, op. cit.). Oxidizing conditions generally occurs within residual soil, however the weathering of sulphides associated with gold deposits can cause acidic conditions. Therefore, Cu, As and Mo are suggested pathfinder elements for soil sampling as their relative mobilities are similar. Ba and Sb are suitable for more detailed follow-up surveys (Levinson, op. cit.).

The use of LANDSAT images forms an integral part of the 'Regional Area Selection' phase of exploration in this project. Features that can be located on LANDSAT images used in this project, that may be an indication of area selection criteria for granite/gneiss-hosted gold mineralization are clay-mineralization (an indication of possible hydrothermal alteration), outcrops with an indication of their composition, lineaments and major fault zones. Further details are given in Chapter 6.

5. The Pietersburg granite-greenstone terrane

The Pietersburg granite-greenstone terrane (Fig. 14) is located in the northern portion of the Kaapvaal Craton, adjacent to the southern marginal zone of the Limpopo Belt (e.g. Brandl, 1986; Van Reenen et. al., 1987; 1988; Smit et. al., 1988 and Roering et. al., 1990a). The first gold deposit in South Africa was discovered in the Pietersburg granite-greenstone terrane on the farm Eersteling 17KS during 1871; and is a shear-zone hosted gold deposit within the greenstones. Table 1 gives the approximate gold production figures of various gold deposits within the Pietersburg granite-greenstone terrane between 1906 and 1937.

Table 1: Approximate production figures of gold from the Pietersburg granite-greenstone terrane.

Goldfield	Farm	Period	Crushed ore (tonnes)	Recovered Au (kg)	Alluvial Au (kg)	Total Production of goldfield (kg Au)
Eerstelling	Eerstelling 17KS	1906-1937	49010	320,43 (1)	97,14	438,94
	Waterval 18KS	1913-1935	1712	4,36		
	Vrischgewaagd 33KS	1906-1937	4275	17,01 (2)		
Roodepoort	Roodepoort 744LS	1905-1937	25778	159,86 (3)	0,42	245,08
	Palmietfontein 24KS	1907-1936	10067	72,44 (4)		
	Wildebeesfontein	1907-1937	2021	12,36 (5)		
Marabastad	Snymansdrift 738LS	1907-1910	21837		-	334,55
	Zandrivier 742LS		5	56,25 (6)		
Mount Robert Occurrence	Potberg Mine	?				Undisclosed

Grand Total recorded = 1018,57 kg.

(1) Includes some from Vrischgewaagd 33KS.
(2) Includes 0,09 kg from an unknown source.
(3) Includes 6,36 kg from an unknown quantity of ore.
(4) Includes 1,1 kg from by-products.
(5) Includes 0,04 kg from an unknown source.
(6) Includes some from Snymansdrif 738LS.

Source: Willemse (1938). (after Franey, 1987).

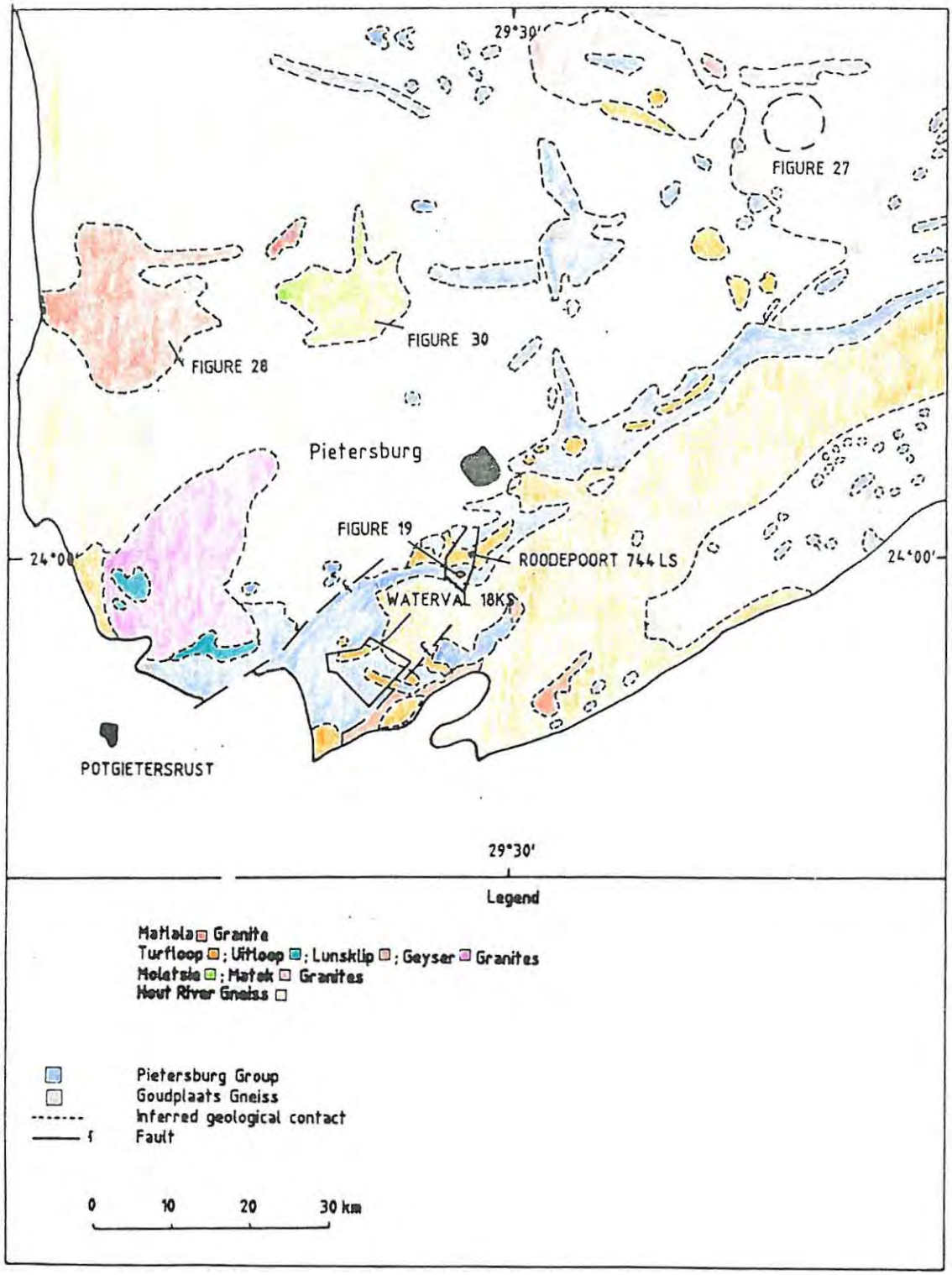

Figure 14. A geological map of part of the Pietersburg granite-greenstone terrane showing the localities of selected granites for this project. This map is compiled from the 1:250000 Geological Survey Maps 2328 and 2428, and from SACS (1980).

Granite-associated gold deposits within the Pietersburg granite-greenstone terrane include:

1) The Roodepoort 744LS deposit. Part of the total gold mineralization occurs within an altered granodiorite locally called the 'Knights or Roodepoort Pluton'.

2). The Palmietfontein 24KS and Wildebeesfontein 20KS deposits. These are shear-zone hosted within Turfloop Granite.

3). The Waterval 18KS deposit. This is also shear-zone hosted, but occurs along the contact of the Turfloop Granite and greenstones of the Pietersburg Group.

Approximately 24% of the gold production between 1906 and 1937 originated from these deposits.

5.1. The geology of the Pietersburg granite-greenstone terrane

The Pietersburg granite-greenstone terrane (Fig. 14) consists of a greenstone belt (the Pietersburg Group) bounded to the north and north-east by the Hout River Gneiss and Goudplaats Gneiss respectively (collectively known as the Baviaanskloof Gneiss; Barton et. al., 1990). Both the greenstone belt and the gneisses have been intruded by two generations of granitic to granodioritic plutons (Barton et. al., op. cit.). The lithostratigraphic subdivision of the Pietersburg greenstone belt is given in Table 2.

5.1.1. The greenstone belt

The Pietersburg greenstone belt comprises two major tectonostratigraphic rock sequences, separated by a well defined unconformity. The lower (older) sequence constitutes the greenstones of the belt, and consists of massive to pillowed and ocelli-bearing metabasalts, mafic metatuffs, metagabbros, and serpentinites (a variety of metaperidotite), interlayered with banded-iron formation (BIF), ferruginous shales, minor cherts, minor metacarbonates and quartz-mica schists (SACS., 1980; De Wit, 1991). These lithologies belong to the Eersteling, Mothiba, Ysterberg and Vrischgewaagd

Formations (Table 2), and have many lithologic, structural, petrologic and chemical similarities to the Onverwacht Group of the Barberton greenstone belt (Grobler, 1972; De Wit, 1990 and Jones, 1990). Whole rock Pb isotopic data from tholeiitic lavas of the Eersteling Formation yield a secondary Pb-Pb isochron age of 3455 +120/-128 Ma (95% confidence level), (Byron and Barton, 1990).

The upper sequence, often referred to as the cover sequence, is composed of a variety of sandstones, siltstones, grits, conglomerates, breccias and shales in varying states of deformation (De Wit, 1991). These rocks comprise the Uitkyk Formation (Table 2), and unconformably overlie the greenstone-BIF sequence.

Table 2: Lithostratigraphic subdivision of the Pietersburg granite-greenstone terrane.

Formation (SACS, 1980)	Lithology	Maximum Thickness (m)	Correlation (de Wit, 1984)
Uitkyk	Quartzites, conglomerates, shale, quartz-mica schists, B.I.F.s.	1500	Cover Sequence
Vrischgewaagd	Chlorite and quartz schists.	500-1000	
Zandrivierspoort *	Mafic meta-lavas with inter-layered magnetite-quartzite.	500	
Eersteling *	Mafic meta-lavas with subordinate ultramafics, quartz-feldspar porphyry and felsic lavas.	10000	Greenstone Sequence
Ysterberg	Felsic lavas and tuffs, shales, inter-bedded quartz schist, banded banded chert, B.I.F., quartzite.	1400	
Mothiba	Ultramafics with minor amphibolite, quartz-schist, quartz-feldspar porphyry, B.I.F.	7500	
Various types of granite and gneiss intrusive into all formations.			
* coeval			(after Franey, 1987).

5.1.2. The granitic rocks

The major granites/gneisses associated with the Pietersburg granite-greenstone terrane are the Goudplaats Gneiss and Hout River Gneiss, Geyser Granite, Matok Granite, Moletsie Granite, Turfloop Granite and Matlala Granite, Uitloop Granite and Lunsklip Granite (Fig. 14).

Goudplaats Gneiss

The Goudplaats Gneiss comprises gneiss, banded-gneiss and migmatite associated with leucocratic granites in varying proportions. The layering is defined by thin bands of alternating melanocratic and leucocratic material. The melanocratic bands generally consist of biotite, hornblende, oligoclase, quartz and hypersthene. The leucocratic material is composed of perthite, oligoclase and quartz; with biotite, garnet and sillimanite as accessories. Chemical analyses indicate that the grey migmatitic gneiss has a tonalitic, and in places, quartz-diorite composition. The leucocratic material ranges in composition from adamellite to tonalite (Brandl, 1986).

Radiometric ages for this rock vary between 2652 and 3054 Ma (Burger and Walraven, 1979b; Walraven et al., 1981), however they may reflect metamorphic overprints. Brandl (1986) suggested that the Goudplaats Gneiss forms the basement of the Pietersburg Group.

Hout River Gneiss

A number of different types of granitic rocks comprise the Hout River Gneiss. They vary from leucocratic migmatite and gneiss, grey and pink hornblende-biotite gneiss, grey biotite gneiss and pegmatitic rocks. These rocks are poorly exposed, hence the actual contact between the Hout River Gneiss and the Goudplaats Gneiss is uncertain (Brandl, 1986). Radiometric ages for this rock cluster around 2700 Ma (Walraven et al., 1981). Brandl (1986) suggests however, that these ages reflect the last metamorphic event.

Geyser Granite

The Geyser Granite is a biotite granite-gneiss (SACS., 1980), and was emplaced about 2900 Ma to 2800 Ma ago (Barton et al., 1990).

Matok Granite

This granite is characterised by the presence of a mafic phase and a younger granitic phase (Du Toit, 1979). The granitic phase consists of various rocks ranging in composition from adamellite to granodiorite. The main variety is a grey and pink, coarse-grained porphyritic granite composed of microcline phenocrysts, oligoclase, quartz and biotite. Minor varieties include a medium-grained hornblende granite and a pink medium-grained biotite-granite. Enclaves of Goudplaats Gneiss are commonly observed in the Matok Granite. The age of the granitic phase is about 2650 Ma (Barton and Ryan, 1977).

Moletsi Granite

This is a medium- to coarse-grained, pink to grey biotite granite. Locally, the granite which has a granodioritic composition contains biotite clusters, now largely altered to chlorite. Inclusions of banded gneiss and leucocratic granite are also present (Van Wyk, 1977). Rb - Sr isotopic ages of this granite ranges from 2546 Ma to 2640 Ma (Barton, 1990; pers. comm).

Turfloop Granite

This granite is a major batholithic intrusion, and flanks the southern edge of the Pietersburg Group. It forms numerous isolated hills, and is located near many Archaean gold deposits. It is a medium- to coarse-grained, grey to pink biotitic rock of adamellitic to granodioritic composition, and contains orthoclase, microcline, quartz, sodic plagioclase and biotite with apatite, alunite, sphene and zircon as accessories (Jantsky, 1978). Ages range between 2566 and 2660 Ma (Burger and Walraven 1977, 1979a).

Matlala Granite

The Matlala Granite is a roughly circular batholith northwest of Pietersburg. It is composed of eight varieties of granite ranging from fine- to coarse-grained, and in colour from light grey through pink to red. The most widespread type is a fine-grained pinkish-grey biotite rock of granodioritic composition. Assimilated inclusions of gneiss are often present near the contacts with country rock (Potgieter, 1976). Radiometric ages vary between 2236 and 2491Ma (Burger and Walraven 1979a,b).

Uitloop and Lunsklip Granites

These are homogenous, coarse-grained to porphyritic biotite-granites with minor hornblende (SACS, 1980). Their ages are as follows:

Uitloop Granite	2545 ± 55 Ma.
Lunsklip Granite	2610 ± 55 Ma.

(after Burger and Coertze, 1975-76).

5.1.3. Deformation

The Pietersburg granite-greenstone lithologies have been dismembered by movements along a series of approximately N-110° and N-70° trending shear zones. The N-110° shear zones dip steeply to the south and apparently predate the response phase of the ± 2700 Ma Limpopo Orogeny and the emplacement of the Turfloop batholith (Barton et al., 1990). However, minor movement on these shear zones also post-date the emplacement of the Turfloop batholith (Barton et al., op. cit.; Byron and Barton, 1990).

The N-70° shear zones dip steeply to the north and are believed to be associated with the Limpopo Orogeny (Van Reenen et al., 1987; Smit et al., 1988). Subsequent movement on the N-70° shear zones displaced rocks of the Transvaal Sequence (Willemse, 1938), implying that the shearing also occurred more recently than about 2430 Ma ago (e.g., Roering et al., 1990b; Barton et al., 1990 and Walraven et al., 1990).

A general map of the southwestern part of the Pietersburg granite-greenstone terrane is illustrated in figure 15. De Wit (1991) identified four deformation events in this area (D_1 to D_4). The greenstones have been affected by all these deformation events, whilst the cover rocks (Uitkyk Formation) have been affected by D_2 to D_4 only.

The D_1 event, consisting of lagging, is only recognised at isolated localities within the greenstones (De Wit et al., 1982).

The D_2 event pre-dates 2700 Ma (De Wit et al., 1991), and involved a period of progressive compressional deformation, affecting all rocks of the greenstone sequence. It is the most prominent deformation period characterized by a series of northward verging, south dipping, thrusts followed by continued compression (Fig. 16). An upright cleavage schistosity (S_2; De Wit, 1984) is representative of this deformation event. The displacement along the thrusts is not known, but must have been considerable in places (i.e. >5 km) where the greenstones have been displaced against the cover rocks (e.g., Mount Mare area; De Wit, 1991). At high levels in the crust, the deformation was accompanied by syntectonic sedimentation along active margins or within collisional zones. At the deeper levels, the shear zones were intruded by syntectonic granites (De Wit, op. cit.).

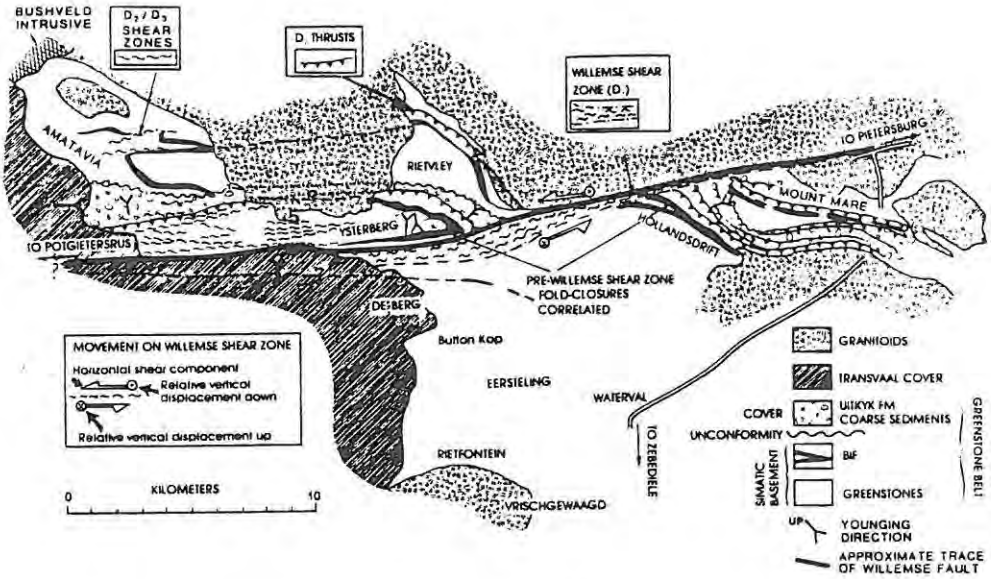

Figure 15. General structural and lithotectonic framework of the southwestern part of the Pietersburg greenstone belt (after De Wit, 1991).

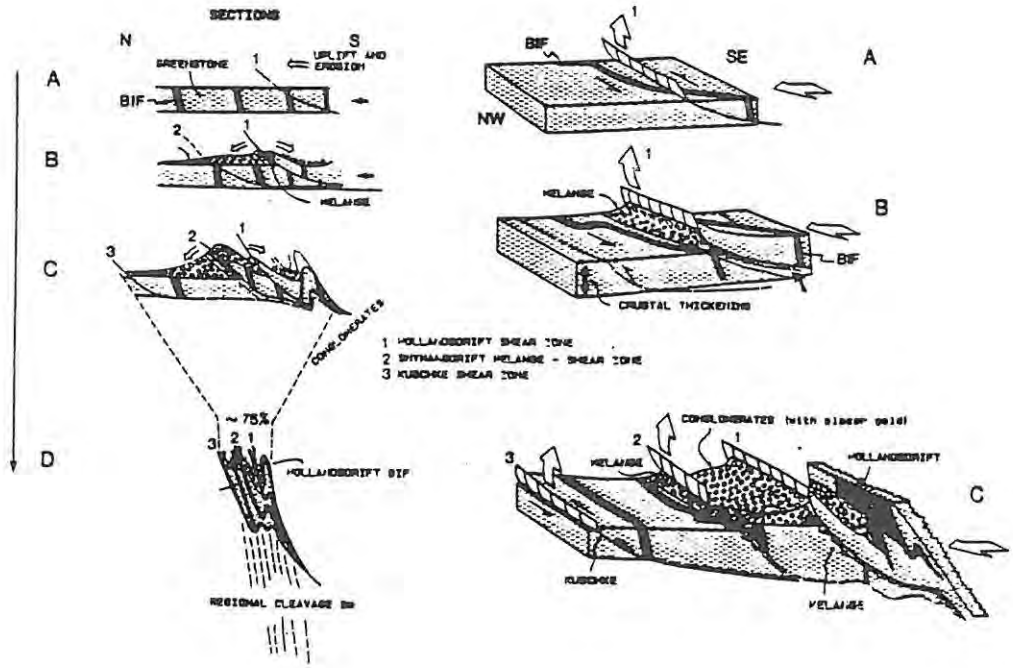

Figure 16. Schematic representation of the D_2 tectonic evolution of the south western part of the Pietersburg greenstone belt (after De Wit, 1991).

Horizontal movement of up to 10s of kilometres along NE-SW shear zones affected the greenstone belt on a regional scale during the later D_3 and/or D_4 deformation periods (Fig. 15). The Willemse shear zone is the most prominent, and also had a vertical displacement of between 3 and 10 km (De Wit, op. cit.).

The N-110° shear zones mentioned above are possibly associated with the D_2 event, whilst the N-70° shear zones could be a product of the D_3 event (Fig. 15). Assuming the above-mentioned deformation events (D_1 to D_4) are correct, the Limpopo Orogeny and the associated Turfloop batholith, should be of D_3 age, or younger.

5.1.4. Metamorphism

M_1 is confined to the greenstones of the Pietersburg Group and was a period of regional hydration under greenschist- to lower amphibolite-facies conditions (De Wit, 1991). The presence of pillow lavas indicates almost instantaneous rock-fluid interaction. De Wit (1990) and Jones (1990) maintain that the entire period of M_1 overlapped with the initial mafic-

ultramafic igneous activity and was of the hydrothermal contact type as shown to be operative along modern mid-oceanic ridges.

M_2 was a period of dynamic metamorphism, syn-kinematic to D_2, which affected the entire Pietersburg Group. It is characterised by the introduction of low-temperature greenschist-facies minerals such as actinolite, tremolite, chlorite and hornblende into the above-mentioned rocks (De Wit, 1991). Franey (1987) suggests that the syn-D_2 metamorphic peak is probably related to heat from the syntectonic granitic intrusions which surround (and underlie) the greenstone belt.

The M_3 and M_4 events were relatively static periods or thermal peaks under lower greenschist facies metamorphic conditions. Possibly, these metamorphic events, associated with the D_3 and D_4 shearing, caused the partial remobilization of gold into these shears (De Wit, 1984, Barton et al., 1990), along which some granites were intruding (e.g., Barton et al., op. cit.).

5.1.5. Tectonic Setting

An original oceanic or back-arc basin setting is proposed for the Pietersburg greenstone belt. Tectonic imbrication of this crust occurred between about 2900 Ma and 2700 Ma during northward-directed thrusting (De Wit, 1991). Sedimentary basins formed in response to this thrusting (Fig. 16), and took place predominantly in subaerial environments, in an alluvial fan of an active foreland basin (De Wit, op. cit.). Syntectonic granites intruded these shear zones, and was followed by bulk shortening (Fig. 16). Finally, the rocks were tectonically deformed in a major strike-slip fault system with both transpressional and transtensional kinematics (Fig. 15; De Wit, op. cit.). The intrusion of late to post-tectonic granites such as the Turfloop batholith were probably associated with the latter deformation events (e.g. Barton et al., 1990).

5.2. Selected granites for exploration

Five areas containing granites were selected nearby Pietersburg for logistical reasons. The granites chosen varied from having known gold mineralization to being previously unexplored. Figure 14 illustrates their localities.

5.2.1. Roodepoort 744LS

The Knight's Pluton at Roodepoort is a known altered granodiorite-hosted gold deposit, and served as an orientation survey in this project.

5.2.2. Waterval 18KS

The granite on the farm Waterval is also a 'Turfloop granite'. Previous soil sampling results from A.A.P.S., Pietersburg show that it is anomalous in Au. One soil sample assayed 740ppb Au. A shear-zone hosted old-gold working (Waterval Gold Mine) on the edge of the Turfloop Granite occurs nearby, 2 km NNE of this locality. In addition, the recently closed shear-zone hosted Eersteling Gold Mine is about 5km W of this granite.

5.2.3. Ramagoep

This is a known remote-sensing 'clay-bearing' anomaly (Franey, 1989; pers. comm.), apparantly within the Goudplaats gneiss. It is interesting because there appears to be no outcrop in the area.

5.2.4. Matlala and Moletsie

The Matlala and Moletsie Granites are intrusive into the Hout River Gneiss, and apparantly have similar conpositions to the Turfloop Granite (Brandl, 1986). To date, they are unexplored for gold.

6. LANDSAT Images

The interpretation of LANDSAT images form an integral part of the 'Regional Area Selection' phase of exploration in this project. The images were processed from data obtained from the LANDSAT 5 satellite, which has a thematic mapper (TM) containing six sensors each with a resolution of 30m x 30m. An additional sensor in the thermal infra-red band has a resolution of 120m x 120m. The above sensors cover the various wavebands of the electromagnetic spectrum as shown in Table 3. A general discussion on LANDSAT images is given in Appendix 2, whilst the types of images used in this project; and their application are described below. This is followed by the LANDSAT image interpretations for the areas selected for exploration.

Table 3: Thematic Mapper Spectral Bands

Band	Wavelength (μm)	Nominal Spectral Location	Characteristics
1	0,45 - 0,52	Blue	Maximum penetration of water, which is useful for bathymetric mapping in shallow water. Useful for distinguishing soil from vegetation and deciduous from coniferous plants.
2	0,52 - 0,60	Green	Matches green reflectance peak of vegetation, which is useful for assessing plant vigour.
3	0,63 - 0,69	Red	Matches a chlorophyll absorption band that is useful for discriminating vegetation types.
4	0,76 - 0,90	Near-infrared	Useful for determining vegetation types, vigour and, biomass content, for delineating water bodies, and for soil moisture discrimination.
5	1,55 - 1,75	Mid-infrared	Indicates moisture content of soil and vegetation. In addition, this band gives an indication of brightness (albedo). This is important as some rocks have reflectance spectra with similar structures, but different albedo (i.e. basalt and marl). Basalt has a low albedo and appears dark on images of single bands compared to marl with a high albedo and light appearance.
6*	10,40 - 12,50	Thermal-infrared	Useful in vegetation stress analysis, soil moisture discrimination, and thermal mapping applications.
7*	2,08 - 2,35	Mid-infrared	Coincides with an absorption band caused by hydroxyl ions in minerals. Ratios of bands 5 and 7 are potentially useful for mapping hydrothermally altered rocks associated with mineral deposits.

* Bands 6 and 7 are out of wavelength sequence because band 7 was added to the TM late in the original system design process.

(modified after Lillesand and Kiefer, 1987; and Sabins, JR., 1987).

6.1. Types of Images

The three types of images used in this project are the Maximum Entropy Scale (MES) images, Clay-iron images and Wallis filter images.

6.1.1. MES Images

MES images are images in which the digital numbers (DNs') of a particular image histogram (Appendix 2) are stretched so as to provide the best spectral contrast in an image. This is an 'in-house' Anglo American image enhancement technique. The MES images utilize the Thematic Mapper (TM) bands in combinations of three. The combinations used in this project are 741 and 751. Reds and browns on both the MES 741 and MES 751 images depict areas that are reflective in band 7 of TM, which is usually assumed to be due to weathered iron-rich minerals.

Green on the MES 741 images represent areas reflective in band 4 of TM. The most likely cause of this is strong vegetation cover. The different shades of green represent the different types of vegetation, state of health, etc.. Green on the MES 751 images represent areas reflective in band 5 of TM, and is also probably caused by various types of vegetation and their moisture content.

Blue on the MES 741 and MES 751 images indicates soil cover as opposed to vegetation cover, and also the presence of water.

Grey on the MES 741 and MES 751 images indicates the presence of granite-derived soil.

6.1.2. Clay-iron Images

This image is an 'in-house' product of Anglo American Corporation involving band-ratioing techniques. The following description is based on discussions with Nick Franey.

Red, orange and yellow depict areas in which there is a strong absorption of band 7. This is generally attributed to the presence of clay minerals or

minerals or minerals containing hydroxyl ions (OH^-). Green and blue represent areas in which band 7 is reflective, which means little and no clay mineral content, respectively. In this context, 'clay minerals' mean kaolinite, montmorrilonite, illite, etc., phyllosilicates such as micas (e.g. biotite, muscovite, sericite) and some amphiboles (e.g. tremolite, actinolite, etc.).

Bright colours on the image depict areas in which there is a strong absorption of band 4 which is generally attributed to iron-rich minerals. Pastel shades depict areas in which band 4 is reflecting; this means little or no iron.

The various colours are interpreted as follows:

* Bright red, orange and yellow. These colours indicate high clay/ high iron.

* Pink, pale-orange or pale-yellow. These colours indicate high clay/ low iron.

* Bright green and blue. These colours indicate 'no' or 'low' clay/ high iron.

* Pale green and pale blue. These colours indicate 'no' or 'low' clay/ no iron.

6.1.3. Wallis Images

A Wallis image is derived from a sophisticated local stretching technique. A 41 * 41 pixel square matrix scans over an image, pixel by pixel. At each stop, it calculates the frequency histogram for the above 'matrix window', applies a linear stretch to that data only, and reassigns a DN to the central pixel. This produces good contrast images on the local scale although large area contrasts are lost. Therefore a large light area will look similar to a large dark area after this process. The danger is that valuable large scale information is lost in this process.

6.2. Land features identifiable on LANDSAT images

The LANDSAT images are restricted to a maximum scale of about 1:50000 due to the pixel size of 30m². After this, too much resolution is lost and therefore, small scale features cannot be detected. For the purposes of this project, the following features can be identified as an aid to the exploration of Archaean granite-/gneiss-hosted gold deposits:

6.2.1. Clay-iron images

* Clay-bearing areas; an indicator of possible hydrothermal alteration.
* Iron-rich areas.

6.2.2. MES images

* Vegetation.
* Lineaments.
* Major outcrops.
* An idea of different soil types.
* An idea of rock composition.

6.2.3. Wallis Images

This image is similar to the MES and Clay-iron images, however local contrast is enhanced while regional resolution is lost.

6.3. LANDSAT Image Interpretations

In this section, the image interpretations of the areas chosen for exporation (Roodepoort, Waterval, Ramagoep, Matlala and Moletsie) are discussed. The actual fieldwork resulting from these interpretations is described in Chapters 7, 8, 9 and 10, respectively. The fieldwork of Matlala and Moletsie are both described in Chapter 10.

6.3.1. Roodepoort 744LS

Figures 17 and 18 are photographs of the MES 741 and Clay-iron images used in this interpretation. Figure 19 is a geological sketch based on the image interpretations.

MES 741 Image (Fig. 17).

This image shows a distinct grey-coloured outline (1) surrounded by brownish bands (2), particularly on the southern side. The grey-coloured outline infers granite-derived soil, and the brownish bands are possibly the greenstones. A number of lighter brown areas also exist within the grey-coloured outline (3) and may represent iron-rich soil and disused cultivation fields with dryish vegetation.

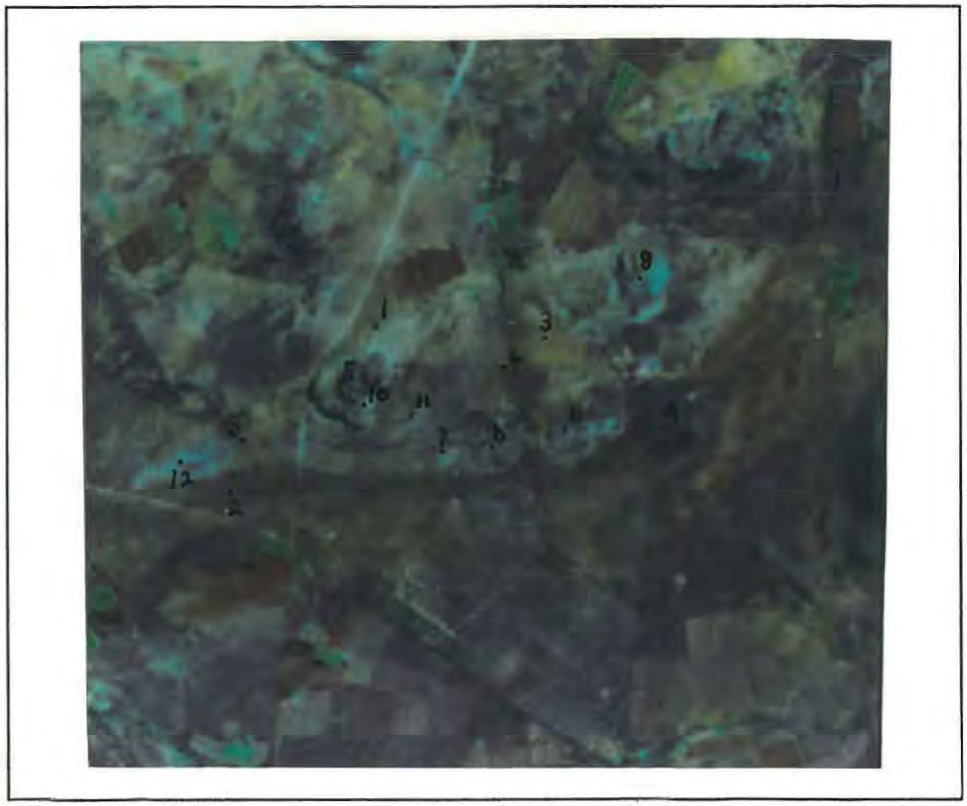

Figure 17. MES 741 image of Roodepoort. The features indicated by numbers 1 to 12 are described in the text. Lateral field of view = 7,5 km.

A NNW-trending lineament (4) is prominent and various outcrops are evident. One occurs just east of the NNE-trending road (5). According to its rounded shape, it is probably a granitic body. Less prominent granitic outcrops (6) are present on either side of the lineament, and also at (7) and (8). The dark grey outcrop (9) just southeast of the grey coloured outline has a very low reflectivity, and is therefore possibly a mafic intrusion.

If this image is examined more closely, it is noted that the grey colours form haloes (10 in Fig. 17) around the proposed granitic outcrops described above, representing granite-derived soil. Possibly, subcropping granites occur at (11) and (12).

Clay-iron image (Fig. 18)

Figure 18. Clay-iron image of Roodepoort. The features indicated by numbers 1, 4 and 13 to 16 are described in the text. Lateral field of view = 7,5 km.

The broad outline (1) is readily seen in the Clay-iron image, although consisting of different colours. The NNW-trending lineament (4) is clearly displayed. Various shades of yellow/orange indicating the presence of clay-minerals (13) are mostly associated with the proposed 'granitic' rocks described in the MES 741 image interpretation. One anomaly is represented by a red dot (14), which also indicates the presence of clay-minerals. Possibly, hydrothermal alteration may be present in some of these areas indicated by (13) and (14). The blue colours (15) indicate areas in which band 7 is strongly reflective, and could be attributed to iron-rich soils derived from greenstone belts or cultivation fields. This tallies with the MES interpretation. The greenish colours (16) could be due to vegetation cover.

Discussion

As illustrated in the geological sketch (Fig. 19), the areas indicating the presence of clay-minerals occur roughly in an ENE-trending band. According to the LANDSAT images, possible area selection criteria for granite/gneiss-hosted gold mineralization in this area are the NNW-trending lineament with proposed granitic rocks on either side. The presence of clay-minerals associated with these outcrops may represent hydrothermal alteration. The other granitic outcrops that appear to be associated with clay-minerals are also worthy of a field visit.

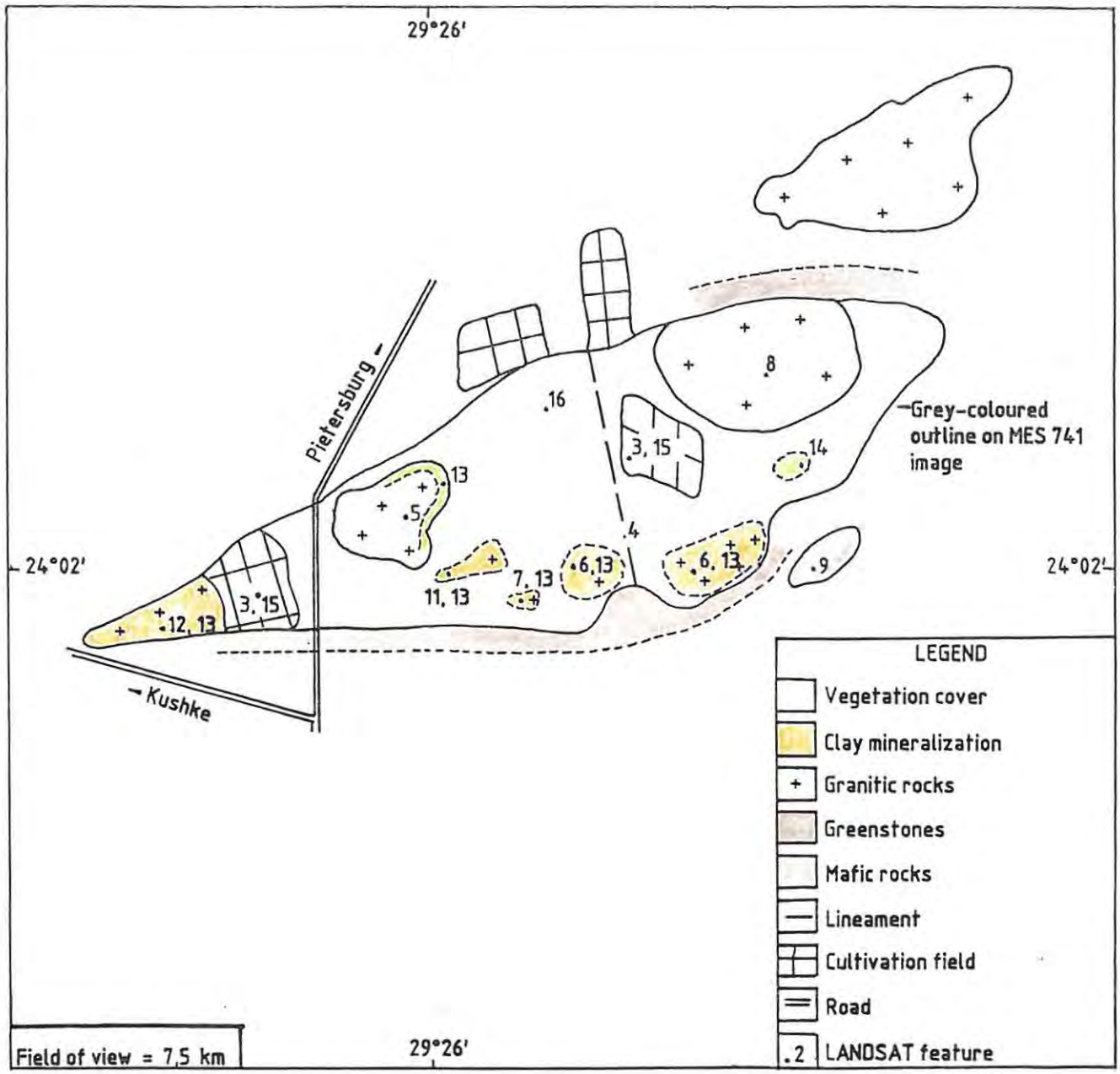

Figure 19. A MES 741 and Clay-iron image interpretation of part of Roodepoort 744LS. The locality of this area is given in figure 14.

present just south of the dyke. The purplish areas on both these images (5) possibly represents iron-rich soil-cover with a lack of vegetation, and is outside the area of interest. The varying shades of green (6) probably represent vegetation cover. The Eersteling and old Waterval gold mines are located at (7) and (8), respectively. The hills on the southwestern corner of the MES and MES Wallis images (9) comprise rocks of the Wolkberg Group.

Figure 21. MES Wallis 751 image incorporating Waterval 18KS. The features indicated by numbers 1 to 9 are described in the text. Lateral field of view = 15 km.

Clay-iron image (Fig. 22)

No distinct outcrops are present in the area outlined by the proposed granite-derived soil (1 in Figs. 20 and 21), however the EW-trending lineament (3) is quite prominent. The Clay-iron image shows that clay-minerals could be present in two areas. The one area is displayed by a yellow-red colour on the southern edge of the proposed subcropping granite (10), and the other area (11) is located alongside the lineament. According

to an aerial photograph of the area (1 in Figs. 20 and 21), (10) coincides with an old cultivation field.

Discussion

The actual interpretation (Fig. 23) is restricted to the north-eastern portion of the images as illustrated in figure 20. The indication of clay-minerals just on the edge of the lineament (11 in Fig. 22) in the vicinity of the proposed granite-derived soil is the only potential area selection criterion for granite/gneiss-hosted gold mineralization in this area. Furthermore, the lineament extends westwards directly towards the recently closed Eersteling Gold Mine. The location of nearby known mineable gold deposits is especially promising.

Figure 22. Clay-iron image incorporating Waterval 18KS. The features indicated by numbers 3, 10 and 11 are described in the text. Lateral field of view = 15 km.

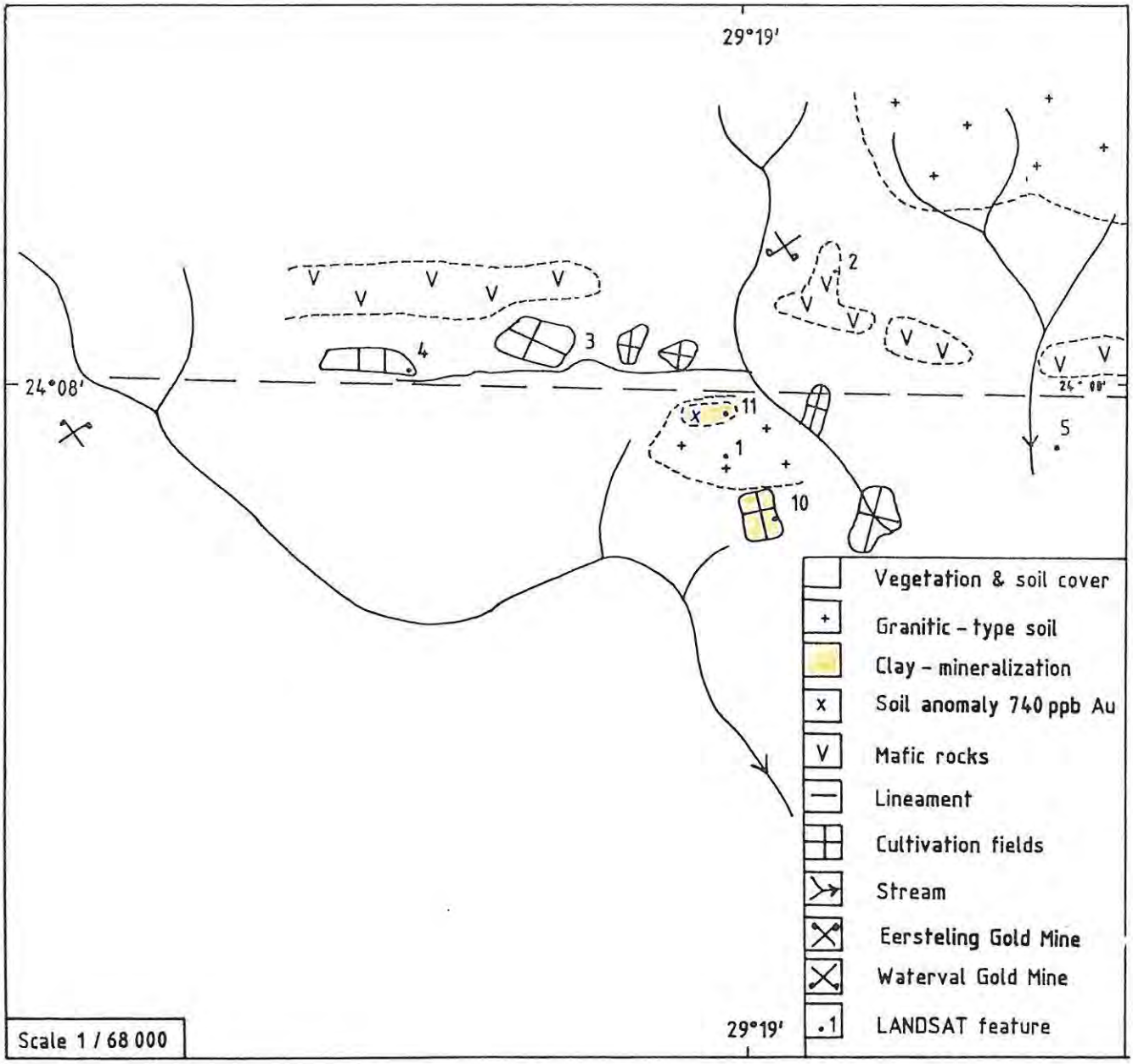

Figure 23. A MES 751, MES Wallis and Clay-iron image interpretation of part of Waterval 18KS. The interpretation is restricted to the north-eastern portion of figure 20. The locality of Waterval is given in figure 14.

6.3.3. Ramagoep

MES 751, MES Wallis 741 and Clay-iron images were used for the interpretation of this area, and are illustrated in figures 24, 25 and 26 respectively. The actual interpretation is illustrated in figure 27.

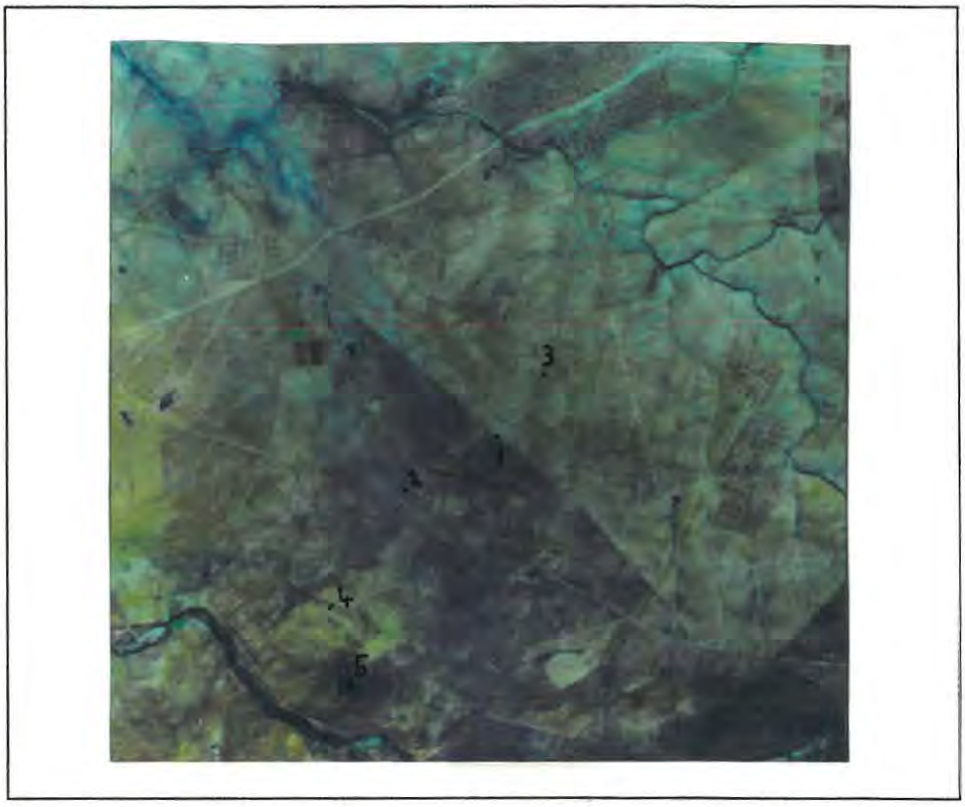

Figure 24. MES 751 image of the Ramagoep area. The features indicated by numbers 1 to 5 are described in the text. Lateral field of view = 15 km.

MES 751 and MES Wallis 741 images (Figs. 24 and 25)

Most of the area outlined by these images appear to be covered by soil with hints of vegetation. A distinct NW-trending diagonal line (1) cross-cuts the central part of the images. Below this line, there is a purplish-coloured area (2), which possibly represents soil cover without vegetation, whereas above this line (3), there is a faint greenish colour (more prominent on the MES Wallis image) that suggests some form of vegetation. Towards the south of these images, faint concentric bands (4) are present,

and are more prominent in the MES Wallis image than the MES image. An outcrop of very low reflectivity, possibly a mafic intrusion occurs in the southern part of the image (5).

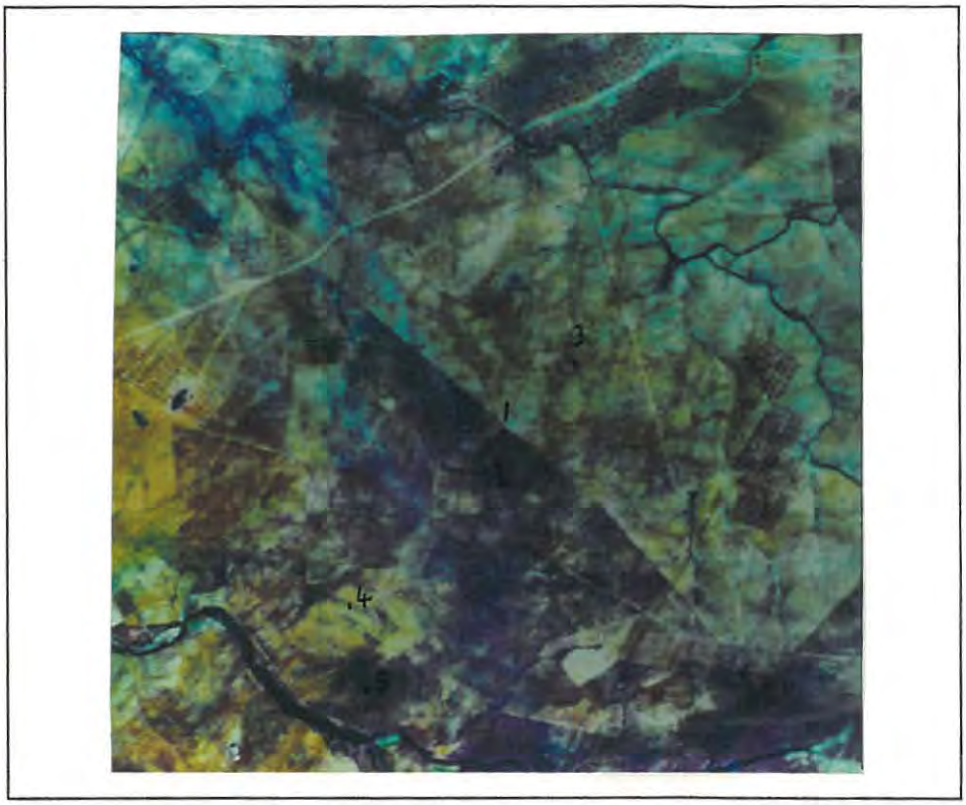

Figure 25. MES Wallis 741 image of the Ramagoep area. The features indicated by numbers 1 to 5 are described in the text. Lateral field of view = 15 km.

Clay-iron image (Fig. 26)

The centre of this image (6) displays a circular feature characterised by orange-yellow colours. This indicates the presence of clay-minerals in the area. The surrounding areas (7) are turquoise in colour, indicating little or no clay-mineral presence. A very prominent purple/blue band (8) is located sub-parallel to the road above the clay-anomaly, inferring iron-rich material, and possibly representing a different rock composition to the turquoise-coloured areas. The concentric bands (4) are also displayed in this image. Less prominent bands (9) subparallel to the concentric bands occur throughout the circular feature.

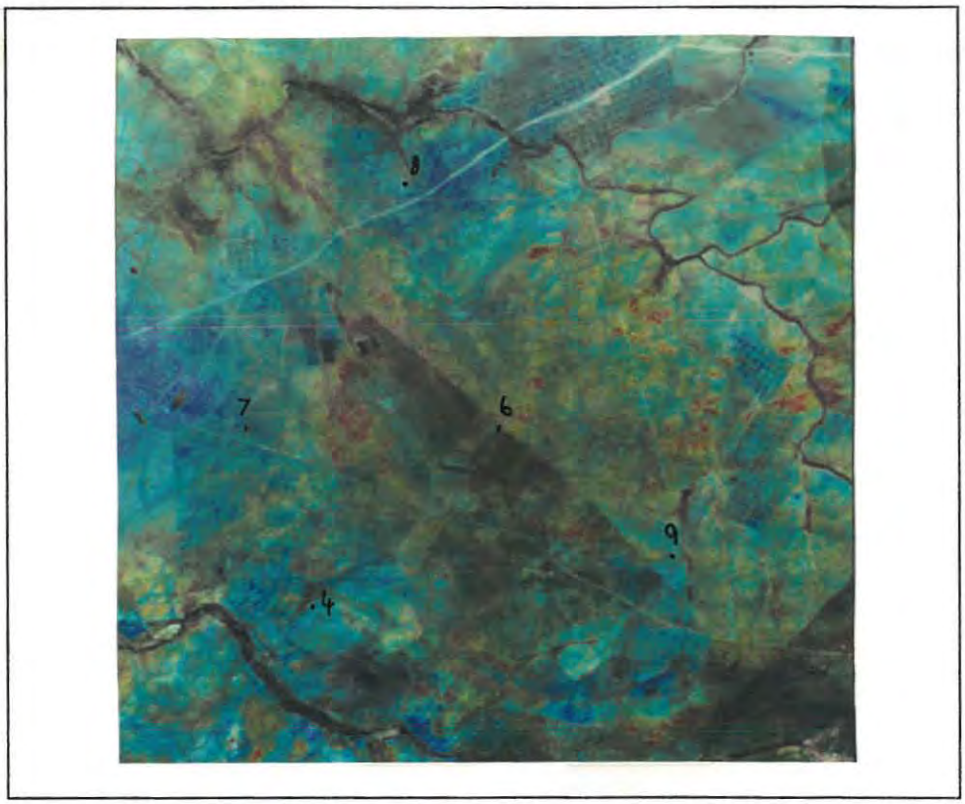

Figure 26. Clay-iron image of the Ramagoep area. The features indicated by numbers 4 and 6 to 9 are described in the text. Lateral field of view = 15 km.

Discussion

The circular feature (Fig. 27) indicating the presence of clay-minerals is the only possible area selection criterion for Archaean granite/gneiss-hosted gold mineralization. If this is an area containing hydrothermal alteration, it may be associated with the 'cupola' of a subcropping granitic intrusive stock. In addition, the concentric bands may be fractures resulting from this intrusion.

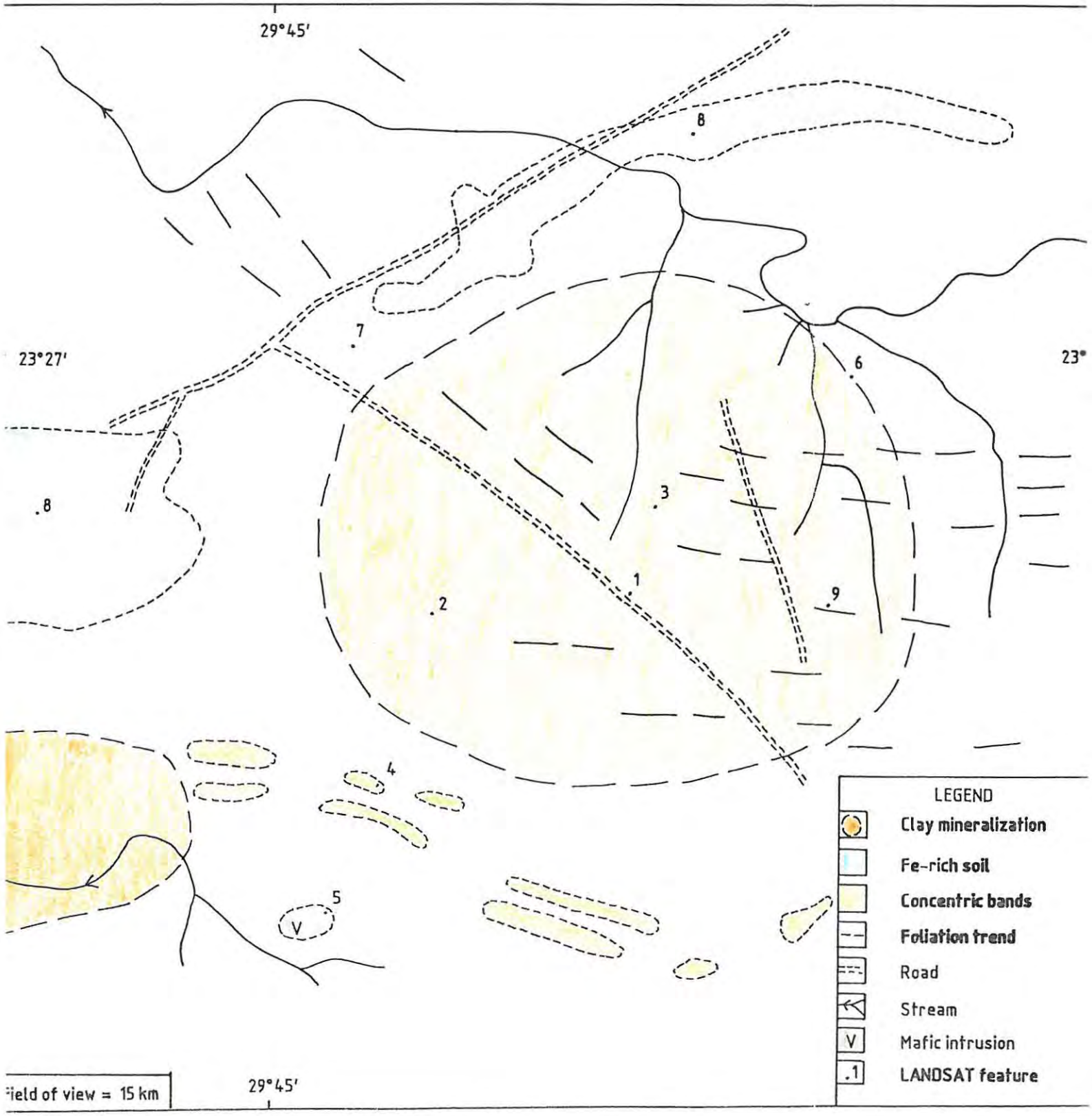

Figure 27. A MES 751, MES Wallis 741 and Clay-iron interpretation of an area in Ramagoep. The locality of this area is given in figure 14.

6.3.4. Matlala

MES 741 and 'Clay-iron + Wallis' images were used to interpret the Matlala area. Photographs of these images are given in figures 28 and 29 respectively. Only the images for the eastern portion of the granite are available.

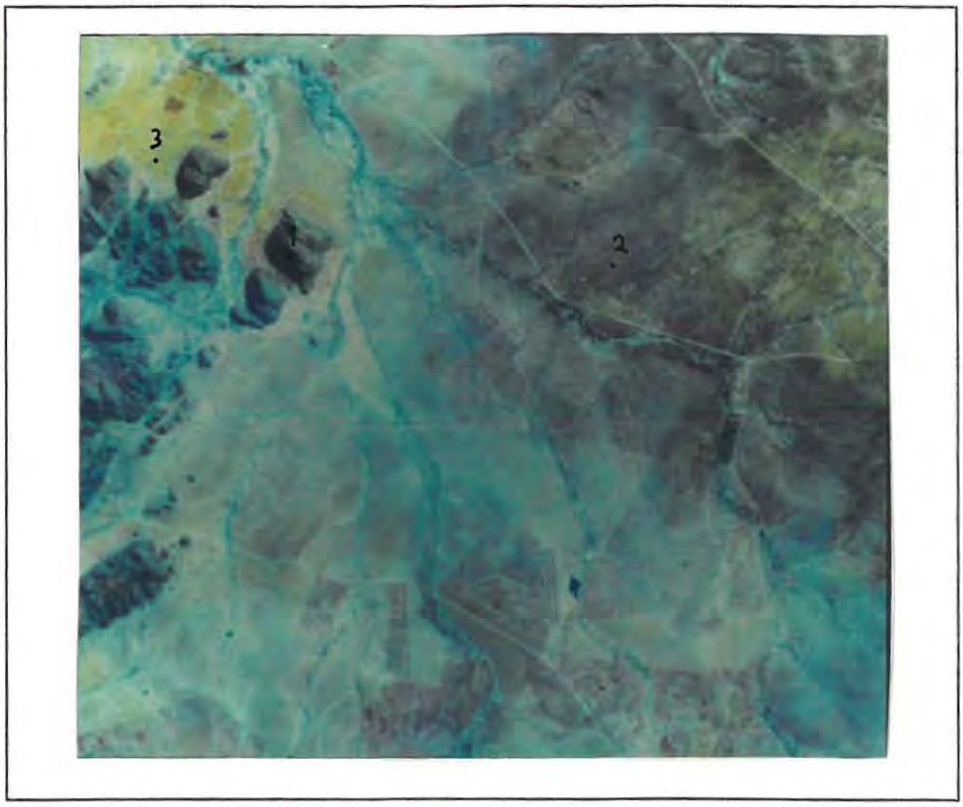

Figure 28. MES 741 image of part of Matlala. The features illustrated by numbers 1 to 3 are described in the text. Lateral field of view = 15 km.

MES 741 image (Fig. 28)

The granitic outcrops (1) are illustrated on the western side of the image. They have a slightly reddish tinge implying that the granites are slightly reflective in band 7. This is generally attributed to the presence of iron-rich weathered minerals. The reddish-brown areas (2) on the eastern side represent soil-covered areas with little or no vegetation. The yellow-green portions of the image (3) represent areas with greater vegetation cover. There is no indication of any lineaments in the area.

Clay-iron and Wallis image (Fig. 29)

The granitic outcrops (1) are also illustrated on the western side of this image. The rest of the image is blue-green in colour; inferring that little or no clay-mineralization is present. This is accentuated by examining the weathering products of the northernmost granite outcrops (4). These are represented by bright blue colours indicating a very high iron content.

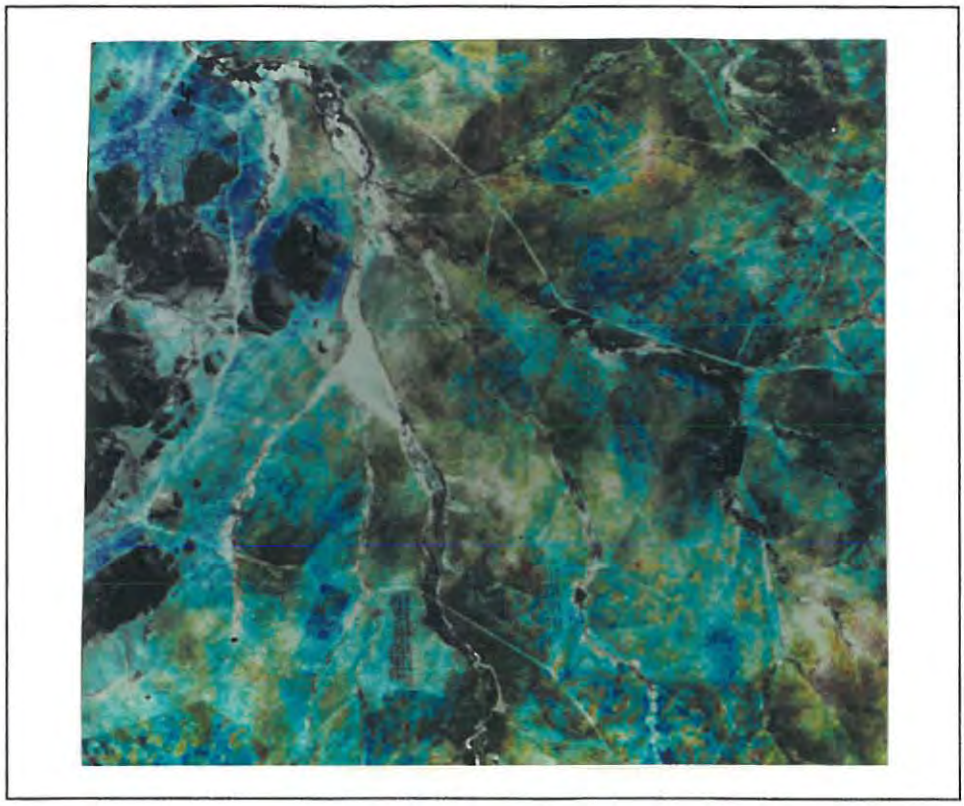

Figure 29. 'Clay-iron + Wallis' image of part of Matlala. The features illustrated by numbers 1 and 4 are described in the text. Lateral field of view = 15 km.

Discussion

The Matlala Granite has different characteristics compared to the granites previously described. As an example, the weathering products of these granitic rocks (their haloes) appear more iron-rich compared to Roodepoort, Ramagoep or Waterval. According to the LANDSAT images of Matlala, there are no features that indicate possible area selection criteria for Archaean granite-/gneiss-hosted gold mineralization in this area.

6.3.5. Moletsie

The area was interpreted using MES 741 and 'Clay-iron + Wallis' images. Photographs of these images are illustrated in figures 30 and 31.

MES 741 image (Fig. 30)

The granitic outcrops (1) are located between the two southeast-trending streams (2), and have a slight reddish 'tinge' indicating the presence of some iron-rich weathered minerals. The yellow-green coloured area (3) surrounding the granites indicates vegetation cover, whilst the reddish-brown coloured areas (4) indicate soil cover with an absense of vegetation.

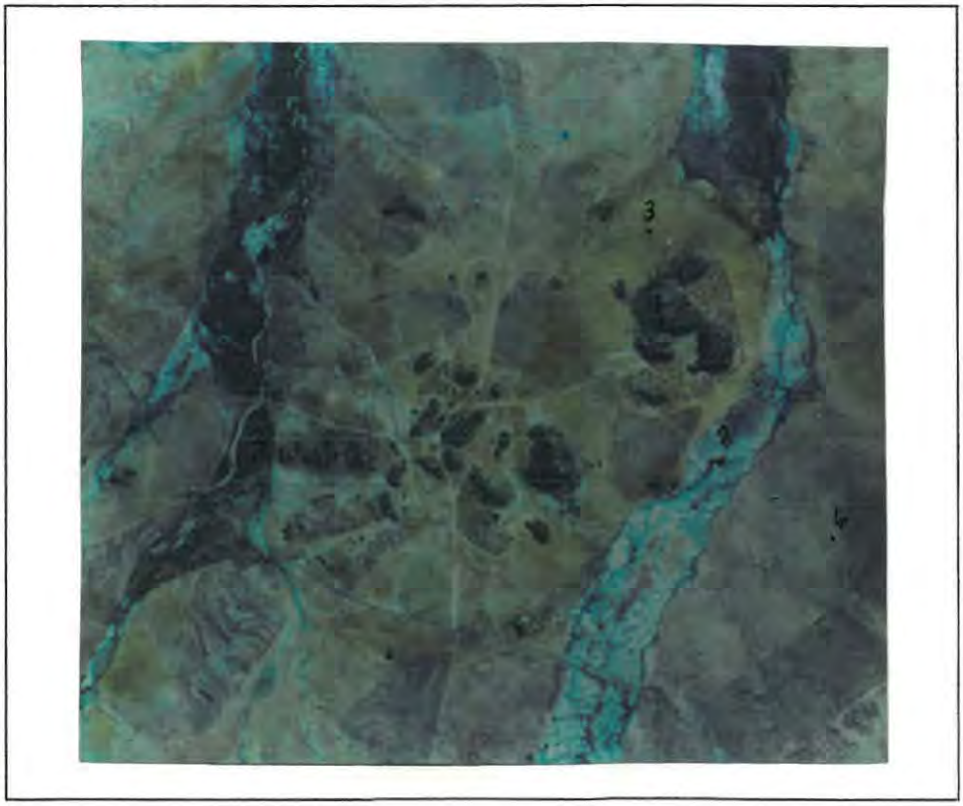

Figure 30. MES 741 image of part of Moletsie. The features illustrated by numbers 1 to 4 are described in the text.

Clay-iron + Wallis image (Fig. 31)

The granite outcrops (1) are quite prominent, and are commonly surrounded by blue-green (5) and bright-blue (6) haloes, thus inferring a lack of clay-minerals required for possible hydrothermal alteration.

Discussion

According to the LANDSAT images of Moletsie, there appears to be no features that indicate possible area selection criteria for Archaean granite/gneiss-hosted gold mineralization in this area. This granite displays similar alteration features to the Matlala Granite.

Figure 31. 'Clay-iron + Wallis' image of part of Moletsie. The features illustrated by numbers 1, 5 and 6 are described in the text.

7. Roodepoort

It is not known when gold mining began, however it is thought that Roodepoort was an extension of the Eersteling goldfield which began production in 1877. Available production records are listed in Table 1. Figure 32 is a simplified geological map of the area showing the positions of the old gold workings.

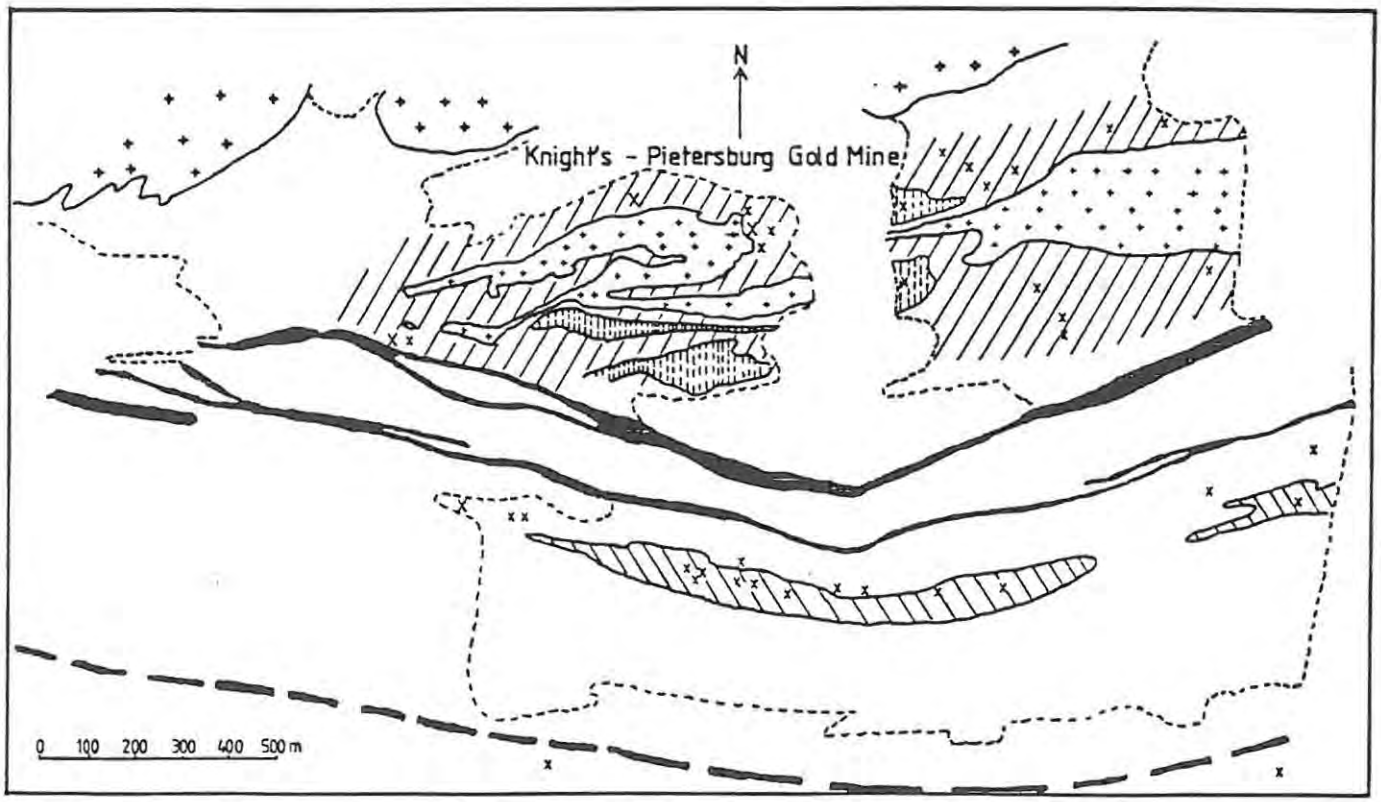

Figure 32. Generalized geological map showing the gold occurrences on the farms Roodepoort 744LS, Langgenoeg 745LS and Palmietfontein 24KS, and the location of the Knight's-Pietersburg Line and gold mine (after Barton et al., 1990).

Gold mineralization occurs in numerous rock types along three sub-parallel ENE-trending shear zones; the Southern Line, Old Freda Line and the Knight's-Pietersburg Line. Gold mineralization at the Southern- and Old-Freda-Lines is shear-zone hosted within the greenstones of the Mothiba Formation. At the Knight's-Pietersburg Line, it is also hosted by the Knight's Pluton in addition to the greenstones.

7.1 LANDSAT anomalies

As described in the LANDSAT images interpretation (section 6.3.1 and illustrated in Fig. 19), a number of anomalies occur at Roodepoort:

1). The 'grey-coloured' outline is probably partly due to granite-derived soil as shown on the MES image. Figure 17 shows that the Turfloop Granite intruded the greenstones of the Mothiba Formation, represented by the brownish bands (2 in Fig. 17).

3). The light brown areas represent old cultivation fields.

4). The only field indication of the lineament is an elongate, well-vegetated depression.

5, 6, 7 and 8). These are granitic outcrops.

9). This outcrop is part of a diabase dyke.

10). These haloes represent granite-derived soil.

11). This anomaly represents granite-derived soil from subcropping granitic rocks.

12). Uitkyk metasediments comprising a series of conglomerates, sandstones, shales and quartz-mica schist outcrop in this area. The indication of clay minerals on the Clay-iron image can be attributed to minerals such as mica within the quartz-mica schist (see Section 6.1.2.).

13). The only granitic outcrops that display distinct alteration in the field are located at (6) and (7). The outcrops at (6) are locally known as the Knight's or Roodepoort Pluton, and the old Knight's Pietersburg gold mine is situated at (6). The minor granite outcrop at (7) appears to be an apophysis of the Knight's Pluton. It is located near the old Northern Hope gold mine within talc-chlorite schist of the Mothiba Formation. Extensive diggings occur in these areas with resultant residual soil which may also contribute to the presence of clay-minerals. A chemical reaction to account for the production of clay from potassic feldspar is:

$$2KAlSi_3O_8 + 3H_2O = Al_2Si_2O_5(OH)_4 + 4SiO_2 + 2KOH$$

K-feldspar Kaolinite (after Levinson, 1980).

14). The red dot is the site of a brick factory.

15). The bright-blue colours represent old cultivation fields that are covered by little or no vegetation. The greenish-coloured areas (16) have greater vegetation cover.

7.2. The geology of part of the farm Roodepoort 744LS

Roodepoort is ideally suited as an orientation survey for this project (Appendix 1), as it contains a known altered granodiorite-hosted gold deposit; the Knight's Pluton. However, outcrop is quite poor, due to extensive soil cover. The area was mapped with emphasis on locating all outcrops of altered granite. The map is illustrated in figure 33. Lithogeochemical samples were collected to determine styles of mineralization and pathfinder elements using the analytical techniques described in Appendix 3. In addition, a vertical drill core through part of the Knight's Pluton (RDP2) was available for logging and petrographical work. The core was previously analysed for gold by the Eersteling Gold Mining Company Limited, using the fire-assay method.

Outcrop within the area mapped comprises rocks of the Mothiba and Uitkyk Formations of the Pietersburg Group, and intrusive Turfloop Granite.

THE GEOLOGY OF PART OF ROODEPOORT 744 LS

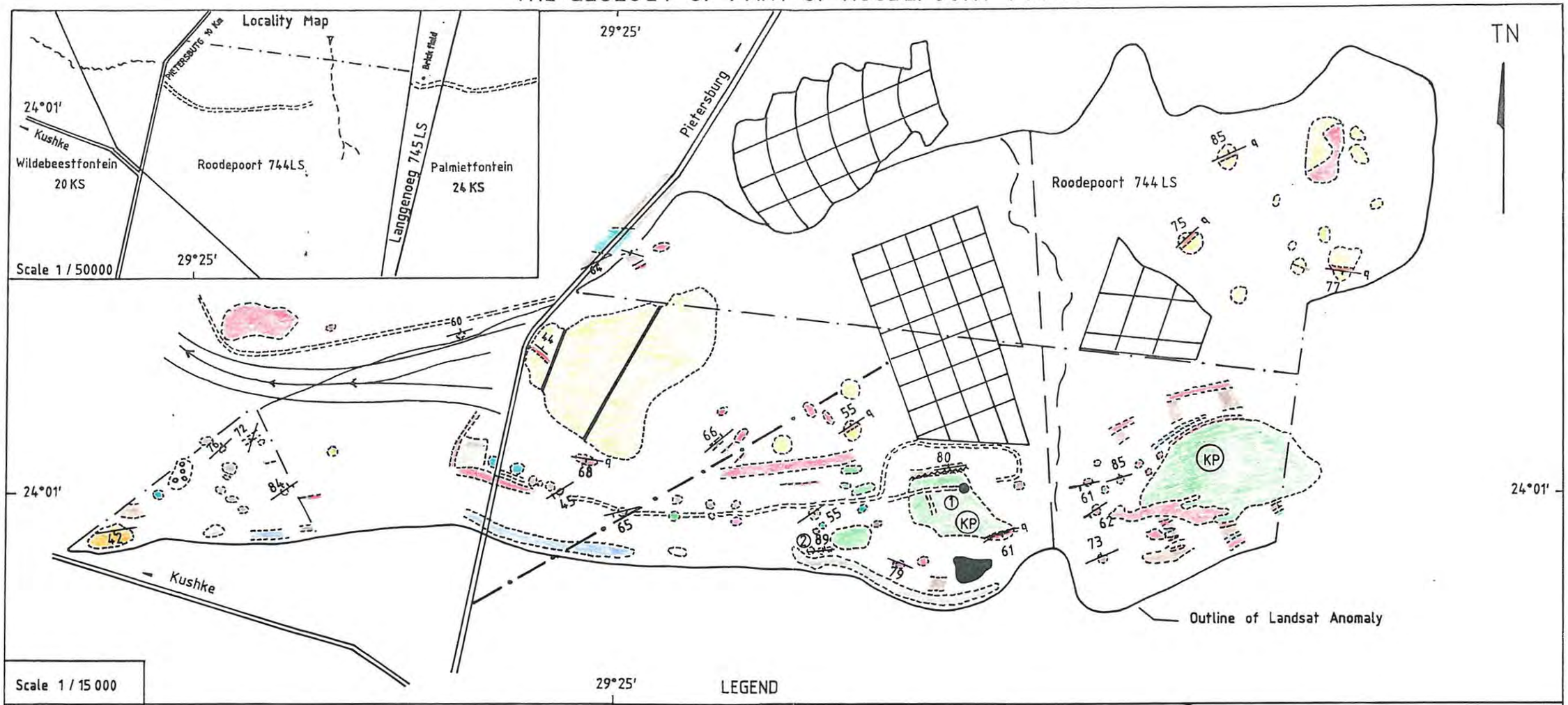

- Soil cover
- Dolerite
- Quartz veins
- Altered granodiorite
- Grandiorite
- Metasediments
- Metabasalt
- Talc - chlorite schist
- Serpentinite (intrusive)
- Banded iron formation
- Carbonate rocks

TURFLOOP GRANITE

UITKYK FORMATION

MOTHIBA FORMATION

PIETERSBURG GROUP

- RDP2 Drill core
- Knight's pluton
- Knight's mine
- Old Northern Hope Mine
- Cleavage-schistocity, 23 Strike and dip of quartz vein
- Shear
- Lineament
- Inferred geological boundary
- Old cultivation fields
- Fence
- Powerline
- Stream
- Kraal
- Road
- Road

Figure 33

7.2.1. Pietersburg Group

The rocks of the Mothiba Formation form the greenstone sequence and consist of quartz-carbonate rocks, banded-iron-formation, serpentinite and talc-chlorite schists. The Uitkyk Formation is represented by an outlier of metasediments in the far west of the area. The metasediments comprise a series of conglomerates, sandstones, shales and quartz-mica schists.

7.2.2. Turfloop Granite

The Turfloop Granite at Roodepoort outcrops within the northern portion of the geological map (Fig. 33) in a roughly ENE-trending band. The granites are transected by steep, north and south dipping quartz veins, commonly with an ENE-trend. A photomicrograph of a Turfloop Granite sample collected at a quarry in Pietersburg, owned by Noordvaal Crushers, Ltd., is illustrated in figure 34.

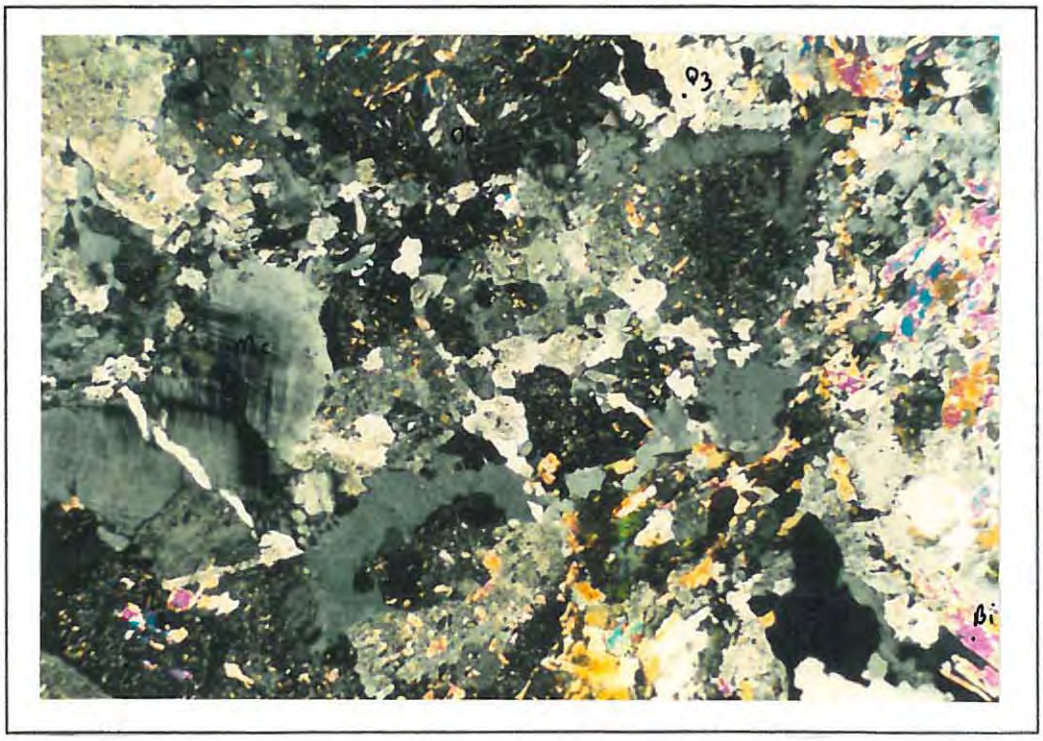

Figure 34. A photomicrograph of Turfloop Granite. It is a porphyritic granodiorite comprising oligoclase (Ol) and microcline (Mc) megacrysts surrounded by a finer-grained groundmass of quartz (Qz) and biotite (Bi). The oligoclase contains sericitic alteration. Cross-polarized light. Lateral field of view = 3,5 mm.

It is a greyish, porphyritic granodiorite consisting of oligoclase and microcline megacrysts, surrounded by a finer-grained groundmass of oligoclase (An_{12}), quartz and biotite. The primary oligoclase is sericitized to varying degrees as opposed to the microcline, which is sericite-free. Apatite, sphene and calcite are present in trace amounts (not visible in Fig. 34). The approximate modal compositions of granitic samples collected at the above-mentioned quarry and determined by thin-section analysis, are given in the Streckeisen plot (Fig. 35). As illustrated, the samples plot mainly as granodiorites and quartz-diorites. One sample plots as a granite.

7.2.3. The Knight's Pluton

The Knight's Pluton (Fig. 33) is a massive body of leucocratic to mesotype rock situated along a steeply northward dipping N-70° trending shear-zone (the Knight's Pietersburg Line) in extensively altered ultramafic and mafic greenstones and banded-ironstones of the Mothiba Formation (Pietersburg Group). It is separated from the Turfloop Granite. Quartz-sericite schist, possibly representing sheared granite, is present along the northern margin of the Roodepoort Pluton in the vicinity of the shear. Minor lit-par-lit intrusions occur west of the Knight's Pluton near the old Northern Hope Mine. A log of the RDP2 core is given in figure 36.

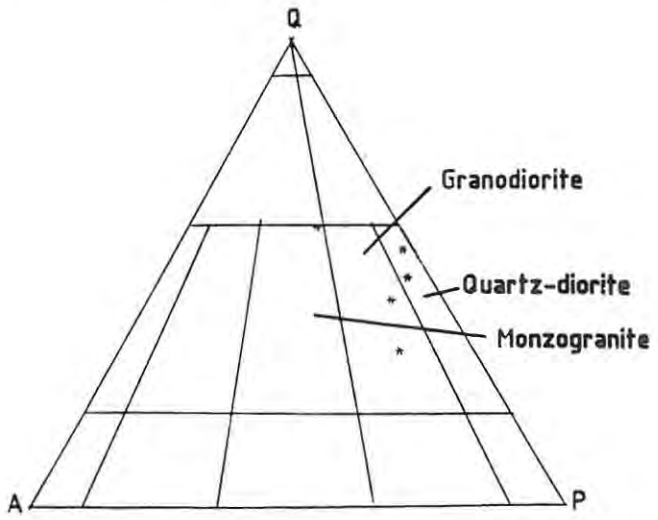

Figure 35. Streckeisen QAP plot of Turfloop Granites (Diagram after Streckeisen, 1976).

LOG OF THE RDP2 CORE

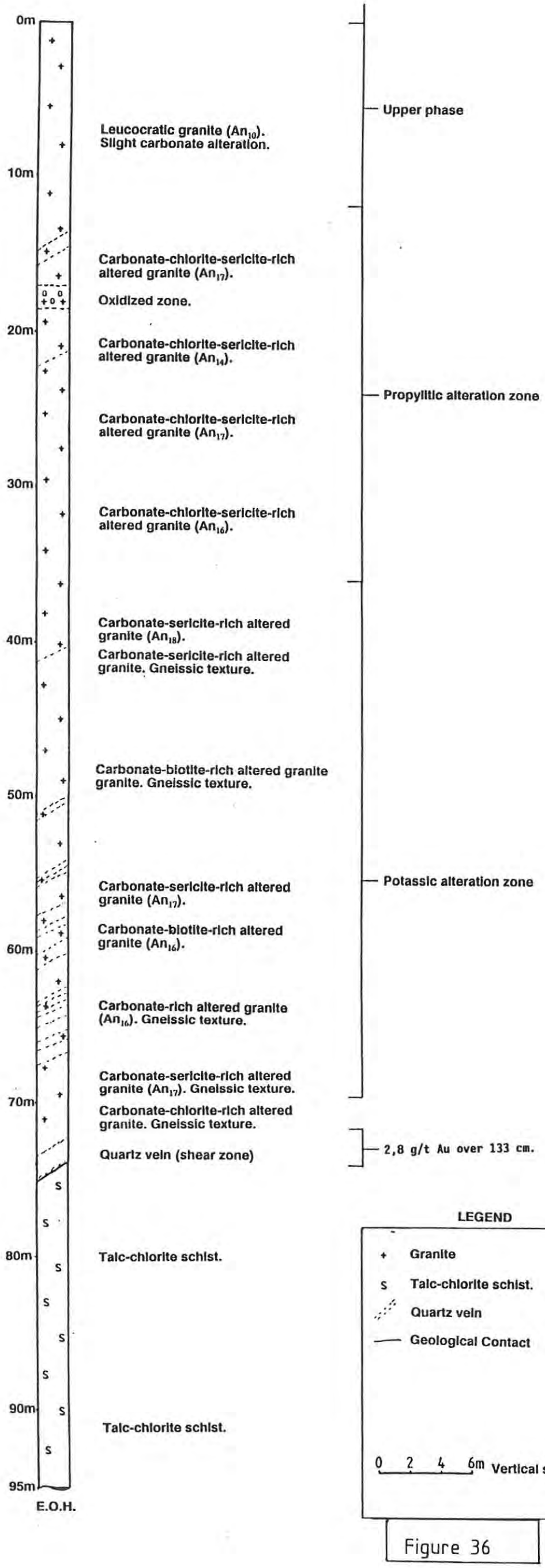

Figure 36

The Knight's Pluton grades from an upper leucocratic phase to a lower grey phase. A photomicrograph of the upper phase (0 - 12m) is illustrated in figure 37. It is a coarse-grained granodiorite composed of albite (± 75 modal %), quartz (± 24 modal %) and muscovite/sericite (± 1 modal %). The production of albite is possibly due to hydrolysis of alkali feldspar, as per the reaction:

$$4(Na,K)AlSi_3O_8 + 2H^+ = NaAlSi_3O_8 + KAl_3Si_3O_{10}(OH)_2 + 6SiO_2 + 2Na+$$

Alkali feldspar — Albite — Sericite — Quartz

(after Colvine et al., 1988).

The propylitic zone of hydrothermal alteration exists between 12 and 36 m (Fig. 36). A photomicrograph representative of this alteration zone is given in figure 38.

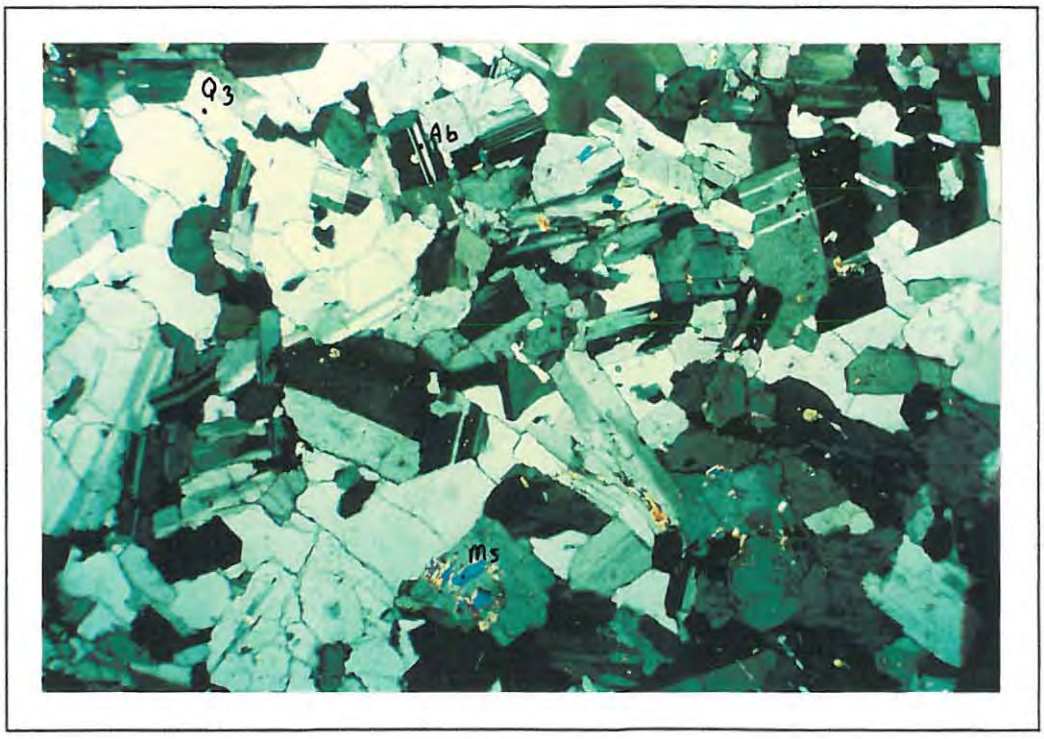

Figure 37. A photomicrograph of the upper phase of the Knight's Pluton. It is a coarse-grained granodioritic rock comprising albite (Ab), quartz (Qz) and minor muscovite/sericite (Ms). Cross polarized light. Lateral field of view = 3,5 mm.

A.

B.

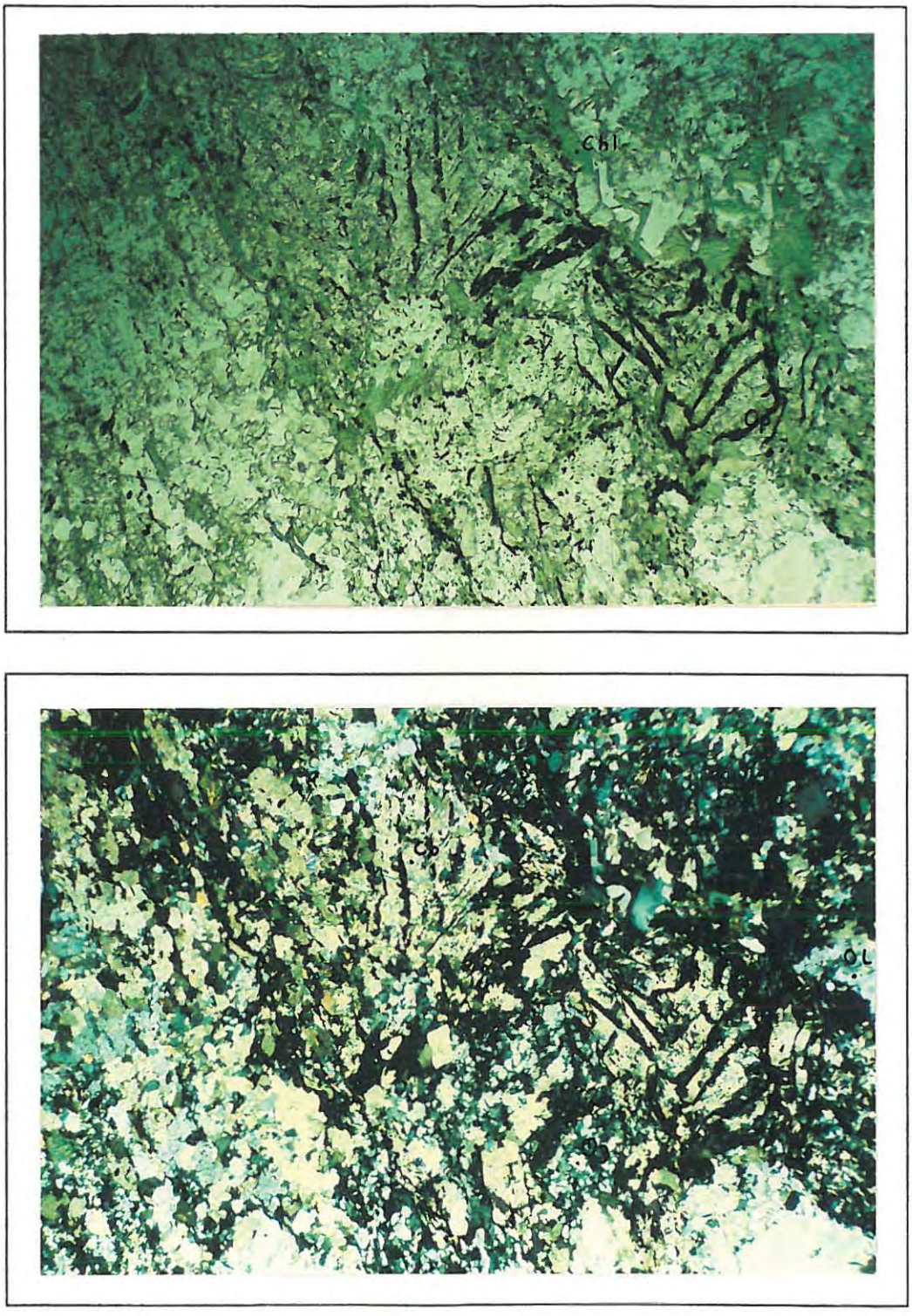

Figure 38. Photomicrograph of the propylitic alteration zone of the Knight's Pluton in the RDP2 core (26,77 m). Chlorite alteration is prevalent. Chl = chlorite, Ol = oligoclase, Op = opaque, Cb = carbonate and Qz = quartz. (A) = plane polarized light, and (B) = cross polarized light. Lateral field of view = 3,5 mm.

As illustrated, it is predominantly a chlorite-rich zone with pervasive calcite and minor sericite. In places, the chlorite and associated opaques (mainly magnetite and some pyrite) display remnants of an amphibolitic cleavage. A possible reaction to account for the alteration of hornblende to a chlorite-calcite -quartz-magnetite assemblage is as follows:

$2Ca_2(Mg,Fe^{2+})4Fe^{3+}AlSi_7O_{22}(OH)_2 + 4CO_2 + 2H_2O + 1/3O_2$
Amphibole

$\longrightarrow Mg5Al_2Si_3O_{10}(OH)_8 + 4CaCO_3 + 5/3Fe_3O_4 + 11SiO_2.$
Mg-chlorite Calcite Magnetite Quartz

(after Colvine et al., 1988).

At a depth of 36 to 75 m, deformation increases to such an extent that a gneissic texture is developed. The propylitic alteration zone is replaced by a potassic alteration zone (Fig.39). Biotite and potassic feldspar are present, but chlorite is essentially absent. The potassic feldspar has been sericitized to varying degrees. According to Burnhan (1979), this sericitization is a common feature of porphyries in which a strong phyllic alteration zone is developed. Chemical reactions that account for the potassic alteration are as follows:

$CaAl_2Si_2O_8(s) + 2KCl(v) + 4SiO_2(s) \longrightarrow 2KAlSi_3O_8(s) + CaCl_2(v)$
Anorthite Quartz K-feldspar

$NaAlSi_3O_8(s) + KCl(v) \longrightarrow KAlSi_3O_8(s) + NaCl(v)$
Albite K-feldspar

(After Burnham, 1979).

A reaction to account for the sericitization of potassic feldspar is:

$3KAlSi_3O_8(s) + 2HCl(v) = KAl_3Si_3O_{10}(OH)_2(s) + 6SiO_2(s) + 2\ KCl(v)$
K-feldspar Sericite Quartz

(After Burnham, 1979).

Phyllic alteration, characterised by quartz-sericite-pyrite alteration and veining, overprints the potassic alteration zone at intervals between depths of 60 and 71,5 m (the lower contact of the granite). Figure 40 is an example of this alteration. Talc-chlorite schist is present below 75m. Pervasive carbonate alteration occurs throughout the Knight's Pluton, but appears minor within the upper leucocratic phase.

It is interesting to note that an argillic zone of hydrothermal alteration in this core is absent. According to Boyle (1984), argillic alteration is a common type of alteration in Tertiary and in some Mesozoic gold-quartz deposits, but is uncommon in Precambrian deposits.

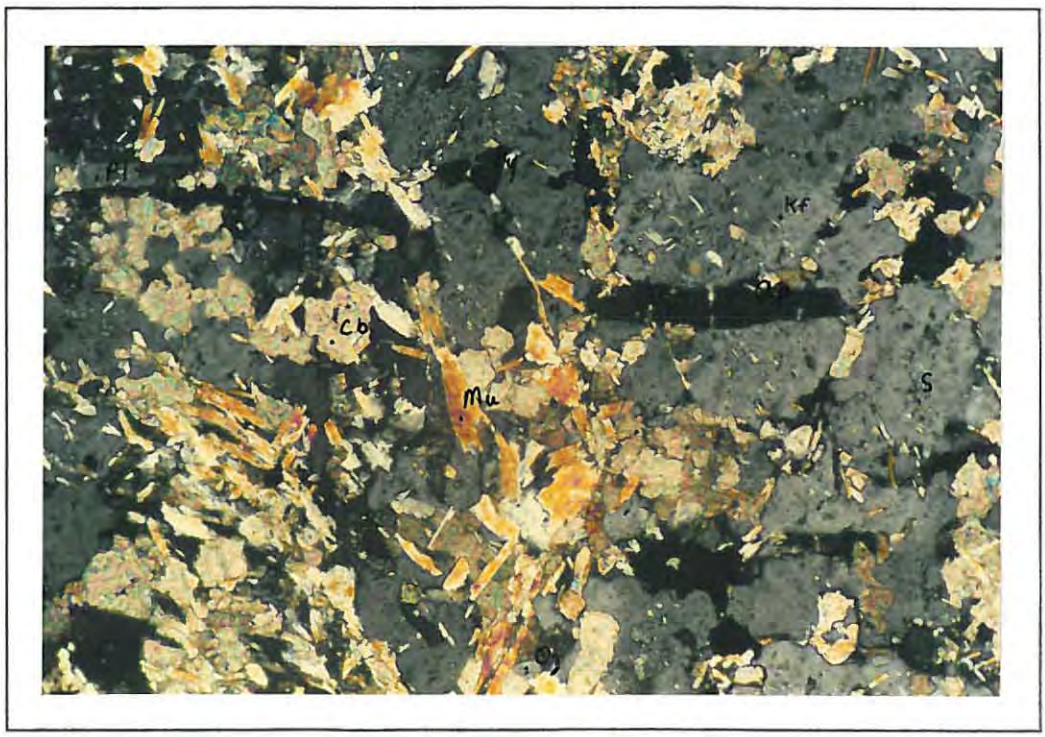

Figure 39. Photomicrograph of the potassic alteration zone of the Knight's Pluton in the RDP2 core (39,33 m). This alteration zone is characterized mainly by the presence of potassium feldspar containing sericitic alteration. Chlorite is absent. Kf = potassium feldspar, Cb = carbonate, Qz = quartz, Mu = muscovite, Ap = apatite, S = sericite, Py = pyrite and Pl = plagioclase. Cross-polarized light, lateral field of view = 0,9 mm.

Figure 40. A typical example of the phyllic alteration (69,66 - 69,74m) within the RDP2 core. The quartz and pyrite alteration are clearly seen. Qz = quartz and Py = pyrite.

7.2.4. Structure

The structure at Roodepoort is extremely complex, and is largely concealed by soil cover. The cleavage-schistocity of the greenstones, the Turfloop Granite and Knight's Pluton all have an approximate ENE-trend. This trend broadly coincides with that of the Knight's Pietersburg Line; one of three subparallel shear zones at Roodepoort. The Turfloop Granite and outcropping Upper Phase of the Knight's Pluton are relatively unfoliated. The Lower Phase of the Knight's Pluton, as indicated by the RDP2 core, becomes increasingly foliated towards the lower, sheared contact with the greenstones.

Extensive, ENE-trending mini-shears occur within the outcropping Upper Phase of the Knight's Pluton. According to the magmatic model, these mini-shears may be due to the physical processes discussed in section 4.1.2., and possibly served as loci for subsequent hydrothermal activity (e.g., Barton et al., 1990). The northern contact of the Knight's Pluton with the

Knight's Pietersburg Line is extensively sheared, and resembles a quartz-sericite schist. This implies that the above-mentioned shear zone was also active after the intrusion of the Knight's Pluton. Late, probably D_4-age, generally ENE-trending quartz-veins truncate all earlier deformation events, and intrude the greenstones, Turfloop Granite and Knight's Pluton. At present, extensive drilling is being done in the area as part of the ongoing exploration at Roodepoort, and should assist in deciphering the structure.

7.3. Geochemical Analyses

The analyses of lithogeochemical samples collected in this project (Table 6), with details of the samples taken, and their positions (Fig. 61), are given in Appendix 4. The analytical techniques used for these lithogeochemical samples are described in Appendix 3. Fire-assay gold analyses of the samples show that notable gold mineralization (>50ppb Au) occurs only within the Knight's Pluton. The gold is mainly associated with shearing (e.g., the quartz-sericite schist, possibly representing sheared granite at the northern contact of the Knight's Pluton with the Knight's Pietersburg Line; Fig. 41), but also occurs within quartz stockworks (Fig. 42). It occurs in the form of free gold (Barton et al., 1986) and associated with pyrite. Fire-assay gold analyses of the RDP2 core (Fig. 36) that were done by Eersteling Gold Mining Co. Ltd., show that significant gold mineralization is also located at the sheared lower contact of the Knight's Pluton with the greenstones.

Figure 43 shows plots of Pb, Sr, Y, Zn, As, Cu, Ba, Nb, Zr and Rb versus Au for the Roodepoort lithogeochemical samples described in Table 6. As illustrated, there appears to be a correlation between Au and Y, As, Ba, Nb and Rb.

The correlation between Rb and Au is due to the substitution of Rb for K, as the upper phase of the Knight's Pluton is enriched in K_2O relative to the Turfloop Batholith (Barton et al., 1990). However, as both the unaltered and altered Turfloop Granites contain minerals such as K-feldspar, Rb is not a good pathfinder-element in the primary environment.

Figure 41. Quartz-sericite schist at the northern contact of the Knight's Pluton with the Knight's Pietersburg Line (shear zone). See RDH 2808, 2811 and 2816 in Appendix 4.

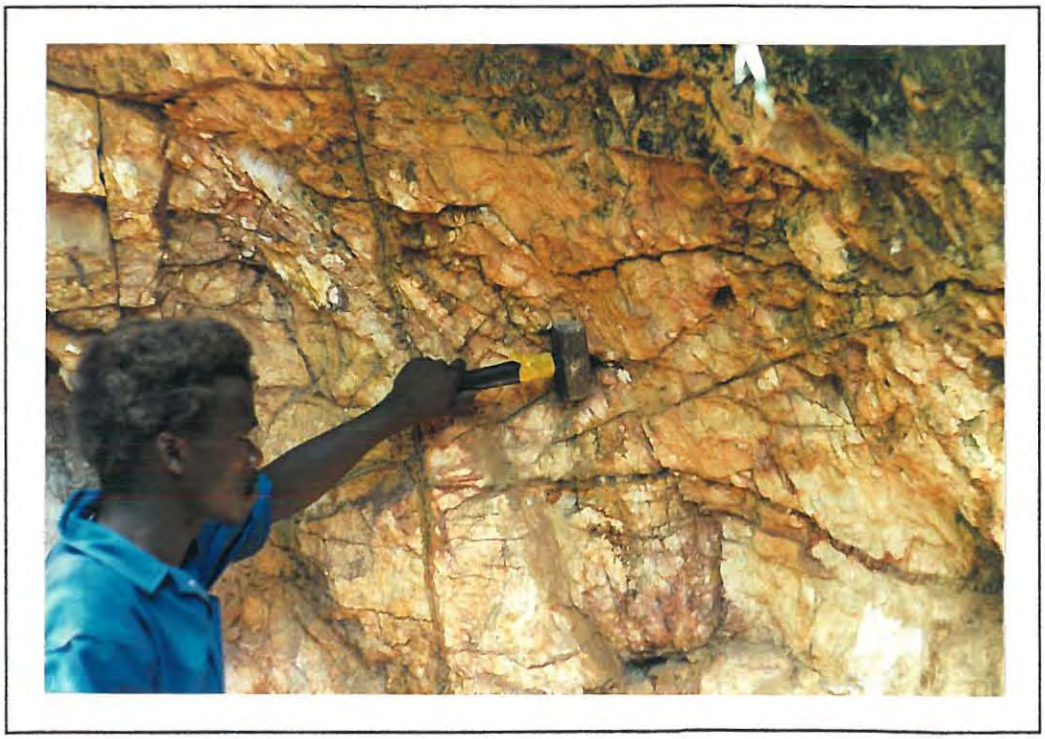

Figure 42. Gold mineralized quartz-stockworks within the Knight's Pluton. See RDH 2805, Appendix 4.

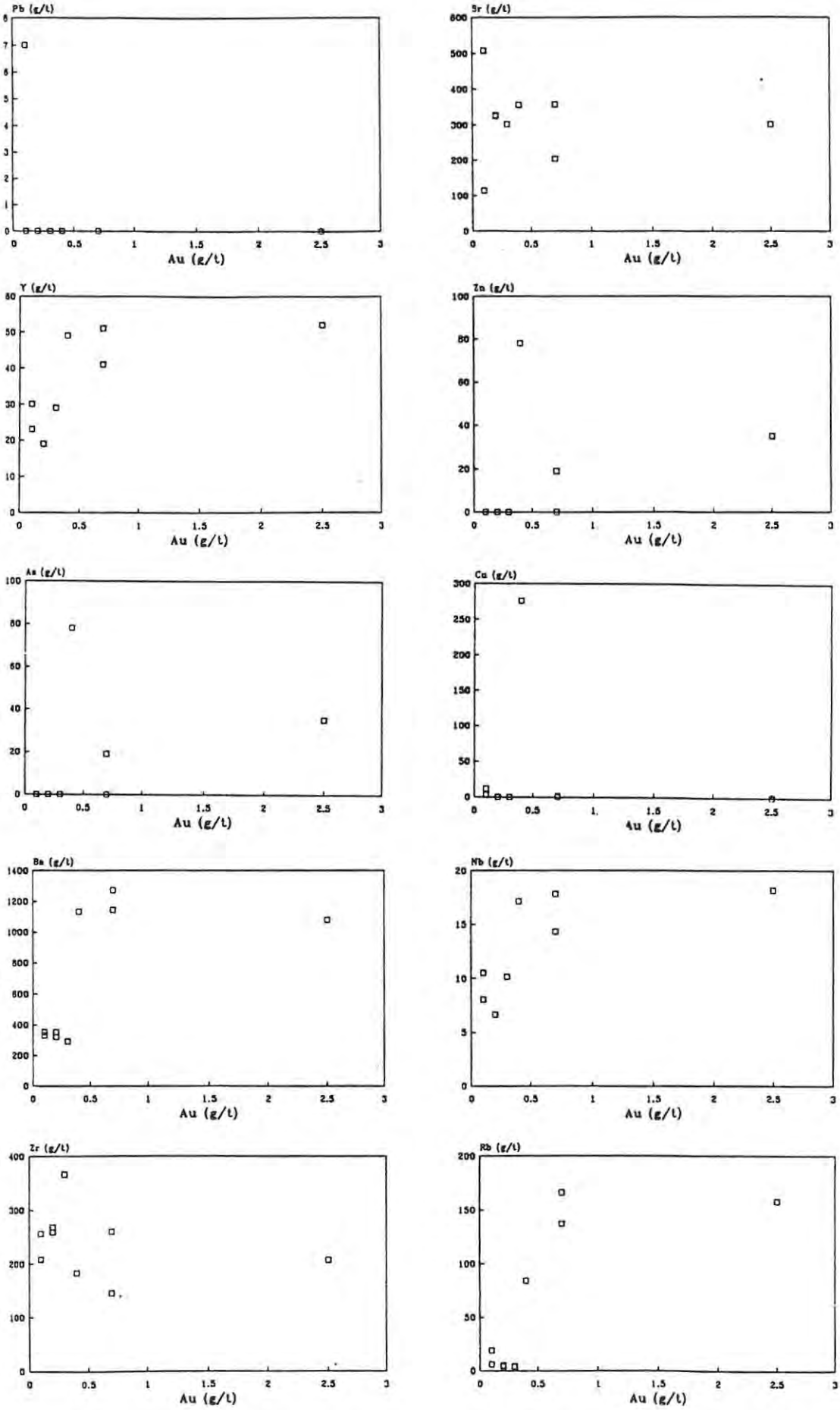

Figure 43. Graphs of As, Cu, Ba, Nb, Pb, Sr, Y, Zn, Zr and Rb vs. Au for the Roodepoort lithogeochemical samples (See Table 6, Appendix 4).

As is known as a good pathfinder element for Au; it has a high mobility in the primary environment, and concentrates within veins and late differentiates; as does gold (Levinson, 1980). Ba also has a high mobility in the primary environment, and is a good pathfinder-element for recognising mineralized granites (Levinson, op. cit.). However, it is important that Ba anomalies are interpreted in conjunction with As anomalies, as Ba also substitutes for elements such as K and Rb. As discussed in Section 4.4., Ba and As tend to form supra-ore haloes (Levinson, op. cit.). Assuming this to be correct, the level of erosion of the Knight's Pluton is not too great.

The correlation between Nb and Au is possibly due to Nb tending to concentrate within albitic granites (Levinson, op. cit.); the same composition as the upper phase of the Knight's Pluton. However, it also substitutes in minerals such as sphene and biotite (Levinson, op. cit.) which are common minerals within the Turfloop Granite. Therefore Nb is not proposed as a pathfinder-element for granite/gneiss-hosted gold mineralization.

The correlation between Y and Au is probably due to the enrichment of CaO in the upper phase of the Knight's Pluton compared to the Turfloop Batholith (Barton et al., 1990). As Y is known to replace Ca in minerals such as apatite (Reedman, 1979); a common mineral within the Turfloop Granite, it is also not a good pathfinder-element for granite/gneiss-hosted gold mineralization.

In summary, As and possibly Ba proved to be suitable pathfinder-elements for granite/gneiss-hosted gold mineralization in the primary environment at Roodepoort, using the analytical techniques described in Appendix 3. As is suggested as a pathfinder-element for stream sediment and soil sampling, whilst Ba should be useful in detailed soil sampling.

7.4. Discussion

Table 4 displays the average chemical compositions of the Turfloop Granite, and the Upper and Lower phases of the Knight's Pluton (sheared and unsheared).

Table 4: Average chemical compositions of rock units mentioned in the text.

Oxide/ Element	Turfloop Batholith Porphyritic Granite (n = 7)	Upper Phase Knight's Pluton (n = 4)	Upper Phase Knight's Pluton (sheared)	Lower Phase Knight's Pluton	Lower Phase Knight's Pluton (sheared)
SiO_2	70,69±0,96	60,69±3,42	57,40	42,4	49,7
TiO_2	0,29±0,07	0,43±0,03	0,54	1,55	1,53
Al_2O_3	14,07±0,20	16,78±0,30	21,09	14,8	15,5
Fe_2O_3	1,84±0,39	2,00±0,81	6,35	10,4	8,81
FeO	0,85±0,46	1,49±0,37	nd	nd	nd
MnO	nd	0,05±0,06	0,11	nd	nd
MgO	0,54±0,24	0,67±0,36	0,70	5,52	3,22
CaO	1,59±0,15	2,51±1,10	1,78	7,84	5,92
Na_2O	4,61±0,19	10,25±1,24	1,94	5,50	4,50
K_2O	4,64±0,20	0,29±0,11	5,97	1,76	0,14
P_2O_5	0,31±0,07	0,19±0,24	0,61	1,14	0,86
Cr_2O_3	-	0,18±0,10	-	-	-
CO_2	0,07±0,01	3,25±1,61	1,50	-	-
H_2O+	0,31±0,08	0,29±0,01	1,95	-	-
H_2O-	0,06±0,01	0,08±0,04	0,19	-	-
LOI	-	-	-	10,25	7,62
S	nd	0,46±0,14	0,57	0,17	0,05
Total	99,86±0,75	99,61±0,43	100,15	99,54	99,42
Au (ppm)	± 0,001	0,5 - 2,0	1,0 - 16,0	0,05	0,01
Pb (ppm)	34± 1,6	22	25	8	7
Cu (ppm)	9± 3,5	11	12	55	16
Zn (ppm)	41± 10,8	5	22	73	124
Zr (ppm)	253± 46,6	175	252	218	210
U (ppm)	nd	nd	nd	6	2
Th (ppm)	12± 3	6	15	27	8
Ba (ppm)	1155±244	441	1187	124	1074
Rb (ppm)	169± 44	1,28± 0,32	20	3,86	0,42
Sr (ppm)	389±100	387±26	468	483	932

nd = not detectable (after Barton et al., 1990).

The Lower Phase of the Knight's Pluton has a meta-aluminous composition, whilst the Turfloop Batholith, the sheared Lower Phase of the Knight's Pluton, the Upper Phase of the Knight's Pluton and the sheared Upper Phase of the Knight's Pluton have per-aluminous compositions.

The meta-aluminous composition of the Lower Phase of the Knight's Pluton supports a magmatic-hydrothermal origin for the gold (see Section 4.1.). This cannot be confirmed however, as the gold mineralization within the Knight's Pluton is now secondary, due to remobilization by later shearing (Barton et al., 1990).

Barton et al., (1990) proposed that the Knight's Pluton was originally part of the granitic magma associated from the Turfloop Batholith, although

separated from the main batholith. It intruded into a shear zone (the Knight's Pietersburg Line) along which alteration involving CO_2 and Au mineralization were occurring, and was itself completely altered. Barton et al., (op. cit.) suggested that crustal thickening and subsequent rapid isothermal decompression during the Limpopo Orogeny about 2700 Ma ago, resulted in appreciable volumes of granitic magma being generated by partial melting of portions of the upper mantle and lower crust in the over-ridden plate, and by hydration of lower portions of the over-riding plate. These granitic magmas then moved along shear zones formed during the Limpopo Orogeny to higher crustal levels. The same shear zones also acted as conduits for fluids derived by crustal dehydration and by crystallization of granitic magmas (Van Reenen et al., 1987, 1988; Barton et al., 1988).

This latter model for the origin of the gold is similar to the metamorphic replacement model described in Section 4.2. A further period of late, probably D_4-age shearing at about 2340 Ma (Barton et al., op. cit.) is represented by the extensive ENE-trending quartz veins found within the mapped area (Fig. 33) that truncate both the granite and greenstones. According to Barton et al., (op. cit.), the gold was remobilized and redistributed into these shear zones.

The favourable area selection criteria for Archaean granite-/gneiss-hosted gold mineralization at Roodepoort are the major ENE-trending shear zone (the Knight's Pietersburg Line), the NNW-trending lineament; shearing quartz-stockworks, hydrothermal alteration and sulphide mineralization associated with the Knight's Pluton.

The MES image interpretation correctly identified the granites, greenstones and the NNW-trending lineament. The Clay-iron image interpretation also correctly located clay-bearing areas. However, field visits were necessary to show that only the altered granites on either side of the lineament contained hydrothermal alteration.

The correlation of Au with As, Ba and Rb in the primary dispersion environment confirms the general enrichment of these elements (amongst others) in Archaean gold deposits, discussed in Chapter 4.

8. Waterval 18KS

The LANDSAT features described in this chapter are illustrated in figure 21. A field visit to the anomalous area (1) confirmed the LANDSAT images interpretation of sparse outcrop and reasonable vegetation cover. The clay-bearing area (10) coincides with an old cultivation field. The only indication of a possible lineament is the stream (3). The dyke-like feature (2) consists of mafic rocks. Trenches were dug at (11) in order to expose the granites. Figure 44 is a locality map of these trenches. A plan view of trenches (1 and 2) is illustrated in figure 45. The other sites (3, 4 and Peg 2400/650) consisted of pits within granite. The samples were analysed by fire assay for gold. The granites sampled at site number 3 assayed 20 ppb Au. Those at site number 4 and Peg 2400/650 both assayed 40 ppb Au.

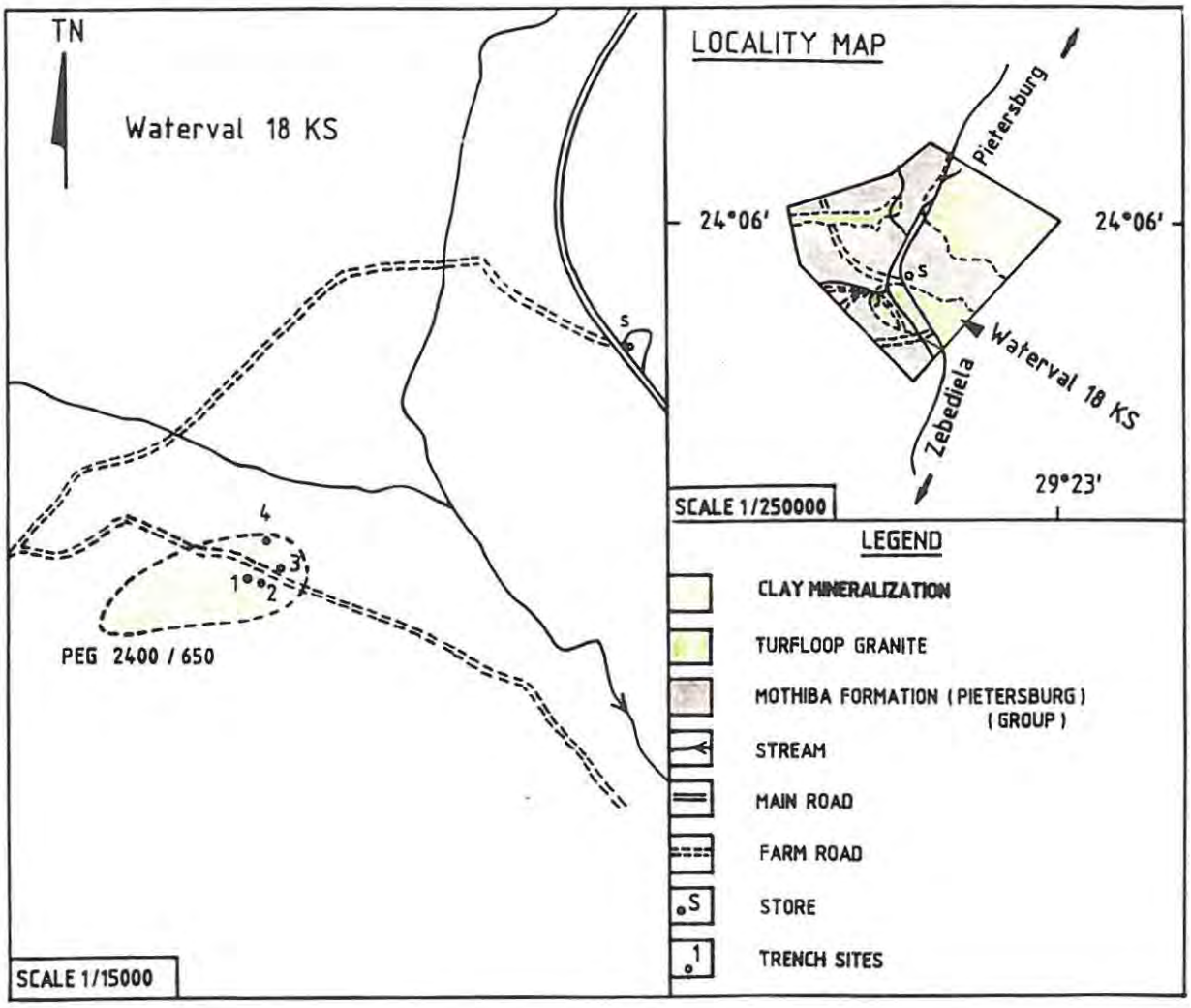

Figure 44. A locality map of the trenches within Waterval 18KS.

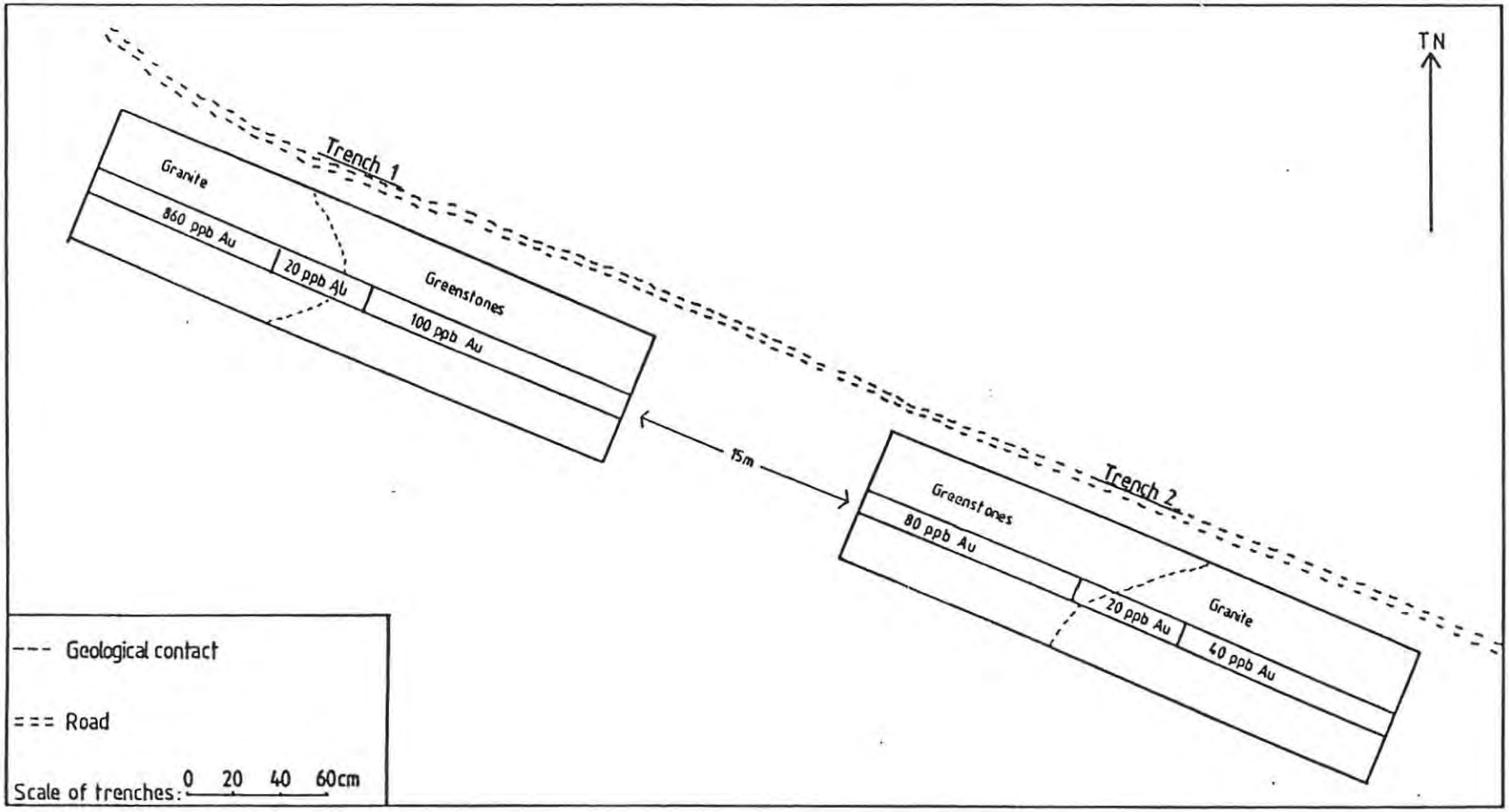

Figure 45. A plan view of trenches 1 and 2.

The other samples, in trenches 1 and 2 assayed between 20 and 100 ppb Au (Fig. 45), however an apophysis of the granite (Trench 1) within the greenstones assayed 860 ppb Au. This particular sample contained traces of pyrite mineralization, however all the granites uncovered contained sericitic alteration.

A photomicrograph of the mineralized granite described above is given in figure 46. It is a coarse-grained granodiorite containing oligoclase (An_{18}, ± 70 modal %) and quartz (± 25 modal %). Sericite (± 2 modal %) and calcite (± 3 modal %) is also present. A reaction to account for the sericitization of the oligoclase is as follows:

$$3NaAlSi_3O_8 + K^+ + 2H^+ = KAl_3Si_3O_{10}(OH)_2 + 6SiO_2 + 3Na^+$$

Na-plagioclase — Fluid — Sericite — Fluid

(after Roberts; 1987).

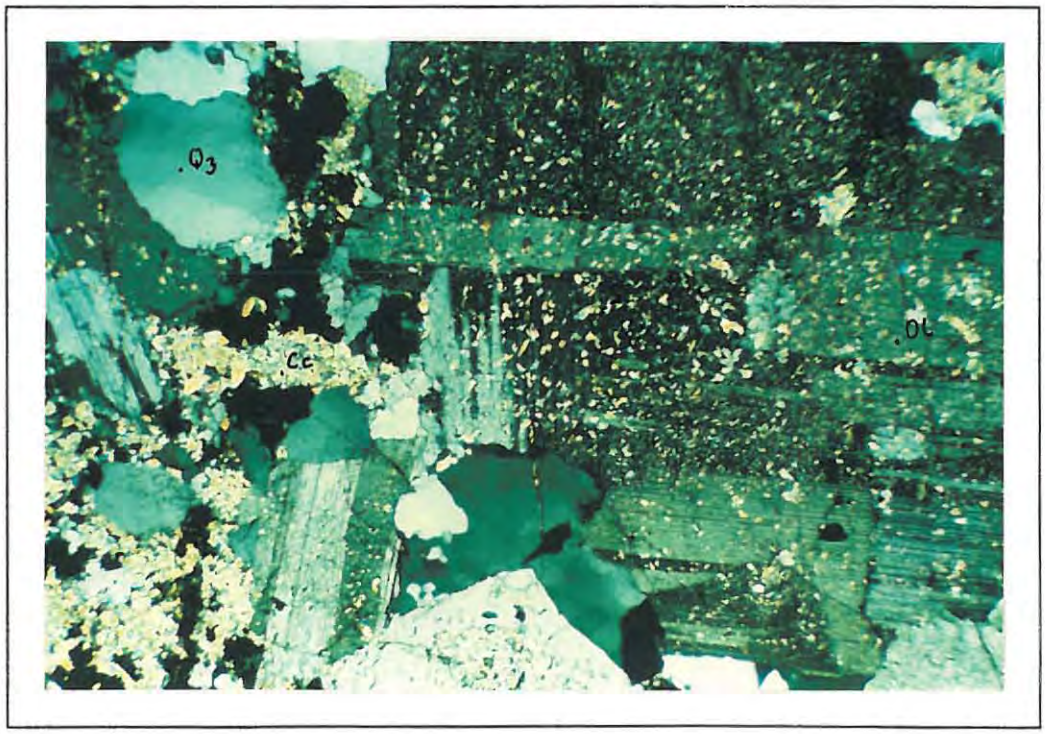

Figure 46. A photomicrograph of the granite at Waterval in trench 1. It is a coarse-grained granodiorite comprising oligoclase (Ol) and quartz (Qz), with sericite-alteration (S) and calcite-alteration (Cc). Cross polarized light. Lateral field of view = 3,5 mm.

8.1. Discussion

The uncovered granites depicted by the clay-bearing area (11) clearly contain sericitic alteration, but lack any significant gold mineralization. Although the granite apophysis within the greenstones was enriched in Au compared to the other granite samples, 860 ppb Au is of no economic significance. A soil sampling program in the vicinity of (10), previously completed by A.A.P.S. Pietersburg, also revealed no geochemical anomalies. Therefore, no further work is recommended in this area.

9. Ramagoep

The Ramagoep area was visited, and a geological map (Fig. 47) produced with the aid of 1:100000 scale LANDSAT images, field-work and the published 1:250000 scale Geological Survey map '2328 Pietersburg'. The area consists of Goudplaats Gneiss, Hout River Gneiss and Matok Granite. Two sub-parallel NE-trending faults cross-cut the area. Isolated bands of amphibolites and banded-iron-formation belonging to the Zandrivierspoort Formation occur towards the south of the area.

All LANDSAT features discussed in this chapter are illustrated in figure 27. The NW-trending diagonal line (1) separates the 'overgrazed' area to the south (2) from the reasonably well vegetated area to the north (3). The concentric bands (4) represent amphibolite bands of the Zandrivierspoort Formation, and not fractures as suggested in the LANDSAT images interpretation (section 7.3.). The outcrop with very low reflectivity (5) consists of banded-iron-formation. The clay-bearing area (6) is underlain by weathered Goudplaats Gneiss; and is surrounded by Hout River Gneiss (7) and Matok Granite (8). The well developed foliation of the Goudplaats Gneiss (Fig. 48) accounts for the faint bands (9).

A photomicrograph of a rock sample collected within the clay-bearing area (RDH2839; Fig. 47) is illustrated in figure 49. It has a granite composition, consisting of quartz (± 30 modal %), perthite (± 65 modal %), muscovite (± 3 modal %) and sillimanite (± 2 modal %). The presence of sillimanite indicates upper-medium- to high-grade metamorphic conditions where temperatures of greater than 600°C prevail, and is attributed to the following reaction:

$$K_2Al_4(Si_6Al_2)O_{20}(OH)_4 + SiO_2 \longrightarrow KAlSi_3O_8 + Al_2SiO_5 + H_2O$$

Muscovite + Quartz = K-feldspar + Sillimanite + Water

(after Winkler, 1979).

The sillimanite indicates a possible pelitic origin for this rock, inferring that it is an S-type granite.

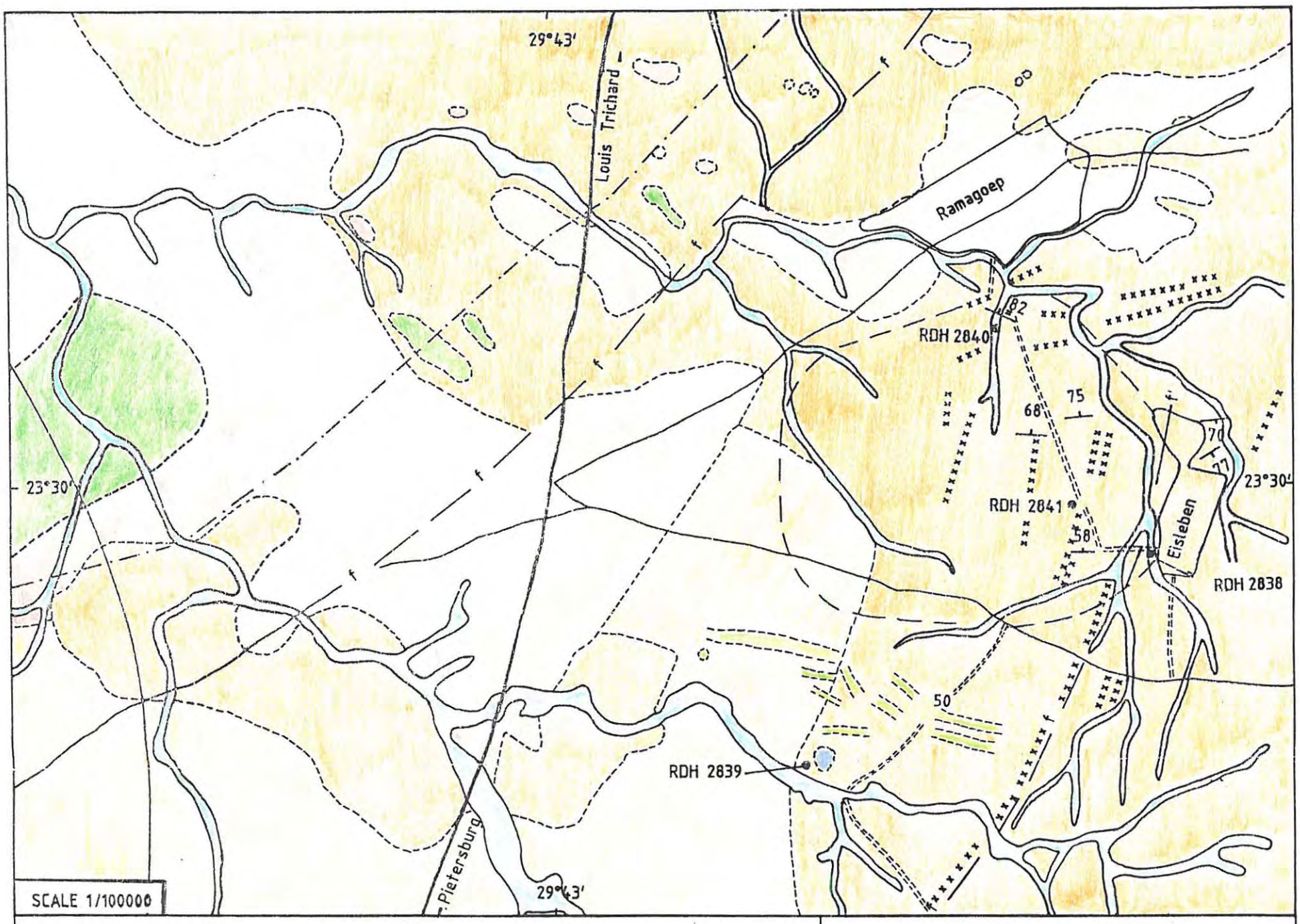

LEGEND

- Diabase dyke
- Matok Granite
- Hout River Gneiss
- Zandrivierspoort Formation (Pietersburg Group) (amphibolite □ :banded - iron - formation □) (minor garnetiferous - schists and) (calc-silicate rocks)
- Goudplaats Gneiss

- RDH 2839 Sample Position
- f —— f Inferred fault
- 23 Foliation
- Roads
- ---- Inferred geological boundary
- Stream
- Clay-anomaly (fig. 27)
- —·— Orthopyroxene isograd

Figure 47. A geological map of part of the Ramagoep area. Compiled from 1:100000 scale LANDSAT images, field visits and the published 1:250000 Geological Survey Map '2328 Pietersburg'.

Figure 48. An outcrop of the extensively foliated Goudplaats Gneiss in the Ramagoep area. Note the pencil for scale.

9.1 Discussion

The idea of a subcropping granitic intrusion with surrounding concentric fractures is completely incorrect. It is proposed that the clay-bearing area (Fig. 47) is a product of the weathering of potassic feldspars within the Goudplaats Gneiss. The most common form of clay produced within climatic areas such as Ramagoep is illite (Levinson, 1980).

The Goudplaats Gneiss probably formed during the first magmatic cycle described in Chapter 2, whereas the Archaean gold mineralization event was coeval with the third magmatic cycle (Chapter 3). Therefore, according to the magmatic model (Chapter 4), it is unlikely that the Goudplaats Gneiss hosts significant gold. There is also an absence of major shears and hydrothermal alteration; requirements for the metamorphic replacement model (Chapter 4). Therefore, no further exploration is recommended for this area. Four geochemical analyses of Goudplaats Gneiss were barren in gold (Appendix 4).

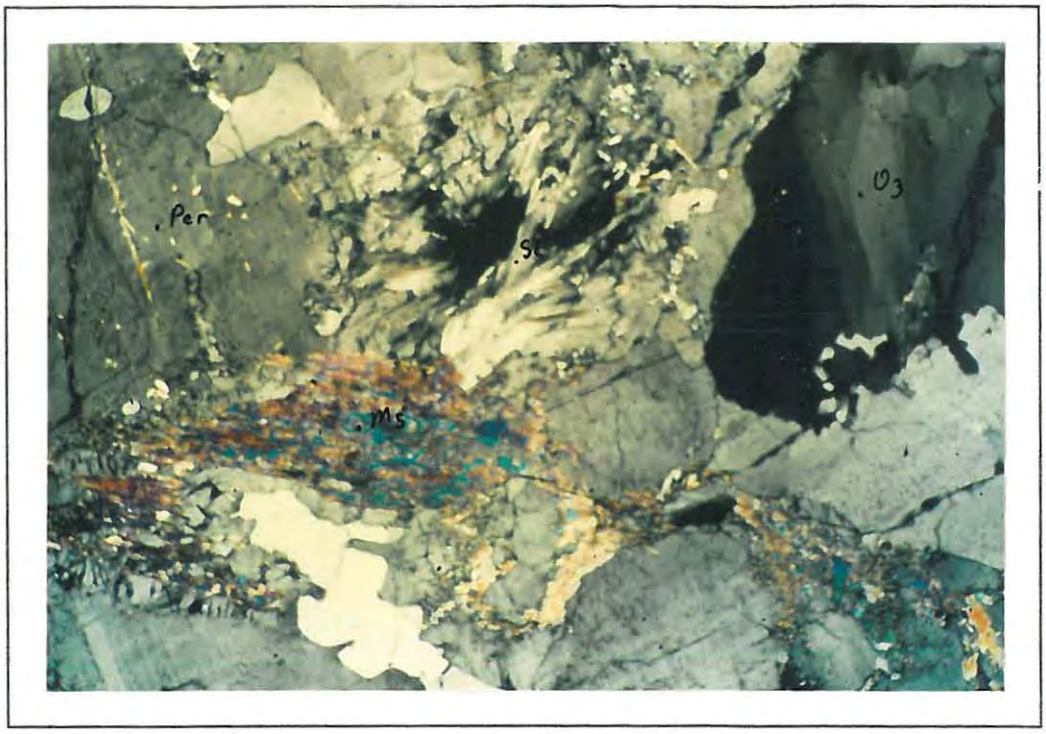

Figure 49. A photomicrograph of a gneissic outcrop within the clay-bearing anomaly (RDH2839; Fig. 47) at Ramagoep. It has a granitic composition and comprises quartz (Qz), sillimanite (Sl), muscovite (Ms) and perthite (Per). Cross polarized light. Lateral field of view = 3,5 mm.

10. Matlala and Moletsie

Figure 50 is a geological map of Matlala and Moletsie. As illustrated, the Matlala and Moletsie Granites are both intrusive into the Hout River Gneiss.

The granite outcrops in both of these areas appear almost identical, and weather into huge, pink-coloured rounded boulders (Fig. 51). They appear undeformed and unaltered. Vegetation cover is quite reasonable in both areas, in the vicinity of the granites. The bright-blue haloes (inferring iron-rich weathered minerals) surrounding some granitic outcrops in figures 28 and 30 represent partially inhabited areas where vegetation cover is removed.

A photomicrograph of the Matlala Granite (sample number 4) is illustrated in figure 52. It is a medium- to coarse-grained, essentially equigranular rock comprising quartz (± 45 modal %), plagioclase (An_9; ± 5 modal %), microcline/microperthite (± 40 modal %) and biotite (± 3 modal %), and plots as a syenogranite on the QAP diagram of Streckeisen, (1976). The individual grains vary in shape from being anhedral to subhedral. Perthitic and myrmekitic exsolution textures are displayed. Greenschist facies metamorphic conditions are indicated by the presence of epidote. Trace amounts of sphene (not shown in Fig. 52) also occurs within this granite .

A photomicrograph of the Moletsie Granite (sample number 1) is illustrated in figure 53. It is a coarse-grained inequigranular rock comprising biotite (± 5 modal %), quartz (± 25 modal %), microcline (± 60 modal %) and plagioclase (An_{10}; ± 10 modal %). Trace amounts of sphene and secondary ilmenite are present. Sericitic alteration occurs within the plagioclase. The presence of epidote indicates greenschist facies metamorphism. It should be noted that the above-mentioned modal percentages are those for the entire thin section. This rock plots as a syenogranite on the QAP diagram of Streckeisen (1976).

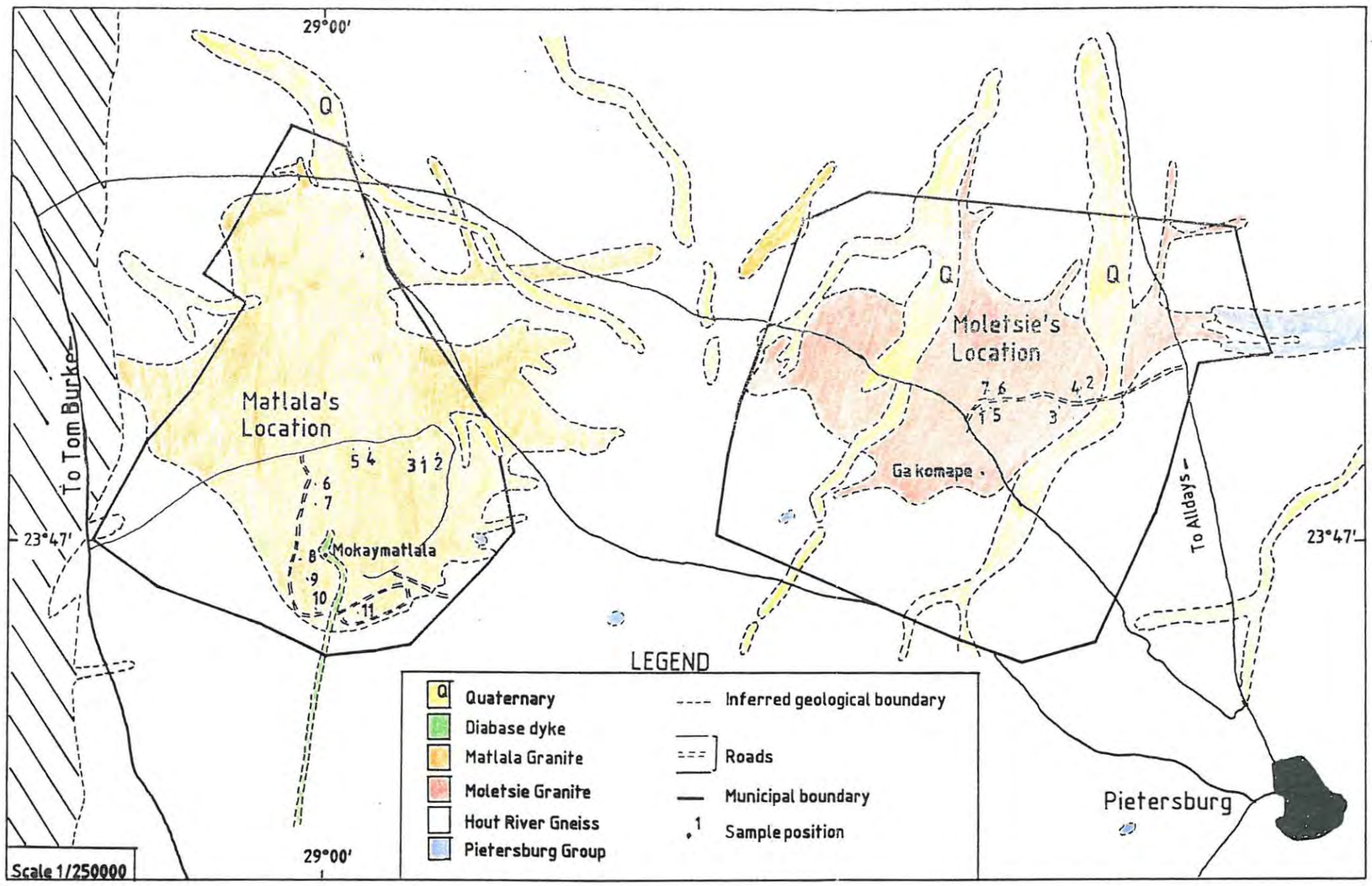

Figure 50. A geological map of the Matlala and Moletsie areas showing sample positions. This map is compiled from the 1:250000 scale published Geological Survey map '2328 Pietersburg'. Geochemical analyses (Appendix 4): RDH2834 = Matlala (5), RDH2835 = Matlala (10), RDH2836 = Moletsie (7) and RDH2836 = Moletsie (3).

Figure 51. A granite outcrop at Moletsie.

10.1. Discussion

A QAP plot of the Moletsie and Matlala Granites, that were determined by thin section analyses, is given in figure 54. As illustrated, all the samples plot as syenogranites and monzogranites. The Matlala Granites appear more quartz-rich than the Moletsie Granites. According to the magmatic hydrothermal model (Chapter 4), the syenogranite and monzogranite compositions, imply that they are unsuitable for magmatic-derived gold mineralization. Furthermore, no evidence of shearing or hydrothermal alteration is present within the granites, to satisfy the metamorphic model (Chapter 4).

It is suggested therefore, that the granites at Matlala and Moletsie are not worthy of further exploration for Archaean granite-/gneiss-hosted gold mineralization. Four geochemically analysed samples were barren in gold (Appendix 4).

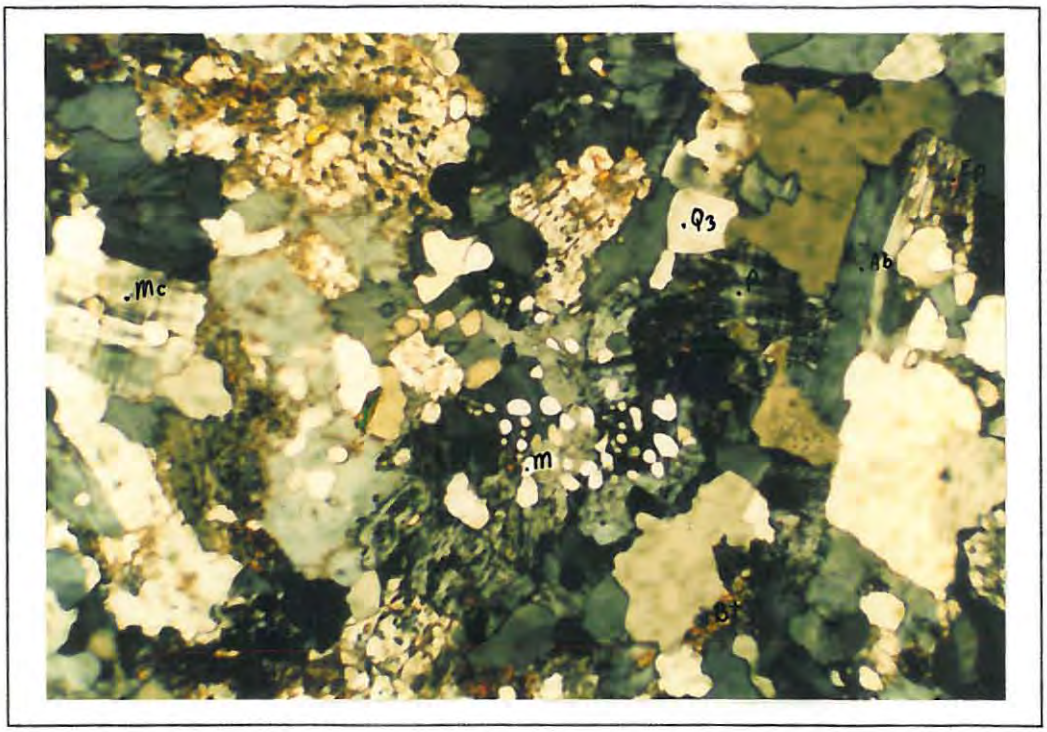

Figure 52. A photomicrograph of the Matlala Granite. It is a medium- to coarse-grained syenogranite comprising biotite (Bt), albite (Ab), quartz (Qz) and microcline (Mc). Perthitic (P) and myrmekitic (M) exsolution textures are displayed. Trace amounts of epidote (Ep) are present. Cross-polarized light. Lateral field of view = 3,5 mm.

The modal mine hosted by Zimbabwean granitic rocks occurs within 2 km of the greenstone contact, and has produced 10 - 100 kg of gold at a yield grade of 5.4 - 8.0 g/t (Mann, 1984). However, the grade and production of these gold deposits decreases exponentially with distance from the greenstone contact. This phenomenon is thought to be partly due to the increase in ferrous iron within the greenstones, which reduces the oxygen fugacity of the granitic melts and enhances the possibility of gold deposition (Mann, op. cit.). It is interesting to note that the Matlala and Moletsie Granites are approximately 30 km from the major Pietersburg greenstone belt.

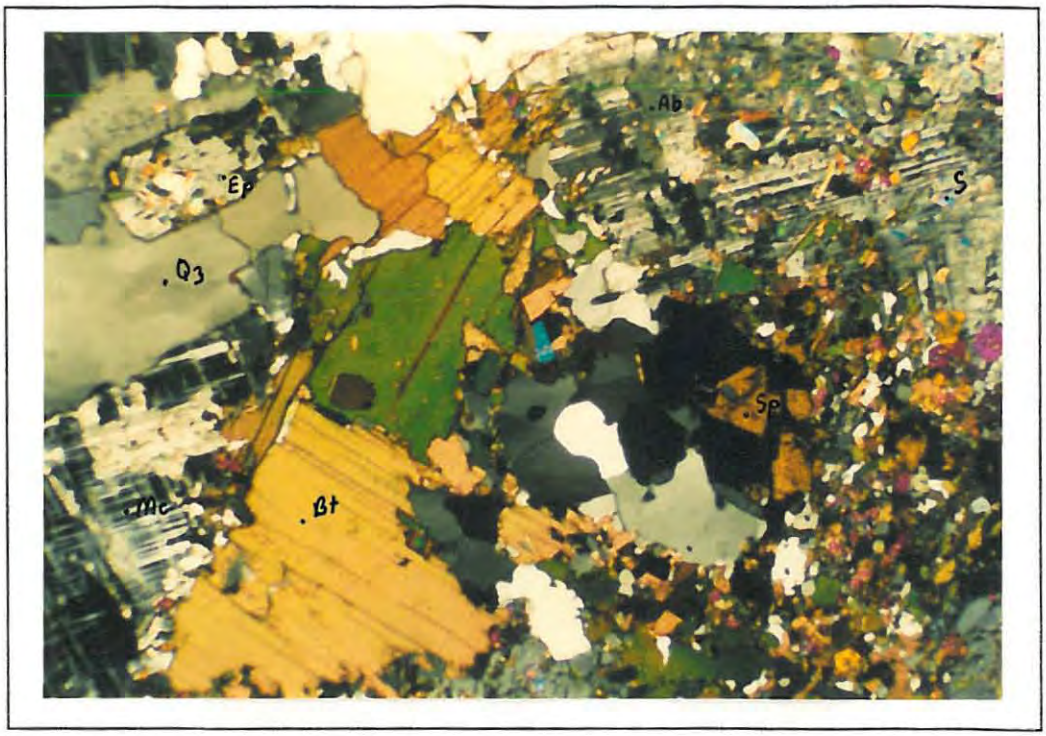

Figure 53. A photomicrograph of the Moletsie Granite. This is a coarse-grained inequigranular syenogranite comprising biotite (Bt), quartz (Qz), albite (Ab) and microcline (Mc). Trace amounts of sphene (Sp) and secondary ilmenite (Il) and epidote (Ep) are present. Sericitic alteration (S) occurs within the albite. Cross-polarized light. Lateral field of view = 3,5 mm.

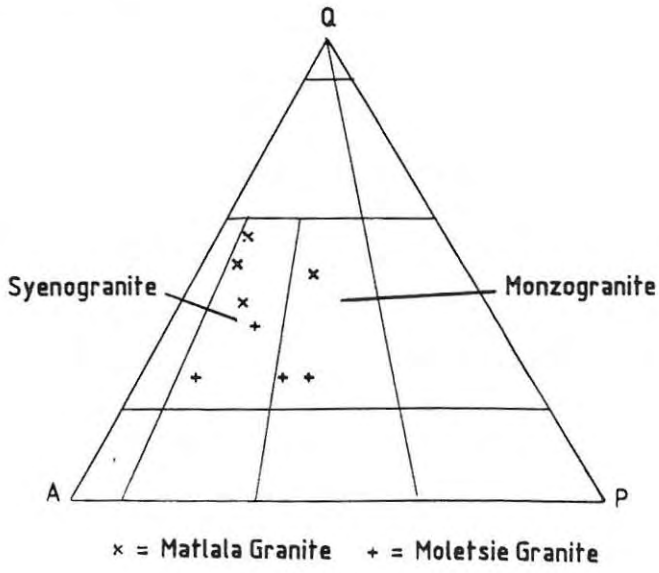

Figure 54. A Streckeisen QAP plot of the Matlala and Moletsie Granites (after Streckeisen, 1976).

11. Conclusion.

Archaean granite-greenstone terranes broadly comprise structurally complex, discontinuous greenstone belts engulfed in a sea of intruded granitic plutons, and are surrounded by extensive high-grade gneissic terranes. Gold mineralization within Archaean granite-greenstone terranes occurs both within the greenstone sequences and the granites. The gold mineralization event occurred during the late Archaean, and followed the intrusion of syn- to late-tectonic felsic plutons into previously deformed volcano-sedimentary sequences in the greenstone belts (Colvine et al., 1988). Fluid inclusion studies and isotopic data identify two possible origins for the auriferous fluids; namely metamorphic and magmatic, but cannot satisfactorily discriminate between the two.

The magmatic model of Archaean gold mineralization proposes that the hydrothermal ore fluids responsible for the gold mineralization are magmatic in origin, and are derived from granitic/porphyritic intrusions. The exploration target for Archaean granite/gneiss-hosted gold deposits according to the magmatic model, is a late Archaean, meta-aluminous, hydrothermally altered granitic intrusion associated with the third magmatic cycle (Chapter 2). The intrusion should be extensively sheared and hydrothermally altered. Magmatic-related gold mineralization generally occurs within quartz veins (concentrated near one or other of the sidewalls) and stockworks within the granites. The gold may occur in its native state, or be associated with sulphide minerals such as pyrite, arsenopyrite, scheelite, molybdenite, chalcopyrite, stibnite, pyrrhotite, galena and sphalerite (Mann, 1984). Large scale area selection criteria for this type of gold deposit are: (1) the intrusion should be of late-Archaean age, (2) it should be hydrothermally altered, and (3) possibly located within a shear zone. Smaller scale area selection criteria are: (1) the intrusion should be extensively sheared with an abundance of quartz veining, and (2) sulphide mineralization should be associated with the quartz veins and quartz stockworks.

The metamorphic replacement model, on the other hand, proposes that the hydrothermal fluids were derived by devolatization of volcanic rocks deep in the greenstone pile during prograde metamorphism at amphibolite facies,

with high geothermal gradients and in the absence of significant melting. In terms of this model, the granites commonly associated with Archaean gold mineralization may represent emplacement of magmas formed by deep crustal melting during the same thermal event that induced metamorphism in the greenstone belts at higher crustal levels. Both the granitic magmas and hydrothermal fluids used available structural channelways (Groves and Phillips, 1987).

The exploration target for Archaean granite/gneiss-hosted gold deposits according to the metamorphic replacement model is a granitic stock that has intruded a zone of crustal weakness such as a shear zone, active during the late Archaean. Alternatively, the granitic intrusion should be affected by late-Archaean shearing. Styles of deformation will depend on local P-T conditions, and will vary from brittle, to brittle-ductile and ductile deformation. This granitic intrusion should also contain hydrothermal alteration. Gold mineralization in this type of deposit occurs predominantly as submicroscopic grains within Fe-sulphides (± arsenopyrite) in the alteration assemblage rather than within penecontemporaneous to slightly later quartz veins (e.g., Groves and Phillips, 1987). Elements such as K, S, W, Ag, Sb, As and B are commonly associated with the gold. Large scale area selection criteria for metamorphic-related gold deposits in granites are: (1) The granitic intrusion should be located within a shear zone, or alternatively the granitic intrusion should be affected by regionally extensive, late Archaean shearing/deformation, and (2) the granitic intrusion should display hydrothermal alteration. Smaller scale area selection criteria are : (1) shearing within the granite and (2) sulphide mineralization together-with associated hydrothermal and possible carbonate alteration, should be present within adjacent wallrocks of the quartz veining, and in quartz stockworks.

Favourable area selection criteria for granite/gneiss-hosted gold mineralization at Roodepoort are the major ENE-trending shear zone (the Knight's Pietersburg line), the NNW-trending lineament, shearing, quartz-stockworks, hydrothermal alteration and sulphide mineralization within the Knight's Pluton.

The origin of the gold within the Knight's Pluton is uncertain. The meta-aluminous, granodioritic composition of the Lower Phase of the Knight's Pluton supports a magmatic-hydrothermal origin for the gold. Alternatively, Barton et al., (1990) proposed that during the Limpopo Orogeny, about 2700 Ma ago, the Knight's Pluton intruded into a late Archaean shear zone (the Knight's Pietersburg line) along which alteration involving CO_2 and Au mineralization were occurring, and was itself completely altered. This model is similar to the metamorphic replacement model for gold mineralization. Subsequent shearing at about 2340 Ma, remobilized and redistributed the gold into these late shears (Barton et al., op. cit.). Geochemical analyses, using the analytical techniques described in Appendix 3, shows that As is a suitable pathfinder-element for granite/gneiss-hosted gold mineralization. Ba is suitable for lithogeochemical sampling and detailed soil sampling. At present, extensive drilling is currently in progress at Roodepoort, as part of the ongoing exploration.

The only area selection criterion for granite/gneiss-hosted gold mineralization at Waterval is the sericitized granites located within the trenches. An apophysis of the granite within the greenstones assayed 860 ppb Au, but is of no economic significance. No further exploration for granite/gneiss-hosted gold mineralization is recommended in this area.

No area selection criteria for granite/gneiss-hosted gold mineralization were located at Ramagoep. The idea of a subcropping granitic intrusion with surrounding concentric fractures is completely incorrect. The clay-bearing anomaly indicated by the Clay-iron image interpretation is probably due to the weathering of the Goudplaats Gneiss to produce clay. No further exploration for Archaean granite/gneiss-hosted gold mineralization is recommended for this area.

No area selection criteria for granite/gneiss-hosted gold mineralization were located within the granites at Matlala and Moletsie. No further exploration for gold is recommended for these areas.

The MES, Clay-iron and Wallis images proved very useful in the exploration for Archaean granite/gneiss-hosted gold deposits. The MES image interpretations were successful in differentiating between granitic

outcrops (grey to brown rounded shapes), greenstones (medium brown bands), very iron-rich and mafic rocks (isolated black colours with low reflectivity), vegetation cover (varying shades of yellow, green and light-brown), soil-covered areas with sparse vegetation (purple and blue), lineaments and granite-derived soil (grey). The Clay-iron images adequately differentiated between iron-rich areas (varying shades of blue) and clay-bearing areas (yellow, orange and red). However, not all clay-bearing areas are associated with hydrothermal alteration; field checks were necessary to discriminate between weathered granites and hydrothermally altered granites. The Wallis images served to locally enhance the contrasts of the MES and Clay-iron images. Hence, although remote sensing techniques are useful in the exploration for Archaean granite/gneiss-hosted gold deposits, field checks are always necessary to confirm the interpretations.

Finally, it is interesting to note that the gold-bearing granites (located on the farms Roodepoort and Waterval) have intruded the greenstones. Possibly, the proximity of greenstone belts to the granites does have an influence on Archaean granite/gneiss-hosted gold mineralization, as discussed by Mann (1984).

12. Acknowledgements.

This thesis represents the final requirements for the M. Sc. in Economic Geology at Rhodes University, Grahamstown. I thank Mr N.J. Franey, Dr L.L. de Gasparis and Dr M. Brown of the Remote Sensing Department (Anglo American Corporation of South Africa, Limited) for organising this project, for financial assistance during the fieldwork and for logistical support. Andy Harrison, Dan Hamer and Steve Smith of the old Nelspruit Regional Office are also thanked for their co-operation and logistical support. My enthusiastic field assistants, Hendrik and Simon are thanked for their help during the fieldwork.

The co-operation of the Bursaries and Scholarship Unit (Anglo American Corporation of South Africa, Limited) is gratefully acknowledged for allowing me to partake in this course, and for providing financial assistance for this thesis.

Professors' F. Pirajno, J.E. Moore, R.E. Jacob and J. Marsh, and Mr C.A. Mallinson must be thanked for their helpful discussions regarding this thesis. Bernd Teigler, Wolfgang Maier, Hugh Smithies, Marilena Moroni, Tom Nowicki, Derek Whitfield, Angela Riganti, Ben Joubert, Murray Biedler, Johan Stiefenhoffer and Ross Whittle-Herbert are also thanked for their useful discussions.

Mr Jim Caulkin, Clive Bradley, Dougall Fraser, Johan Grobler and Pierre Coffee of Freegold South, Welkom, are thanked for allowing me the necessary time off to complete this thesis. Sharon Monaghan deserves special mention for draughting my maps. The staff at the training centre of 1 Shaft, President Steyn Mine are thanked for allowing me to use their printing facilities.

13. References.

Anhaeusser, C.R., Mason, R., Viljoen, M.J. and Viljoen, R.P. (1969). A reappraisal of some aspects of Precambrian shield geology. *Geol. Soc. Amer. Bull.*, **80**, p. 2175 - 2200.

Anhaeusser, C.R., (1973). The evolution of the early Precambrian crust of southern Africa. *Phil. Trans. Roy. Soc. Lond.*, **A273**, p. 359 - 388.

Anhaeusser, C.R., (1976). Archaean metallogeny in southern Africa. *Econ. Geol.*, **71**, p. 16 - 43.

Anhaeusser, C.R. and Robb, L.R., (1980). Magmatic cycles and the evolution of the Archaean granitic crust in the eastern Transvaal and Swaziland. *Econ. Geol. Res. Unit, Univ. Witwatersrand, Inf. Circ.*, **144.**, 11 pp.

Anhaeusser, C.R. and Viljoen, M.J., (1986). Archaean Metallogeny of Southern Africa. 33 - 42. *In*: Annhaeusser, C.R., and Maske, S., (Eds.), *Mineral Deposits of Southern Africa*, **I**. *Geol. Soc. S. Afr.*, 1020 pp.

Barley, M.E. and Groves, D.I., (1990). Deciphering the Tectonic Evolution of Archaean Greenstone Belts: the importance of Contrasting Histories to the Distribution of Mineralization in the Yilgarn Craton, Western Australia. *Precambrian Research*, **46**, p. 3 - 20.

Barton, J.M., Byron, C.L. and Klemd, R., (1986). The setting of some gold mineralization on the farms Eerstelling and Roodepoort, Pietersburg Greenstone belt. *Ext. Absts., Geocongress '86, Geol. Soc. S. Afr., Johannesburg.*

Barton, J.M., Jr and Ryan, B., (1977). A review of the geochronologic framework of the Limpopo Mobile Belt: *Bull. geol. Surv. Botswana*, **12**, p. 183 - 200.

Barton, J.M., Jr., Klemd, R., Byron, C.L., and Beattie, M., (1990). *Albitization and the gold-bearing Roodepoort Pluton, Pietersburg granite-greenstone Terrane, South Africa.* Trans. Geol. Soc. S. Afr., **93**, p. 776 - 784.

Binns, R.A., Gunthorpe, R.J. and Groves, D.I., (1976). Metamorphic patterns and devolopment of greenstone belts in the eastern Yilgarn Block, Western Australia. *In:* B.F. Windley (ed.). *The early history of the earth.* Wiley, London, p. 303 - 313.

Brandl, G., (1986). The Geology of the Pietersburg Area. *Unpubl. rep., Geol. Surv. S. Afr.*, 43 pp.

Burger, A.J. and Coertze, F.J., (1977). Summary of age determinations carried out during the period April, 1974 to March, 1975. *Ann. Geol. Surv. S. Afr.*, **11**, p. 323 - 329.

Burger, A.J. and Walraven, F., (1977). Summary of age determinations carried out during the period April 1975 to March 1976: *Ann. geol. Surv. S. Afr.*, **11**, p. 323 - 329.

Burger, A.J. and Walraven, F., (1979a). Summary of age determinations carried out during the period April 1976 to March 1977: *Ann. geol. Surv. S. Afr.*, **12**, p. 199 -207.

Burger, A.J. and Walraven, F., (1979b). Summary of age determinations carried out during the period April 1977 to March 1978: *Ann. geol. Surv. S. Afr.*, **12**, p. 209 - 218.

Burley, A.J., Evans, R.B., Gillingham, J.M. and Masson Smith, D., (1970). Gravity anomalies in Swaziland. *Geol. Surv. Mines Dept. Swazld., Bull.* **7**, p. 4 - 16.

Burnham, C.W., (1979). Magmas and hydrothermal fluids. *In:* H.L. Barnes (ed.), *Geochemistry of Hydrothermal Ore Deposits, 2nd edit.* John Wiley and Sons, Inc., p. 71 - 136.

Burnham, C.W. and Ohmoto, H., (1980). Late-stage processes of felsic magmatism. *Mining Geology Special Issue*, **8**, p. 1 - 11.

Burrows, D.R., Thomas, A.V. and Spooner, E.T.C., (1986). A magmatic origin for Archaean gold-quartz vein mineralization in the Mink Lake granodiorite stock, NW Ontario, and from the Hollinger Au deposit, Timmins, Ontario. *In:* Geocongress '86: Extended Abstracts. *Geol. Soc. S. Afr.*, p. 283 - 286.

Burrows, D.R. and Spooner, E.T.C., (1987). Generation of a magmatic H_2O-CO_2 fluid enriched in Mo, Au and W within an Archaean sodic granodiorite stock, Mink Lake, northwestern Ontario. *Econ. Geol.*, **82**, p. 1931 - 1957.

Burrows, D.R. and Spooner, E.T.C., (1988). Relationships between Archaean Au-quartz veins/shear zone mineralization and igneous intrusions in the Val d'Or and Timmins areas, Abitibi sub-Province, Canada; the geochemical characteristics of gold related magmas. *In:* A.D.T. Goode and L.I. Bosma (eds.), *Bicentennial Gold '88: Extended Abstracts - Oral Programme*. Geol. Soc. Aust., p. 302 - 306.

Byron, C.L. and Barton Jr., J.M., (1990). The setting of mineralization in a portion of the Eersteling goldfield, Pietersburg granite-greenstone terrane, South Africa. *Trans. Geol. Soc. S. Afr.*, **93**, p. 463 - 472.

Cameron, E.M. and Hattori, K., (1987). Archaean gold mineralization and oxidized hydrothermal fluids. *Econ. Geol.*, **82**, p. 1177 - 1191.

Carmichael, I.S.E., Turner, F.J. and Verhoogen, J., (1974). *Igneous petrology*. McGraw Hill, Inc., 739 pp.

Colvine, A.C., Fyon, J.A., Heather, K.B., Marmont, S., Smith, P.M. and Troop, D.G., (1988). Archaean Lode gold deposits of Ontario. *Ontario Geol. Surv., Misc. Pap.*, **139**, 136 pp.

Condie, K.C., (1989). *Plate Tectonics and Crustal Evolution.* Pergammon Press. 476pp.

Darracott, B.W., (1975). The interpretation of the gravity-anomaly over the Barberton Mountain Land, South Africa. *Geol. Soc. S. Afr., Trans.*, **78**, p. 123 - 128.

de Beer, J.H., Stettler, E.H., Duvenhage, A.W.A., Joubert, S.J. and Raath, C.J. de W., (1984). Gravity and geoelectrical studies of the Murchison greenstone belt., South Africa. *Geol. Soc. S. Afr., Trans.*, **87**, p. 347 - 359.

de Wit, M.J., Fripp, R.E.P. and Stanistreet, I.G., (1982). Tectonic and stratigraphic implications of new field observations along the southern part of the Barberton greenstone belt. *Geol. Soc. S.A. Special Publi.* **9**, p. 21 - 29.

de Wit, M.J., (1984). *Geology of the Pietersburg Greenstone Belt*. Progress Report to Anglo American (unpubl.), Anglo American Prosp. Serv. Ltd., Nelspruit, pp. 28.

de Wit, M.J., (1990). Low grade, least deformed lithologies in the Pietersburg greenstone belt. *In:* D.D. van Reenen and C. Roering (Eds.), *The Limpopo belt, a field workshop on granulites and deep crustal tectonics*. Rand Afrikaans University publication, Johannesburg, p. 61 - 68.

de Wit, M.J., (1991). Archaean greenstone belt tectonism and basin development: some insights from the Barberton and Pietersburg greenstone belts, Kaapvaal Craton, South Africa. *Journ. of Afr. Earth Sci.*, **13(1)**, p. 45 - 63.

Drury, S.A., (1987). *Image Interpretation in Geology*. Allen and Unwin.

Du Toit, M.C., (1979). *Die geologie en struktuur van die gebiede Levubu en Bandelierkop in Noord-Transvaal*: Ph.D. thesis, Rand Afrikaans University, (unpubl.).

Eisenlohr, B.N., Groves, D. and Partington, G.A., (1989). Crustal-scale shear zones and their significance to Archaean gold mineralisation in Western Australia. *Mineral. Deposita* **24**, 1 - 8.

Feather, C.E. and Baumgartner, F.C., (1983). Simultaneous Determination of 36 Elements By X-Ray Fluorescence Spectrometry as a Prospecting Tool. *In*: Hubbard, R.H., Barrett, C.S., Predecki, P.K. and Leyden, D.E., (eds.), *Advances in X-ray analysis, Vol. 26.*

Franey, N.J., (1987). *A Geological Model Of Shear Zone Gold Deposits* In *The Pietersburg Greenstone Belt, South Africa*. M. Sc. thesis (unpubl.), Rhodes Univ., Grahamstown, 114 pp.

Fyfe, W.S. and Kerrich, R., (1984). Gold: natural concentration processes. *In*: R.P. Foster (ed.), *Gold '82: the Geology, Geochemistry and Genesis of Gold Deposits*. Balkema, Rotterdam, p. 99 - 127.

Fyon, A., MacDonald, A.J., Marmont, S. and Troop, G., (1988). Shield wide introduction of gold into Archaean crust, Superior Province, Ontario: Coupling between mantle initiated magmatism and lower crustal maturation. *In:* A.D.T. Goode and L.I. Bosma (eds.), *Bicentennial Gold '88: Extended Abstracts - Oral Program*. Geol. Soc. Aust., p. 313 - 318.

Grobler, N.J., (1972). *The geology of the Pietersburg Greenstone Belt*. PhD-thesis (unpubl.), University of Orange Free State, Bloemfontein, 156 pp.

Groves, D.I. and Batt, W.D. (1984). Spatial and temporal variations of Archaean metallogenic associations in terms of evolution of granite-greenstone terranes with particular emphasis on the Western Australian Shield. *In*: Kroner, A., Hanson, G.H. and Goodwin, A.M., (Eds.), *Archaean Geochemistry*. Springer - Verlag, Heidelberg. p. 73-98.

Groves, D.I. and Phillips, G.N., (1987). The genesis and tectonic control on Archaean gold deposits of the Western Australian Shield - A metamorphic replacement model. *Ore Geol. Rev.*, **2**, p. 287 - 322.

Groves, D.I., Barley, M.E., Cassidy, K.C., Hagermann, S.G., Ho, S.E., Hronsky, J.M.A., Mikicki, E.J., Muellar, A.G., McNaughton, N.J., Perring, C.S. and Ridley, J.R., (1991). Archaean lode-gold deposits: The products of crustal-scale hydrothermal systems. *In:* E.A. Ladeira (ed.)., *Proceedings of Brazil Gold '91, An International Symposium on the Geology of Gold: Belo Horizonte, 1991*. A.A. Balkema, Rotterdam, p. 299 - 305.

Henley, R.W., (1973). Solubility of gold in hydrothermal chloride solutions. *Chemical Geology*, 11, p. 73 - 87.

Hodgson, C.J. and Troop, D.G., (1988). A new computer-aided Methodology for Area Selection in Gold Exploration: a Case Study from the Abitibi Greenstone Belt, Ontario. *Econ. Geol.*, 83, p. 952 - 977.

Hodgson, C.J., (1990). Uses (and Abuses) of Ore Deposit Models in Mineral Exploration. *Geoscience Canada*, 17(2), p. 79 -89.

Hunter, D.R., (1991). Crustal processes during Archaean evolution of the southeastern Kaapvaal Province. *Journ. of Afr. Earth Sci.*, 13 (1), p. 13 - 25.

Jantsky, G.J., (1978). The geology of the Bosbult and Munnik areas (Sheets 2329 DA and DB): *Unpubl. Rep. geol. Surv. S. Afr.*

Jones, M.G., (1990). *The geology of the Mount Mare area, Pieterburg greenstone belt, South Africa*. PhD-thesis (unpubl.), Imperial College, Univ. London, 298 pp.

Keays, R.R., (1984). Archaean gold deposits and their source rocks: the upper mantle connection. *In:* R.P. Foster (ed.), *Gold '82: The Geology, Geochemistry and Genesis of Gold Deposits*. A.A. Balkema, Rotterdam, p. 17 - 51.

Kerrich, R., (1986). Fluid infiltration into fault zones: chemical isotopic and mechanical effects. *Pure Appl. Geophys., Vol. 124*, p. 225 - 244.

Levinson, A.A., (1980). *Introduction to Exploration Geochemistry (second edition)*. Applied Publishing Ltd, 924 pp.

Lillesand, T.M. and Kiefer, R.W., (1987). *Remote Sensing and Image Interpretation (Second Edition)*. John Wiley and Sons, New York. 721 pp.

Mann, A.G., (1984). Gold mines in Archaean granitic rocks in Zimbabwe. *In:* R.P. Foster (Editor), *Gold '82: The Geology, Geochemistry and Genesis of Gold Deposits*. Balkema, Rotterdam, p. 553 - 568.

Neall, F.B., (1985). *Application of thermodynamics to the study of two Archaean hydrothermal gold deposits in Western Australia.* Ph.D. thesis, Univ. of Western Australia, Nedlands, W.A. (unpubl.).

Neall, F.B., (1987). Sulphidation of iron-rich rocks as a precipitation mechanism for large Archaean gold deposits in Western Australia: thermodynamic confirmation. *In*: Ho, S.E., Groves, D.I. (eds.). *Recent advances in understanding Precambrian gold deposits.* Geol. Dept. and Univ. Extension, Univ. West. Australia Publ., **11**, p. 265 - 269.

Ohmoto, H. and Rye, R.O., (1979). Isotopes of sulphur and carbon. *In:* H.L. Barnes (ed.), *Geochemistry of Hydrothermal Ore Deposits, 2nd edit.*, John Wiley and Sons, Inc., p. 509 - 567.

Perring, C.S., Groves, D.I. and Ho, S.E., (1987). Constraints on the source of auriferous fluids for Archaean gold deposits. *In:* S.E. Ho and D.I. Groves (eds.), *Recent Advances in Understanding Precambrian Gold Deposits.* Geology Dept. and Univ. Extension, Univ. Western Australia, Publ., **11**, p. 287 - 306.

Perring, C.S., Groves, D.I., Shellabar, J.N. and Hallberg, J.A., (1991). The 'porphyry-gold' association in the Norseman-Wiluna Belt of Western Australia: implications for models of Archaean gold metallogeny. *In:* I. Haapala and K.C. Condie (eds.), *Precambrian Granitoids-Petrogenesis, Geochemistry and Metallogeny.* Precambrian Res., **51**, p. 85 - 113.

Peters, W.C., (1978). *Exploration and Mining Geology.* John Wiley & Sons, New York. 696 pp.

Phillips, G.N. and Groves D.I., (1983). The nature of Archaean gold-bearing fluids as deduced from gold deposits of Western Australia. *Jour. Geol. Soc. Aust.*, **30**, p. 25 - 39.

Phillips, G.N., (1985). Interpretation of Big Bell/Hemlo-type gold deposits: precursors, metamorphism, me;ting and genetic constraints. *Trans. Geol. Soc. S. Afr.*, **88**, p. 159 - 173.

Potgieter, G.J.A., (1976). Geologiese verslag oor kartering van 1:50000 velle Pietersburg 2329CD, Ga Mashashane 2329CC en Limburg 2328DD: *Unpubl. Rep. geol. Surv. S. Afr.*

Reedman, J.H., (1979). *Techniques in Mineral Exploration.* Applied Science, 533 pp.

Roberts, R.G., (1987). Ore deposit Models #11. Archaean Lode Gold Deposits. *Geoscience Canada*, 14, p. 37 - 52.

Robertson, I.D.M., (1976). The geology of the country around Battlefields. *Geol. Surv. Rhod., Bull. 76*, 258 pp.

Roering, C. et al. (14 authors), 1990a. A geotransect across the Limpopo belt (Extended Abstracts). *In:* J.M. Barton (ed.). *A geotransect across the Limpopo Belt: a field workshop on granulites and deep crustal tectonics.* Rand Afrikaans Univ., Johannesburg, p. 105 - 106.

Roering, C., Barton, J.M., Jr. and Winter, H. de la R. (1990b). The Vredefort structure: a perspective with regard to new tectonic data from adjoining terranes. *Tectonophysics*, 171, p. 7 - 22.

Saager, R. and Meyer, M., (1984). Gold distribution in Archaean granitoids and supracrustal rocks from southern Africa: A comparison. *In:* R.P. Foster (ed.), *Gold '82: The Geology, Geochemistry and Genesis of Gold Deposits.* A.A. Balkema, Rotterdam, p. 53 - 70.

Sabins, F.F., (1983). *Remote sensing laboratory manual (second edition).* Remote Sensing Enterprises, La Habra, Calif.

Sabins, F.F., Jr., (1987). *Remote Sensing Principles and Applications (Second Edition).* Freeman and Co., New York. 449 pp.

Seward, T.M., (1979). Hydrothermal transport and deposition of gold. *In:* J.E. Glover and D.I. Groves (eds.), *Gold Mineralization.* Univ. Western Australia. Geol. Dept. Ext. Service, Publ., 3, p. 56 -65.

Seward, T.M., (1984). The transport and deposition of gold in hydrothermal systems. *In*: R.P. Foster (ed.), Gold '82. *The Geology, Geochemistry and Genesis of Gold Deposits*. Balkema, Rotterdam, p. 165 - 181.

Smit, C.A., Roering, C., Van Reenen, D.D. and Barton, J.M., Jr. (1988). Deep crustal deformation in the Limpopo belt and adjacent granite-greenstone terranes. *Extended Abstracts Geocongress 1988, Geol. Soc. S. Afr.*, p. 567 - 570.

South African Committee for Stratigraphy (SACS), (1980). Stratigraphy of South Africa. Part 1 (Comp. L.E. Kent). *Lithostratigraphy of the Republic of South Africa, South West Africa/Namibia and the Republic of Bophutatswana, Transkei and Venda*. Geological Survey of South Africa, Handbook 8, Pretoria, 690 pp.

Spooner, E.T.C., (1991). The magmatic model for the origin of Archaean Au-quartz vein ore systems: An assessment of the evidence. *In:* E.A. Ladeira (ed.), *Proceedings of Brazil Gold '91, An International Symposium on the Geology of Gold: Belo Horizonte*. A.A. Balkema, Rotterdam, p. 313 - 318.

Stagman, J.G., (1961). The geology of country around around Sinoia and Banket, Lomagundi District. *Geol. Surv. Rhod., Bull. 49*, 107 pp.

Streckeisen, A., (1976). To each plutonic rock its proper name. *Earth Sci. Rev., 12*, p. 1 - 33.

Van Reenen, D.D., Barton, J.M., Jr., Roering, C., Smit, C.A. and Van Schalkwyk, J.F. (1987). Deep crustal response to continental collision: the Limpopo belt of southern Africa. *Geology*, **15**, p. 11 - 14.

Van Reenen, D.D., Roering, C., Smit, C.A., Van Schalkwyk, J.F. and Barton, J.M., Jr., (1988). Metamorphic evolution of the northern high-grade margin of the Kaapvaal craton, South Africa. *Jour. Geol.*, **96**, p. 549 - 560.

Van Wyk, J.P., (1977). Geologiese verslag van die gebied 2329C Pietersburg: *Unpubl. Rep. geol. Surv. S. Afr.*

Walraven, F., Burger, A.J. and Allsop, H.L., (1981). Summary of age determinations carried out during the period April 1979 to March 1980: *Ann. Geol. Surv. S. Afr.*, **15(1)**, p. 89 - 94.

Walraven, F., Armstrong, R.A. and Kruger, F.J., (1990). A chronological framework for the north-central Kaapvaal Craton, the Bushveld Complex and the Vredefort Structure. *Tectonophysics*, **171**, p. 23 - 48.

Watkins, K.P., Fletcher, I.R. and de Laeter, J.R., (1991). Crustal evolution of Archaean granitoids in the Murchison Province, Western Australia. *Precambrian Res.*, **50**, p. 311 - 336.

Whitney, J.A., (1988). The origin of granite: The role and source of water in the evolution of granitic magmas. *Geol. Soc. of America Bulletin*, **100**, p. 1886 - 1897.

Willemse, J., (1938). The gold occurrences south-west of Pietersburg. *Bull. Geol. Surv. S. Afr.*, No. 12, pp. 38.

Windley, B.F., (1984). *The Evolving Continents* (second edition). John Wiley and Sons, 399 pp.

Winkler, H.G.F., (1979). *Petrogenesis of Metamorphic Rocks*. Springer-Verlag, New York. 348 pp.

Wood, P.C., Burrows, D.R., Thomas, A.V. and Spooner, E.T.C., (1986). The Hollinger-McIntyre Au-quartz vein system, Timmins, Ontario, Canada; geologic characteristics, fluid properties and light stable isotope geochemistry. *In:* MacDonald, A.J., (ed.), *Gold '86: Proceedings Volume, Toronto, Canada*. p. 56 - 80.

Appendix 1: The Exploration of Archaean granite/gneiss-hosted gold deposits

The objective of mineral exploration is to focus attention progressively on the most favourable parts of an area, so that as exploration proceeds, the chances of an economic mineral deposit being found continuously increases (Hodgson, 1990). Two factors are critical to a good exploration strategy; namely:

1) optimizing on the cost in relation to the effectiveness of methods used to determine the presence or absence of features on which the area selection process is based, and

2) using the appropriate criteria for exploration area selection. Large scale area selection criteria define the geological environment which is favourable for mineralization, whilst the smaller scale features define the deposit (e.g., Fig. 55). These area selection criteria should be relatively easily identified by field techniques (Hodgson, op. cit.).

As described in Section 4.4., large scale area selection criteria for magmatic-related gold deposits within granites are: (1) the intrusion should be of late-Archaean age, (2) it should be hydrothermally altered, and (3) possibly be located within a shear zone. Smaller scale area selection criteria are: (1) the intrusion should be extensively sheared with an abundance of quartz veins in brittle and brittle-ductile fractures, and (2) sulphide mineralization should be associated with these quartz veins (concentrated near one or other of the sidewalls), and also quartz stockworks.

Large scale area selection criteria for metamorphic-related gold deposits in granites are: (1) the granite intrusion should be located within a shear zone, or alternatively the granite intrusion should be affected by regionally extensive, late-Archaean shearing/deformation, and (2) the granite intrusion should display hydrothermal alteration. Smaller scale area selection criteria are: (1) shearing within the granite. The style of shearing could vary from brittle to brittle-ductile to ductile, depending on the grade of local metamorphism, and (2) sulphide mineralization together-with associated hydrothermal and carbonate alteration should be present within the immediate wallrocks of the quartz veining, and in quartz stockworks.

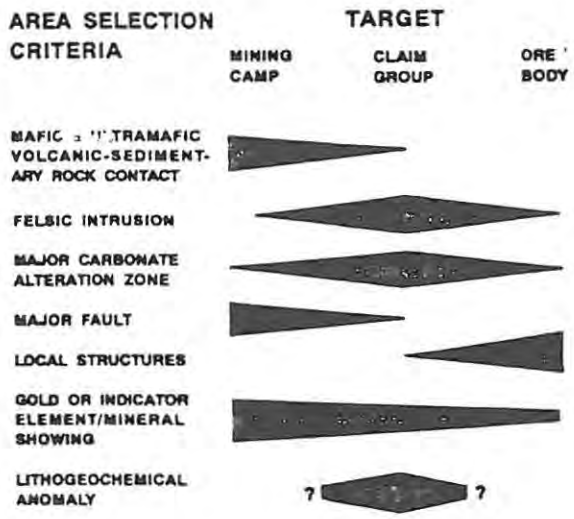

Figure 55. Diagrammatic illustration showing how the distinction between geological characteristics of the 'deposit', and the geological characteristics of the 'deposit environment' depends on the scale of the geological feature associated with mineralization (after Hodgson, 1990).

Pathfinder-elements for geochemical exploration depend on the type of sampling being undertaken, the sampling media and associated Eh/Ph conditions, local geographic and climatic conditions, the type of geochemical analyses available to exploration geologists and the phase of exploration involved. As discussed in Section 4.4., suggested pathfinder-elements/ratios for Archaean granite/gneiss-hosted gold deposits are as follows:

Lithogeochemical samples: Ba, Cu, Mo, K/Na, Sb and As.
Stream sediment samples: Mo and As.
Soil samples: Mo, As and Cu.
Ba and Sb (for more detailed soil surveys).

Prior to proceeding with the exploration, it is useful to do an orientation survey over an orebody, similar to those being explored for. The orientation survey should establish the local geographical conditions under which the exploration is to proceed, and the response of the exploration techniques to be used in the particular phase of exploration (e.g., LANDSAT images and geochemical analyses techniques available for the exploration

program). In addition, a vertical profile of the gold deposit (perhaps an old drill core) should be examined/logged, and the nature of the mineralization determined (Peters, 1978). The Knight's Pluton at Roodepoort is a known gold deposit, hosted by altered granodioritic intrusion within the Pietersburg granite-greenstone terrane, and served as an orientation survey for this project (see Chapter 7).

The exploration sequence is displayed in figure 56. As illustrated, each exploration phase is separated by a decision point, prior to proceeding to the next exploration phase. Ideally, the exploration techniques used in each exploration phase should have the lowest cost/benefit ratio. The 'Regional Area Selection' phase of exploration that is applicable to this project, and proposed programs for further exploration are described below.

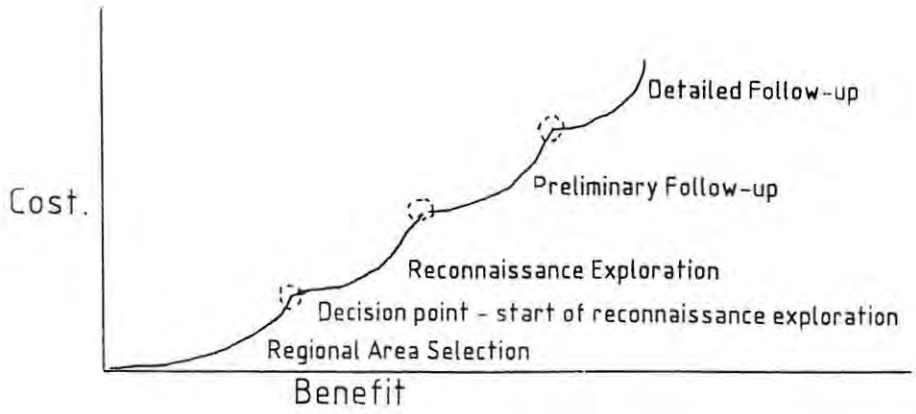

Figure 56. Diagrammatic representation of the exploration sequence, in terms of cost/benefit ratio. The optimal exploration strategy is that succession of exploration activities which in aggregate has the lowest total cost, relative to the economic return. Each type of exploration activity gives a diminishing return on investment as it is pursued, and is replaced by the next most cost-efficient type of activity at the decision points where the size of the area being explored is reduced (after Hodgson, 1990).

Regional Area Selection

Area selection in mineral exploration is based on the presence or absence of the above-mentioned 'area selection criteria' (Hodgson, 1990). In this project, the use and interpretation of LANDSAT images formed an integral part of the exploration techniques (Fig. 2); to assess their usefulness in the exploration of Archaean granite/gneiss-hosted gold deposits. They also represent a potentially cost-effective exploration tool; an important component of a good exploration strategy (Hodgson, op. cit.). The LANDSAT images used in this project were processed and made available by the **Remote Sensing Department, Anglo American Corporation of South Africa Limited.** The images were interpreted with emphasis on identifying possible large-scale 'area selection criteria' described above.

The fieldwork consisted of locating the latter features on the ground and carrying out preliminary exploration for both large and smaller scale 'area selection criteria'. This involved geological mapping and trenching where necessary, and the collection of lithogeochemical samples. Representative samples were analyzed by fire assay for gold and the multi-element XRF (X-ray fluoresence) analytical technique available to exploration geologists of A.A.C. (Appendix 3). Laboratory work involved petrographic examinations of selected granitic samples from each of the five areas chosen for exploration; to determine their approximate modal compositions and types of alteration.

Finally, recommendations for the future of each area, in terms of gold exploration, were offered. The recommendation for the 'Regional Area Selection' phase of exploration to be upgraded to the 'Reconnaissance' phase of exploration (Fig. 56) is based on the presence of 'area selection criteria' within the selected areas chosen for exploration.

Reconnaissance Exploration

Having established the presence of 'area selection criteria' within an area selected for exploration, the next stage is to use appropriate rapid sampling techniques that are able to delineate mineralized areas for follow-up studies, and eliminate barren ground. It must be recognised that

most potential orebodies discovered during present-day exploration are likely to be blind deposits. The resultant geochemical anomalies caused by these potential orebodies at surface will probably be very subtle. Initially, the best technique for reconnaissance exploration is stream sediment sampling. An orientation exercise should be conducted within the streams to determine the the optimum size sampling fraction. An initial sample spacing of 400m is recommended. In addition, every confluence must be sampled; slightly upstream.

The stream sediment analyses should be plotted on sampling map overlays, and as cumulative frequency diagrams on log-probability graph paper; to enable the different sample populations (i.e. background and anomalous) to be determined with a reasonable level of confidence. The decision to proceed to the 'Preliminary Follow-up' phase of exploration is based on whether suitable anomalies exist. According to Levinson (1980), at least two contiguous anomalous samples are necessary for mineralization to be considered significant. Reedman (1979) stated that the average abundance of As and Mo within stream sediments are 1-50 ppm and 1-5 ppm, respectively.

Preliminary Follow-up Phase of Exploration

Having established the existence of a geochemical anomaly, its source must be located, and cause determined. Closer spaced stream sediment sampling followed by bank sampling, where possible, are proposed as methods of isolating the source and possible causes of the anomaly. Examples of causes may be actual mineralization, groundwater seepages, contamination, etc..

The next step in the follow-up work is a soil sampling program within the drainage basin of the anomalous stream sediments. A soil sampling grid is suggested for the areas selected for exploration in this project. The base line of the grid should be placed subparallel to the strike of major shears or lineaments in the area, and the soil samples should be collected at right angles to the strike of the base line. If shear zones or lineaments are absent, a square or rectangular shaped grid should be used. As the most likely gold deposit is shear-zone hosted, the grid needs to have a reasonably narrow spacing, such as 100m by 50m. A big problem regarding soil geochemistry however, especially in a long-established gold producing

area such as the Pietersburg granite-greenstone terrane, is contamination from pre-existing gold workings, and should be borne in mind during any interpretation of soil geochemical data. Analyses should be plotted, as grid overlays and contoured. Geophysical techniques such as ground magnetometer surveys and IP surveys are recommended as an aid to locate shear zones and to indicate areas of possible disseminated mineralization.

Ideally, a small orientation soil sampling program should be done at the relevant area, prior to the follow-up soil sampling program. Soil samples should be taken from the B-horizon of the soil profile, and sieved to various mesh sizes, prior to being submitted for XRFME analyses (Appendix 3). The mesh size with optimum Cu, As and Mo values should be used. The decision to proceed to the 'Detailed' phase of exploration is based on a significant non-cultural anomaly being located.

Detailed Exploration Phase

Detailed exploration involves evaluating anomalies and outlining the location of mineralization as closely as possible prior to drilling or initiating major surface/subsurface excavations (e.g., extensive trenching, adits), (Levinson, 1980). The anomalous area located during the 'Preliminary Follow-up' phase of exploration should be soil sampled, using a smaller spaced grid of 50m by 25m. The soil samples should be analyzed for Au, Cu, As, Ba and Sb using atomic absorption spectroscopy (AAS). Results should also be plotted as grid overlays and and anomalous areas determined. These areas should be geologically mapped at a scale of 1:500 or 1:1000, and lithogeochemical samples collected where possible. The lithogeochemical samples should be collected along traverses at regularly spaced intervals within the mapping area, and analyzed using the above-mentioned technique for K and Na in addition to Au, Cu, As, Ba and Sb. The increasing K/Na ratio can be used as an indicator of hydrothermal alteration. If no outcrop exists, at least one percussion drill hole in the most anomalous area is recommended. The samples should be analyzed as described above.

Particular attention must be given to locating shears, quartz-carbonate veins and alteration-types (phyllic, propylitic, potassic, carbonatization,

alunitization) during the geological mapping. Alteration is often revealed by a bleached appearance on weathered surfaces, although some surfaces are reddish due to iron-staining, and others are black due to manganese oxide staining. Where possible, thin-section petrographic work should be done in conjunction with the geological mapping as an aid for identifying the different haloes of hydrothermal alteration. Gold mineralization is usually greatest in the potassic and phyllic alteration zones, alongside shears and in areas of quartz-carbonate veining. The recognition of the propylitic alteration halo is however, important for exploration purposes.

As described in Section 4.4., the anomalous area located during the 'Detailed Exploration Phase' is considered to be a gold deposit if gold assays indicate values of 1g/metric ton over widths of at least several metres, or higher grades over narrower widths and/or verbal descriptions that indicate such values (e.g. Hodgson and Troop, 1988).

The decision to further evaluate the prospect depends on numerous factors such as Company policy, gold price, the economic climate, logistical factors (e.g., availability of electricity, ease of access, type of mining required, mining costs) and political climate. At a present gold price of approximately R35000/kg and total operating costs of about R30000/kg for underground gold mining operations, it is suggested that an open pit operation is the only viable economic target. Ideally, the mineralized granite should be in a semi-weathered state to keep processing costs such as crushing at an absolute minimum.

Appendix 2. LANDSAT Images

The images used in this project are acquired from the 'Earth Observation Satellite Company', USA; and originates from the LANDSAT 5 satellite launched in 1984. They are received in the form of a computer compatible tape, and are processed on a VAX 8600 computer using Anglo American Corporation 'in house' computer programs written by Dr Neil Pendock.

The LANDSAT 5 satellite has a thematic mapper (TM), which contains six sensors each with a resolution of 30m x 30m. An additional sensor in the thermal infra-red band has a resolution of 120m x 120m.

The above sensors cover the various wavebands of the electromagnetic spectrum as shown in Table 3.

Each of the sensors gather data simultaneously, but are restricted to their individual wavebands. The data in each sensor is collected as picture elements (pixels). Each pixel has a digital number (DN) assigned to it, and this represents the energy associated with the range of EMR wavelengths to which each detector is sensitive (Drury, 1987). For the visible and near-infrared range, the energy is that reflected by the earth's surface together with a minor component scattered by the atmosphere. The data are stored as electrical potentials produced in a radiation detector by photons. These potentials are rescaled and transmitted to an earth receiving station as an 8-bit binary digit number.

The DN's from the different bands for a particular pixel along a particular line coincide with one another. Therefore the data obtained from the different sensors can be correlated. As this data is in digital form, it can be manipulated using various mathematical techniques during the various processes neccessary for the final product. These processes consist mainly of pre-processing and image enhancement, and are described below. Details of these processes are obtained mainly from Sabins Jr., (1987), and will not be specifically referenced.

Preprocessing

Preprocessing involves applying corrective proceedures such as replacing dropped lines and geometrical corrections on original data. Dropped lines occur due to brief failures in the circuits of a detector which results in spurious signals during a scan. Geometrical rectification takes curvature of the earth into account, and converts the position of pixels to a two-dimensional space.

Image Enhancement

Image enhancement covers all 'processing' operations concerned with making an image 'better' or more interpretable. These operations are of two types; point operations and neighbourhood operations.

Point operations act upon the brightness values of individual pixels whereas neighbourhood operations change the pixel values as a function of the values of other pixels.

The image histogram (Fig. 57) forms the basis of all image enhancement operations.

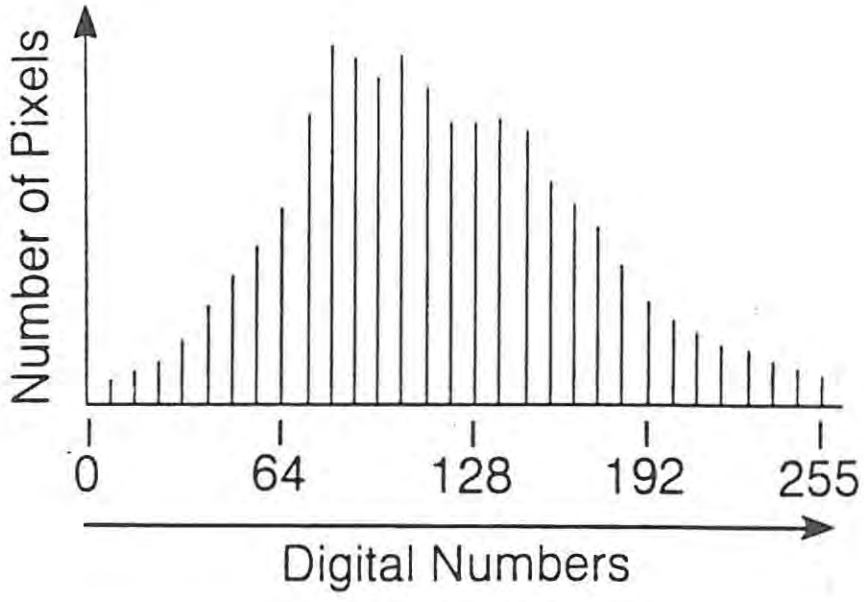

Figure 57. An image histogram (after Sabins Jr., 1987).

It is a plot of the brightness value represented by digital numbers (DNs') versus the frequency of their occurrence. The shape of the histogram and spread of its values determines the methods of enhancement. The most commonly applied methods are contrast stretches, band ratioing and edge enhancement.

Contrast Stretches

Contrast stretches are the basic working tools of the image analyst. Remote sensing systems are designed to record the full range of reflectances possible from all conceivable surface materials. Values range from black (DN = 0) to white (DN = 255), however such extremes are rare on the earth's surface. Furthermore, the human eye is capable of only discriminating only about 30 grey levels providing they are adjacent to each other and sharply contrasting. Therefore it is preferable to stretch the image in order to highlight contrasts. The in-house Anglo American MES images are produced in such a manner. The major methods of stretching available are the Linear Contrast Stretch, and Non-linear Contrast Stretch consisting of the Uniform Distribution Stretch and the Gaussian Stretch as illustrated in figure 58.

The Linear Contrast Stretch is the most commonly used method and involves assigning a DN value at the low end of the original histogram to 0 (black) and a DN value at the high end of the original histogram to 255 (white). All the data between these two values are then linearly stretched. This stretching improves the contrast of the image, thus enabling the enhancement of features such as fractures and individual rock-units, etc.. A disadvantage is that contrast is decreased at the extreme high and low end of the original image histogram.

The Uniform Distribution Stretch is similar to the Linear Contrast Stretch and redistributes all the values of the original histogram uniformly over the entire horizontal axis. This stretch applies the greatest contrast enhancement to the middle brightness values (DNs') of the original histogram. The loss of contrast at the extreme light and dark ranges is not as severe as in the Linear Contrast Stretch.

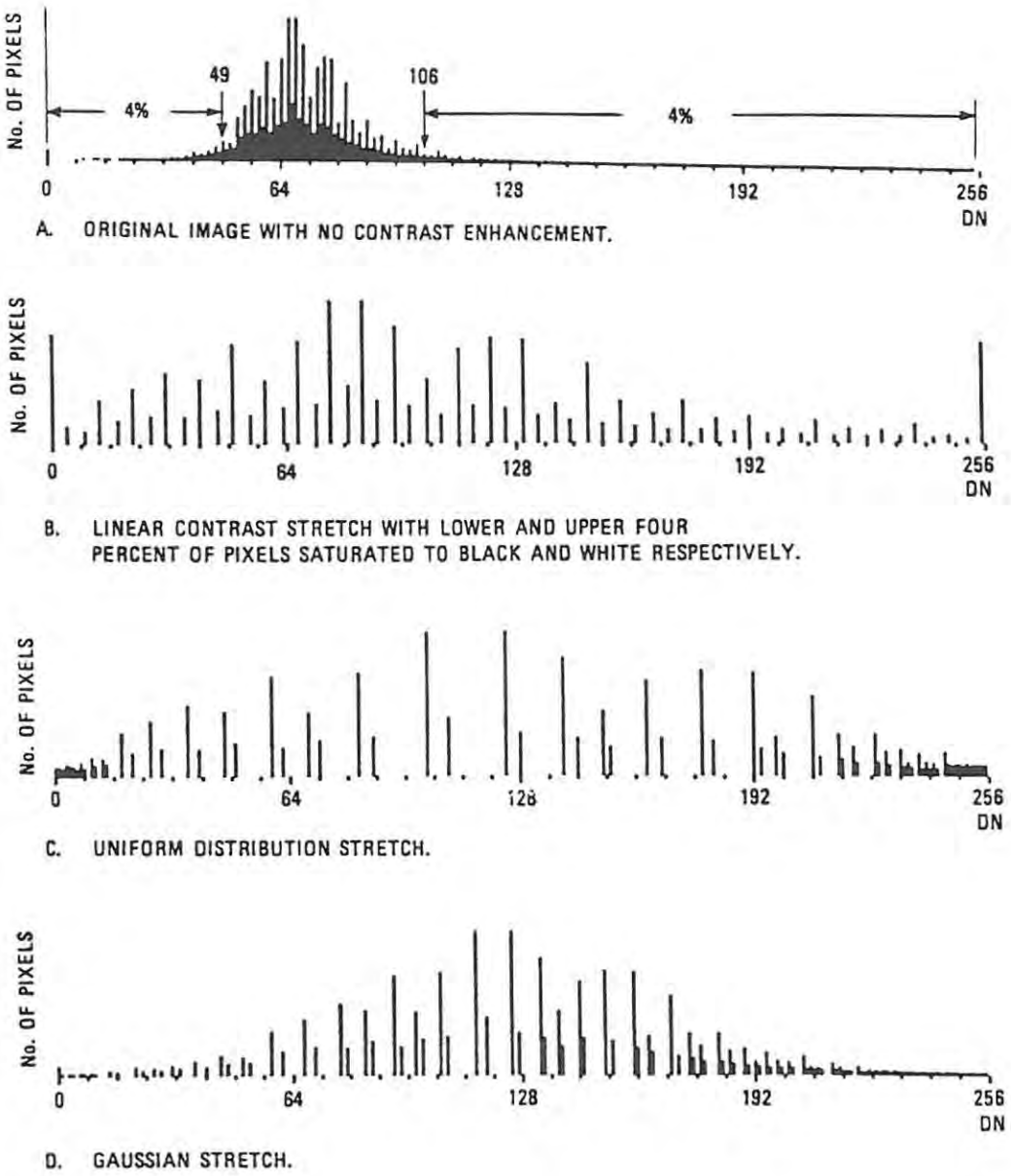

Figure 58. Contrast enhancement methods (modified after Sabins Jr., 1987).

The Gaussian Stretch approximates the original histogram to a normal distribution, thus enhancing the contrast within the tails of the histogram (i.e. it improves contrast between the light and dark ranges of the image at the expense of contrast in the middle ranges).

Ideally, the user should inspect the original image and determine the elements of the scene (e.g. fractures, granites) that are of greatest interest. The appropriate stretching technique should then be applied.

Band Ratioing

A lot of minerals have spectra with diagnostic absorption and reflectance characteristics (spectral signatures). Some are illustrated in figure 59, which shows laboratory measured reflectance spectra for a number of common minerals over the wavelength range 0,4 - 2,5 µm. As illustrated, kaolinite, alunite, montmorillonite and illite have prominent absorption features within band 7, and high reflectances associated with band 5. Limonite, hematite and goethite have weak reflectances in band 1, but strong reflectances in band 3.

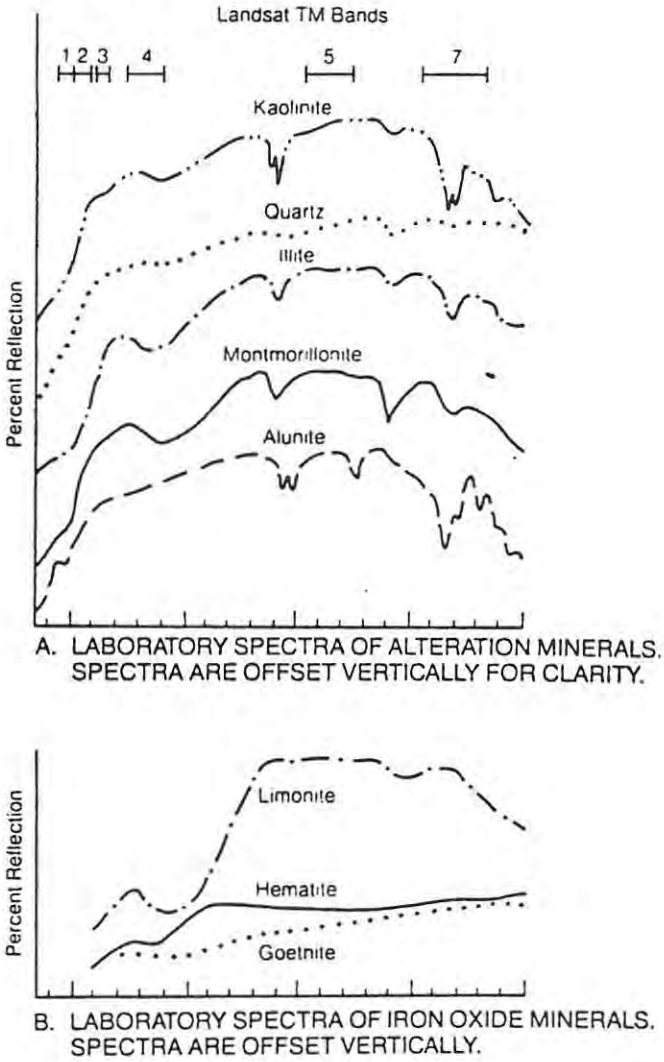

Figure 59. Reflectance spectra of some minerals (after Sabins, JR., 1987).

Unlike the laboratory determined spectra using band-widths of 0,01 μm, the thematic mapper takes readings over larger band-widths, and therefore cannot diagnose the individual spectral differences. Instead, the individual band reflectance values are representative of the overall rock composition derived from a number of different minerals. This also applies to vegetation, soil, etc..

Figure 60 shows spectral reflectance curves for vegetation, hydrothermally altered rocks and unaltered rocks according to the LANDSAT TM. As illustrated, there is a distinct difference between the reflectance percent of hydrothermally altered rock and unaltered rock. This property is useful, especially as Archaean granite/gneiss-hosted gold mineralization is commonly associated with hydrothermal alteration. It should be noted that Band 6 of TM (10,4 - 12,5 μm) lies in the thermal IR region beyond the range of figure 60.

Note that the altered rocks have high reflectances at 1,6 μm corresponding to band 5 and low reflectances at 2,2 μm corresponding to band 7. Therefore an image using the ratio 5/7 would enhance the reflectance of the altered rocks to a ratio of approximately 1,5 : 1 as the lower reflectance values of band 7 are in the denominator. The unaltered rocks have nearly equal reflectance values for bands 5 and 7; and therefore a ratio of approximately 1 : 1. The percentage reflection is usually represented by 'grey-scales' with the lowest reflection being black and the highest reflection being white. These 'grey-scales' can be converted to colour by using a colour density slice, and is more 'pleasing' to the eye. Red and yellow colours for example, can be assigned to the highest ratio values; thereby suggesting the possible presence of altered rocks. Green and blue can be assigned to those rocks with the lowest ratio values, suggesting unaltered rocks.

Similarly, spectra of weathered iron-rich minerals (Fig. 59) have weak reflectance in the blue region (band 1) and strong reflectance in the red region (band 3). Therefore an image using the ratio 3/1 results in high reflectances for iron-rich areas, causing bright tones on the image.

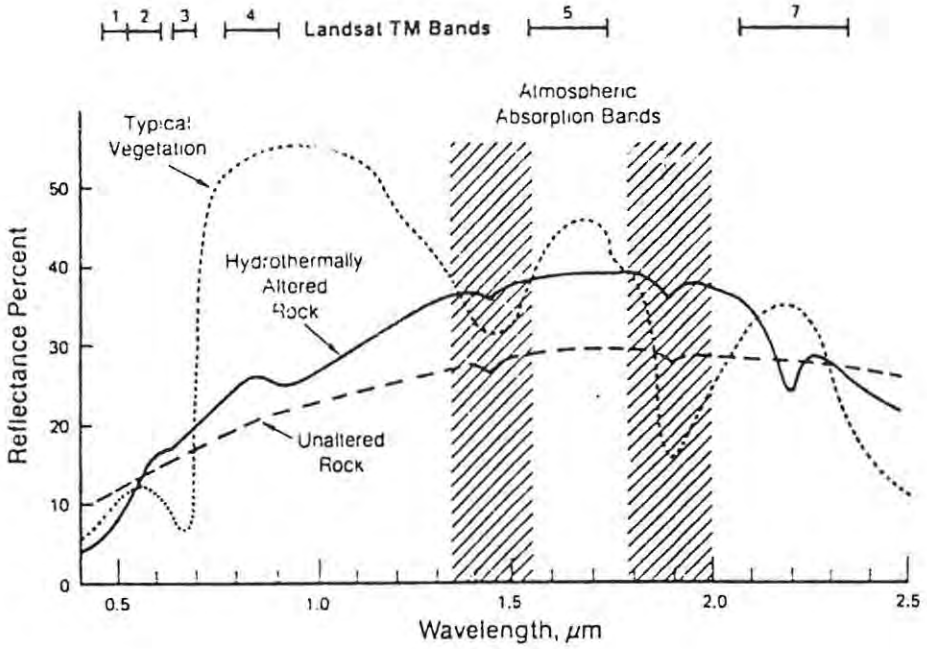

Figure 60. Spectral bands for the TM system. Reflectance curves for vegetation, unaltered rocks, and hydrothermally altered rocks (after Sabins, 1983).

It is also possible to produce an image using the ratios 5/7, 3/1 and 3/5. If one had to apply a 'colour density slice' to these ratios by assigning red, green and blue to these ratios respectively, orange and yellow tones would delineate possible altered rocks whilst blue would represent areas with little clay alteration. This type of image is often called a 'clay-iron' image. Other combinations of band ratios are also possible and often used (e.g. the in-house Anglo American clay-iron image).

Another effect of band ratioing is to remove the influence of topography and shadow caused by varying illumination from the sun. Theoretically any surface should recieve the same proportion of energy in all wavebands irrespective of its orientation to the sun. Hence the ratio between two bands for pixels containing the same kinds of surface material should be the same despite their varying orientations. In addition, the brightness (albedo) variation of the ground surface is decreased and the colour (spectral) differences increased. Problems related to band-ratioing include (Drury, 1987):

1). Emphasizing random noise, thereby enhancing spurious data.

2). Removing surface brightness effects. This can in some instances remove the very parameter by which the analyst discriminates materials; two rocks can have similar spectra, but different albedos.

It should be emphasized however, that not all alteration features indicated in Clay-iron images necessarily involve hydrothermal alteration. Therefore field visits are always needed to determine their cause.

Edge Enhancement

Edge enhancement techniques are specifically used for enhancing linear features, using various linear algebraic techniques. They fall into two categories; non-directional filters and directional filters. Non-directional filters enhance linear features having almost any orientation in an image (except those features that are orientated parallel to the direction of filter movement). Directional filters on the other hand, enhance specific linear trends in an image.

Appendix 3: Geochemical analytical techniques used in this project

In this project, selected rock samples were analysed using the Anglo American Research Laboratory Xray Fluorescence Multi-element (XRFME) technique for base-metals and fire-assay for gold. The XRFME package is the standard geochemical analysis method available for exploration. Table 5 gives the limits of detection and precision for relevant elements using the XRFME method. The limit of detection of Au using the fire-assay method is 50ppb.

Table 5

Geochemical Analyses Using The A.A.R.L.* XRFME Technique

Element	Working Range		Precision
	L.L.D.	Upper	(1 std. dev.)
Ba	50ppm	1100ppm	38ppm @ 300ppm
Rb	2ppm	1400ppm	2.5ppm @ 100ppm
Sr	2ppm	1000ppm	0.9ppm @ 100ppm
Nb	1ppm	1000ppm	1ppm @ 100ppm
Zr	2ppm	5000ppm	0.9ppm @ 100ppm
Y	2ppm	1000ppm	1.7ppm @ 100ppm
Cu	5ppm	1000ppm	3ppm @ 100ppm
Zn	5ppm	1000ppm	6.1ppm @ 100ppm
Pb	3ppm	1000ppm	3.9ppm @ 100ppm
As	5ppm	1000ppm	5.1ppm @ 100ppm

(modified after Feather and Baumgartner, 1983).

*Anglo American Research Laboratories.

Appendix 4: Geochemical Analyses

The geochemical analyses of the Roodepoort, Ramagoep, Moletsie and Matlala granitic rocks are given in Table 6. They were all analysed using the techniques described in Appendix 3. The granitic samples from Waterval were analysed separately by the Eersteling Gold Mining Company, Ltd. for gold only, using the fire-assay technique. The results of these analyses are given in Chapter 8 and figure 45.

As shown in Table 6, most of the samples are obtained from Roodepoort, the only really promising area for gold mineralization. Sample positions are illustrated in figure 61. The sampling positions for Roodepoort that are not illustrated in figure 61, are taken from pits, trenches and adits within the Knight's Mine. The sample positions at Ramagoep, Moletsie and Matlala are illustrated in figures 47 and 50 (Moletsie and Matlala) respectively.

Table 6: Geochemical analyses

Table of gold analyses

Sample No	Ba (g/t)	Rb (g/t)	Sr (g/t)	Zr (g/t)	Y (g/t)	Nb g/t	Cu (g/t)	Zn (g/t)	Pb (g/t)	As (g/t)	Au (g/t)		Description of Samples
RDH2801	276.0	86.0	22.0	31.0	24.0	8	BLD	2.0	BLD	BLD	<0.05	Roodepoort	Pyrite-mineralised leucocratic granite
RDH2802	699.0	44.0	519.0	51.0	6.0	2	BLD	14.0	17.0	BLD	<0.05	Roodepoort	Muscovite-rich leucocratic granite
RDH2803	567.0	BLD	368.0	58.0	4.0	0	11.0	39.0	19.0	28.0	<0.05	Roodepoort	Leucocratic granite at contact with greenstones
RDH2804	344.0	19.0	251.0	53.0	5.0	0	BLD	14.0	25.0	4.0	<0.05	Roodepoort	Leucocratic granite at contact with greenstones
RDH2805	1079.0	158.0	301.0	207.0	52.0	18	BLD	7.0	BLD	35.0	2.50	Roodepoort	Quartz stockworks in pit at Knight's Mine (see fig. 39)
RDH2806	124.0	BLD	325.0	314.0	18.0	6	10.0	22.0	24.0	72.0	<0.05	Roodepoort	Pyrite-rich leucocratic granite from Knight's Mine
RDH2807	696.0	83.0	213.0	111.0	8.0	3	3.0	23.0	8.0	BLD	<0.05	Roodepoort	Pyrite-rich leucocratic granite from Knight's Mine
RDH2808	344.0	22.0	63.0	11.0	10.0	3	8.0	0.0	BLD	BLD	2.80	Roodepoort	Quartz veins at the contact between the granite and schist at Knight's Mine
RDH2809	271.0	8.0	278.0	63.0	8.0	3	BLD	BLD	BLD	BLD	<0.05	Roodepoort	Pyrite-rich leucocratic granite
RDH2810	410.0	7.0	287.0	160.0	11.0	4	BLD	BLD	BLD	BLD	<0.05	Roodepoort	Leucocratic granite
RDH2811	1143.0	137.0	358.0	145.0	41.0	14	2.0	10.0	BLD	19.0	0.70	Roodepoort	Granite contact with schist at Knight's Mine (see fig. 40)
RDH2812	330.0	6.0	114.0	256.0	23.0	8	3.0	42.0	7.0	BLD	0.10	Roodepoort	Gossanous granite at Knight's Mine
RDH2813	345.0	4.0	128.0	346.0	27.0	9	BLD	BLD	BLD	BLD	<0.05	Roodepoort	Pyrite-rich leucocratic granite
RDH2814	900.0	185.0	346.0	314.0	28.0	10	1.0	10.0	7.0	8.0	0.05	Roodepoort	Leucocratic granite from Knight's Mine
RDH2816	1132.0	84.0	357.0	183.0	49.0	17	276.0	201.0	0.0	78.0	0.40	Roodepoort	Schist contact with granite at Knight's Mine (see fig. 40).
RDH2817	515.0	46.0	413.0	50.0	6.0	2	BLD	17.0	7.0	BLD	<0.05	Roodepoort	Leucocratic granite from Knight's Mine
RDH2818	610.0	34.0	441.0	107.0	6.0	0	0.0	38.0	18.0	45.0	<0.05	Roodepoort	Granodiorite from quarry (Noordvaal Crushers Ltd., Pietersburg)
RDH2819	657.0	89.0	317.0	113.0	8.0	3	2.0	24.0	6.0	BLD	<0.05	Roodepoort	Granodiorite
RDH2820	291.0	4.0	302.0	366.0	29.0	10	BLD	BLD	BLD	BLD	0.30	Roodepoort	Silicified granite in pit at Knight's Mine
RDH2821	677.0	20.0	284.0	87.0	11.0	4	BLD	BLD	BLD	BLD	<0.05	Roodepoort	Pyrite-rich leucocratic granite at Knight's Mine
RDH2822	352.0	19.0	507.0	208.0	30.0	10	12.0	21.0	BLD	BLD	0.10	Roodepoort	Pyrite-rich leucocratic granite at Knight's Mine
RDH2823	455.0	9.0	242.0	175.0	12.0	4	BLD	5.0	17.0	BLD	<0.05	Roodepoort	Silicified leucocratic granite at Knight's Mine
RDH2824	608.0	49.0	501.0	79.0	8.0	3	BLD	9.0	0.0	BLD	<0.05	Roodepoort	Leucocratic granite at Knight's Mine
RDH2825	321.0	5.0	328.0	259.0	19.0	7	BLD	BLD	BLD	BLD	0.20	Roodepoort	Quartz-veined leucocratic granite at Knight's Mine
RDH2826	351.0	4.0	325.0	268.0	19.0	7	BLD	BLD	BLD	BLD	0.20	Roodepoort	Gossanous leucocratic granite at Knight's Mine
RDH2827	1273.0	166.0	204.0	260.0	51.0	18	BLD	2.0	BLD	BLD	0.70	Roodepoort	Leucocratic granite at Knight's Mine
RDH2828	369.0	5.0	171.0	422.0	32.0	11	1.0	BLD	BLD	BLD	<0.05	Roodepoort	Leucocratic granite at Knight's Mine
RDH2829	696.0	51.0	754.0	53.0	8.0	3	BLD	26.0	9.0	BLD	<0.05	Roodepoort	Dynamite-blasted leucocratic granite
RDH2830	298.0	3.0	108.0	87.0	9.0	3	BLD	5.0	BLD	BLD	<0.05	Roodepoort	Leucocratic granite
RDH2831	1762.0	85.0	382.0	229.0	59.0	21	35.0	85.0	BLD	14.0	<0.05	Roodepoort	Pyrite-rich quartz-sericite schist at Knight's Mine
RDH2833	599.0	75.0	433.0	113.0	8.0	3	2.0	27.0	13.0	BLD	<0.05	Roodepoort	Granodiorite
RDH2834	535.0	307.0	114.0	181.0	38.0	13	BLD	22.0	22.0	BLD	<0.05	Matlala	Coarse-grained K-rich granite
RDH2835	1437.0	147.0	231.0	719.0	80.0	28	BLD	68.0	18.0	BLD	<0.05	Matlala	Coarse-grained K-rich granite
RDH2836	224.0	175.0	55.0	68.0	20.0	7	BLD	15.0	35.0	35.0	<0.05	Moletsie	Coarse-grained K-rich granite
RDH2837	845.0	184.0	167.0	363.0	26.0	9	BLD	33.0	10.0	BLD	<0.05	Moletsie	Coarse-grained K-rich granite
RDH2838	409.0	15.0	660.0	12.0	3.0	0	BLD	BLD	BLD	BLD	<0.05	Ramagoep	Gneiss
RDH2839	804.0	78.0	126.0	21.0	13.0	5	BLD	6.0	40.0	BLD	<0.05	Ramagoep	Gneiss
RDH2840	476.0	34.0	555.0	67.0	9.0	3	2.0	12.0	14.0	BLD	<0.05	Ramagoep	Gneiss
RDH2841	1088.0	150.0	231.0	350.0	65.0	23	BLD	38.0	14.0	BLD	<0.05	Ramagoep	Gneiss

BLD = Below limit of detection

THE GEOLOGY OF PART OF ROODEPOORT 744 LS

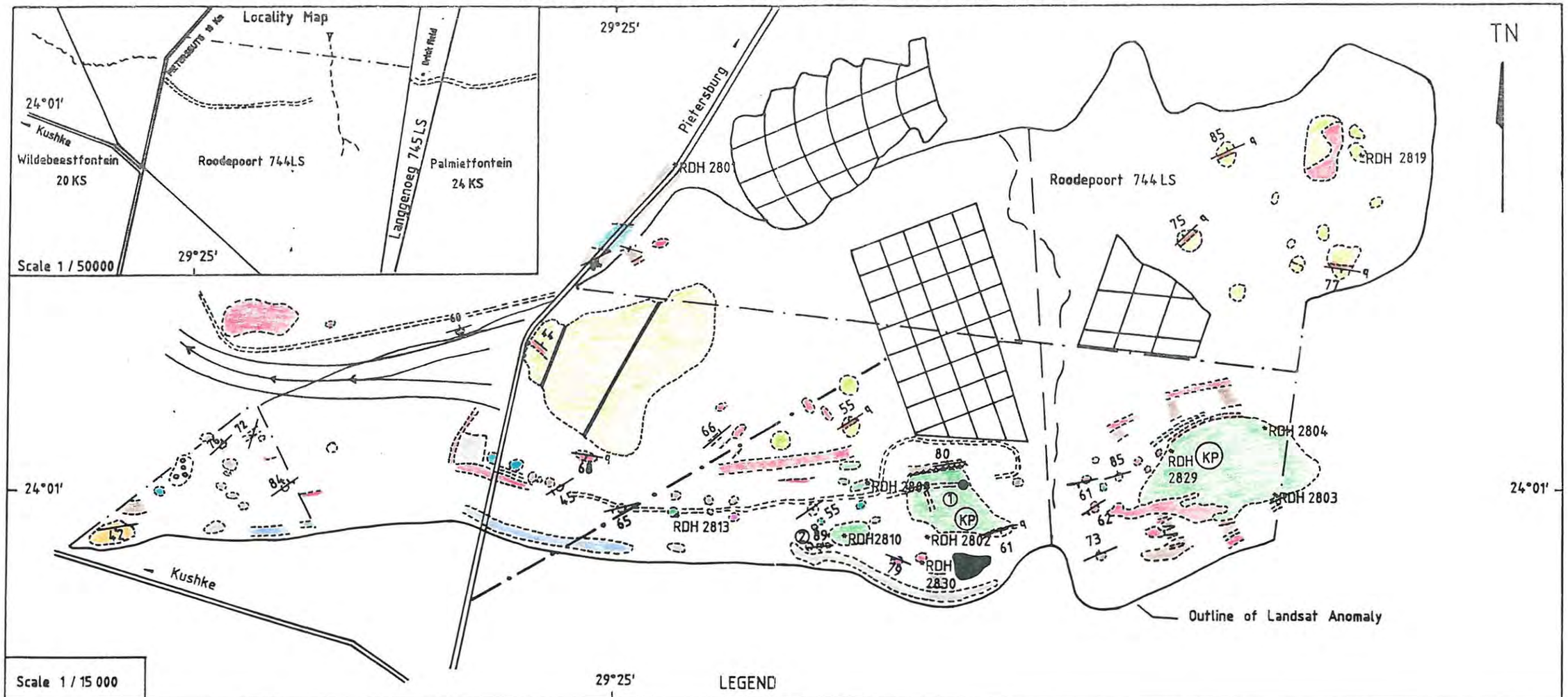

- Soil cover
- Dolerite
- Quartz veins
- Altered granodiorite
- Grandiorite
- Metasediments
- Metabasalt
- Talc - chlorite schist
- Serpentinite (intrusive)
- Banded iron formation
- Carbonate rocks

TURFLOOP GRANITE

UITKYK FORMATION

MOTHIBA FORMATION

PIETERSBURG GROUP

- RDP2 Drill core
- (KP) Knight's pluton
- (1) Knight's mine
- (2) Old Northern Hope Mine
- 23 — Cleavage-schistocity, 23 q Strike and dip of quartz vein
- Shear
- Lineament
- Inferred geological boundary
- Old cultivation fields
- RDH 2801 Lithogeochemical sample number

- Fence
- Powerline
- Stream
- Kraal
- Road
- Road

Figure 61